

**DESIGN AND CONSTRUCTION OF NON-IMAGING DISH
CONCENTRATOR SYSTEM (COOLING SYSTEM)**

NG SHIAU PING

**A project report submitted in partial fulfilment of the
requirements for the award of Bachelor of Engineering
(Hons.) Mechatronics Engineering**

**Faculty of Engineering and Science
Universiti Tunku Abdul Rahman**

May 2013

DECLARATION

I hereby declare that this project report is based on my original work except for citations and quotations which have been duly acknowledged. I also declare that it has not been previously and concurrently submitted for any other degree or award at UTAR or other institutions.

Signature : _____

Name : NG SHIAU PING

ID No. : 09UEB08352

Date : 10th May 2013

APPROVAL FOR SUBMISSION

I certify that this project report entitled “**DESIGN AND CONSTRUCTION OF NON-IMAGING DISH CONCENTRATOR SYSTEM (COOLING SYSTEM)**” was prepared by **NG SHIAU PING** has met the required standard for submission in partial fulfilment of the requirements for the award of Bachelor of Engineering (Hons.) Mechatronics Engineering at UniversitiTunku Abdul Rahman.

Approved by,

Signature : _____

Supervisor: Dr. Chong Kok Keong

Date : _____

The copyright of this report belongs to the author under the terms of the copyright Act 1987 as qualified by Intellectual Property Policy of University Tunku Abdul Rahman. Due acknowledgement shall always be made of the use of any material contained in, or derived from, this report.

© Year 2013, Ng Shiau Ping. All right reserved.

Specially dedicated to
my beloved grandmother, mother, father and eldest sister.

ACKNOWLEDGEMENTS

I would like to thank everyone who had contributed to the successful completion of this project. I would like to express my gratitude to my research supervisor, Dr.Chong Kok Keong for his invaluable advice, guidance and his enormous patience throughout the development of the research.

In addition, I would like to thank my group mates for being so cooperative in completing this final year project. Without all the discussion and analysis together with the group member, the project may not be completed.

Moreover, I would like to express my gratitude to mr. Tan Woei Chong, mr. Yew Tiong Keat, mr. Nicholas and mr. Wong Chee Woon, for their teaching, guidance and advice in the process of designing the system; Mr Ho Chan Cheong for teaching, guidance and advice in the process of fabrication of the main frame.

Furthermore, I would like to thank my family for giving me full support in completing this final year project. Without their support and encouragement, I would not complete this project.

DESIGN AND CONSTRUCTION OF NON-IMAGING DISH CONCENTRATOR SYSTEM (COOLING SYSTEM)

ABSTRACT

The sunlight is captured and converted to electricity by using solar cells made of a semiconductor material in all CPV systems. The performance of solar cells is dependent on the temperature. The higher the temperature, the power output from the cells will be lower and it also threatens the long-term stability of the solar cells. In the interest of maintaining the optimal performance of the solar cell, a good design of heat dissipation system is a must in the CPV System. In this report, I have been assigned to design and construct the cooling system for the CPV receiver module. The cooling block has been designed for the cooling system and the automotive radiator is used as key element for heat rejection. Tap water is used as medium for cooling and it is recyclable. Theoretical study on both the automotive radiator and cooling block has been carried out to determine the factors that will affect the heat rejection rate. Furthermore, Computational Fluid Dynamic simulation has been carried out to determine the performance of the cooling block. In addition the Solidworks software has been used to design the cooling block under stress. We have performed on-site actual measurement to validate the simulated result of cooling block in the cooling system. The Prototype of the Non-Imaging Dish Concentrator has been fabricated and tested. The NIDC has a total reflective area of 3.82m^2 and solar concentration ratio of 84 suns. The experimental results show that the cooling system has performed heat rejection well by maintaining the temperature of the system. The relationship between the electrical conversion efficiency of CPV system and the temperature of the cell is determined too. From the results, the highest net electrical output power is 595.78W, with the solar power input of 2188.31W and the conversion efficiency is at 34.08%.

TABLE OF CONTENTS

DECLARATION	ii
APPROVAL FOR SUBMISSION	iii
ACKNOWLEDGEMENTS	vi
ABSTRACT	vii
TABLE OF CONTENTS	viii
LIST OF TABLES	xi
LIST OF FIGURES	xiii
LIST OF SYMBOLS / ABBREVIATIONS	xix

CHAPTER

1	INTRODUCTION	1
	1.1 Background	1
	1.1.1 Natural Energy on Earth	1
	1.1.2 Concentrated Photovoltaic System (CPV)	2
	1.1.3 CPV world map	5
	1.2 Aims and Objectives	8
2	LITERATURE REVIEW	9
	2.1 Types of Concentrator Design	9
	2.1.1 Parabolic Concentrator	9
	2.1.2 Fresnel Lens	10
	2.2 Studies on the Characteristic of the Solar Cell	12
	2.2.1 Current voltage (IV) characteristic of the Solar Cell	12

2.2.2	Measurement of the Efficiency for the solar cell	14
2.2.3	Other Parameters of the solar cell	15
2.2.4	Bypass diode in Solar cell	16
2.3	Cooling System for High Concentration Photovoltaic (CPV) System	17
2.3.1	Concentrator Geometries	17
2.3.2	Importance of Cooling System Design for a Receiver	21
2.3.3	Example of Cooling System for Densely Packed Cells	23
2.3.4	Element to be Considered in CPV cooling system design.	25

3 METHODOLOGY 27

3.1	Design of the Cooling System for Dish Shape Concentrator Photovoltaic Receiver Module	27
3.1.1	Main Component Used for the Cooling System	29
3.1.2	Theoretical Study of Automotive Radiator	31
3.1.3	Cooling block design for the Densely Packed Concentrated Photovoltaic (CPV) Receiver Module	37
3.1.4	Technical Design of the Cooling Block	38
3.1.5	Theoretical Study On The Cooling Block	40
3.1.6	Software Simulation Studies for the Cooling Block Design	45
3.2	Fabrication of the Hardware of the Concentrated Photovoltaic (CPV) Frame	47
3.2.1	Process Planning of The Main Frame Parts Fabrication.	48
3.2.2	Fabrication Process of the Mirror Supporter for the Concentrated Photovoltaic (CPV) Frame	49
3.3	Design and Fabrication of the Mirror Tilting System	55
3.3.1	Material Used for the Mirror Tilting Purpose	56
3.4	Setup of Experiment	59

3.4.1	Non Imaging Dish Concentrator	60
3.4.2	Experimental setup To Test the Cooling System	62
3.4.3	Experimental Analysis on the Heat Rejection Rate and Efficiency of Conversion of CPV module	67
4	RESULTS AND DISCUSSIONS	70
4.1	Results for The Cooling Block Design, Analysis and Fabrication	70
4.1.1	Stress Analysis	70
4.1.2	Result of Calculated Fin Efficiency	76
4.1.3	Computational Fluid Dynamic (CFD) Analysis Results	77
4.1.4	Comparison between theoretical study and simulated results of the Cooling block	78
4.1.5	Fabrication Results of the cooling block	83
4.2	Fabrication Results of the whole cooling system	84
4.3	Fabrication result for the Hardware of the Concentrated Photovoltaic (CPV) Frame	86
4.3.1	Fabrication Result of the Mirror Supporter for the Concentrated Photovoltaic (CPV) Frame	86
4.3.2	Problem Encounter During On site Prototype Setup	90
4.4	Result for the NIDC Experiment	92
4.5	Result on the On Site Testing Of the Cooling System and Power Conversion Efficiency of the CPV module	93
5	CONCLUSION AND RECOMMENDATIONS	103
5.1	Conclusion	103
5.2	Recommendation for Future Work	104
	REFERENCES	106
	APPENDICES	110

LIST OF TABLES

TABLE	TITLE	PAGE
	Table 2.1: Summary on the Characteristic of Types of Solar Concentrators.	12
	Table 3.1: Specification of the automotive radiator	31
	Table 3.2: Calculated Parameter Result For The Heat Rejection Rate	34
	Table 3.3: Some Common Metals Thermal Conductivity	37
	Table 3.4: Rounded Off Measurement for the Square Aluminium Bar	49
	Table 3.5: Rounded Off Measurement for the Main Frame Support Square Aluminium Bar	53
	Table 3.6: Mass result of number of experiment	64
	Table 3.7: Summary of the specification in whole experimental setup.	65
	Table 3.8: Thermal conductivity value for different material and the different material's thickness	69
	Table 4.1: Parameter Used To Carry Out the CFD Analysis	77
	Table 4.2: Parameters calculated for heat rejection analysis at different temperature	78
	Table 4.3 Thermal load calculated for heat rejection analysis at solar constant	79
	Table 4.4: Solar Power Input, Heat Rejection Rate, Cooling Block Temperature and from 11am to 12:15pm at every 5 minutes of interval	94

Table 4.5: Solar Power Input, Heat Rejection Rate, Cooling Block Temperature recorded from 11:00am to 3:30pm at every 15 minutes of interval	94
Table 4.6: Conversion Efficiency comparison with fan	95
Table 4.7: Conversion Efficiency comparison without fan	96
Table 4.8: Comparison of the net electrical output between the case of cooling system with fan and without fan	101

LIST OF FIGURES

FIGURE	TITLE	PAGE
Figure 1.1:	Semiconductor with p-n junction (Miñano and Benítez 2008)	2
Figure 1.2:	Generating electricity from the Sun, with and without a solar concentrator. (Miñano and Benítez 2008)	3
Figure 1.3:	30 Years of field-proven CPV technology around the world (PV insider, 2012).	5
Figure 1.4:	HCPV plant in USA (PV insider, 2012)	6
Figure 1.5:	HCPV plant in China (PV insider, 2012)	6
Figure 1.6:	HCPV plant in other places (PV insider, 2012)	7
Figure 2.1:	The Sun rays are focused at the focal point of the parabola (Stine and Geyer 2009)	10
Figure 2.2:	Fresnel Lenses (Stine and Geyer 2009)	11
Figure 2.3:	As the incident light increases, the development of the solar cell IV curve is shown. (Vorster and Dyk 2004)	13
Figure 2.4:	The area of the biggest rectangle shown in the IV curve is maximum power of solar cell delivered. (Vorster and Dyk 2004)	13
Figure 2.5:	Simplified corresponding circuit drawing of a solar cell (Ellingson and Heben 2008)	15
Figure 2.6:	On the left is IV curve and on the right is power vs load resistance curve. Two plots can be converted to each other due to same information content. (Ellingson and Heben 2008)	16

Figure 2.7: Influence of single bypass diodes on behalf of each cell (Vorster and Dyk 2000)	17
Figure 2.8: Single cell points focus assembly. The obtainable space for heat dissipation is indicated by the dashed line (Royne 2005)	19
Figure 2.9: Linear assembly. The area available for heat sinking is indicated by the dashed line (Royne 2005)	20
Figure 2.10: Cutaway section of the Entech module (McDanal A, 1984)	20
Figure 2.11: Densely Packed assembly. The rear side of the cell is only the area available for heat sinking (Kreske 2002)	21
Figure 2.12: The impact of temperature on the current-voltage characteristics of a solar cell. (Honsberg and Bowden 2010)	22
Figure 2.13: Horne's suggested Cooling method for dense module (Horne 1993)	24
Figure 3.1: Cross flow type of automotive radiator (Boe 2011)	29
Figure 3.2: The cooling system's automotive radiator with the model "Proton Wira 1500 c.c." with 1.5-liter water capacity. It is used as the main component for the rejection of heat in the cooling system. (Chong and Tan 2012)	30
Figure 3.3: Graph of rate of heat rejection of automotive radiator VS different in temperature among radiator and ambient, with different speed of wind and area of heat being transfer	36
Figure 3.4: The physical drawing of CDO 100, C3MJ cell assembly. (Emcore 2010)	39
Figure 3.5: Illustration of the heat transfer in the cooling block	41
Figure 3.6: The triangular plate with marking and with hole drilled.	51
Figure 3.7: Connection that needed the L bar support	52

Figure 3.8: Example of aluminium bar with the four L bar connected to it.	52
Figure 3.9: Main frame picture showing that each side contain 4 cutting angle square bars for mirror support.	53
Figure 3.10: Square aluminium bar with angle cutting.	54
Figure 3.11: Old mirror tilting syst	55
Figure 3.12: Main component of the mirror tilting system	56
Figure 3.13: Testing on the main component of the mirror tilting system	57
Figure 3.14: fully filled silicon with bad finishing causes uneven surface	57
Figure 3.15: 3D outlook of the structure of the mirror tilting system.	58
Figure 3.16: Mirror being placed onto the main frame.	59
Figure 3.17: Results of solar flux distribution for NIDC prototype shown in 2-D form. The total flux distribution area is 18cm ×18cm	60
Figure 3.18: Results of solar flux distribution for NIDC prototype shown in #-D form. The total number of Suns is 84.	60
Figure 3.19: The prototype of the NIDC positioned at latitude of 32N and longitude of 107.7E in the campus.	61
Figure 3.20: Situation where all the group member performing the NIDC experiment	62
Figure 3.21: Situation the Sunlight focuses on the cooling block causes the sand paper to be burned	62
Figure 3.22: The schematic diagram shows the entire component for the automotive radiator cooling system.	63
Figure 3.23: The on-site experiment performed to measure the water mass flow rate.	63
Figure 3.24: Commercialized solar cell mounted to the cooling block	66

Figure 4.1: Cooling block drawn by using Solidworks software with the dimension of 245mm × 245mm × 16mm	70
Figure 4.2: Aluminium cover drawn by using Solidworks software with the dimension of 245mm × 315mm × 5mm	71
Figure 4.3: Angle bar for cooling block mounting drawn by using Solidworks software with the thickness of 3mm and angle of 113 degree	71
Figure 4.4: Maximum stress analysis result for the 14mm height cooling block	72
Figure 4.5: Maximum stress analysis result for the 15mm height cooling block	72
Figure 4.6: Maximum stress analysis result for the 16mm height cooling block	72
Figure 4.7: Maximum displacement analysis result for the 14mm height cooling block	73
Figure 4.8: Maximum displacement analysis result for the 15mm height cooling block	73
Figure 4.9: Maximum displacement analysis result for the 16mm height cooling block	73
Figure 4.10: Maximum stress analysis result for the cooling block cover	74
Figure 4.11: Maximum displacement analysis result for the cooling block cover	74
Figure 4.12: Maximum stress analysis result for the angle bar of the cooling block	75
Figure 4.13: Maximum displacement analysis result for the angle bar of the cooling block	75
Figure 4.14: Guide to assign fin length and fin height	76
Figure 4.15: Figure of full assembly of cooling block used for thermal-load simulation	78
Figure 4.16: Graph of temperature at the center of cooling block (°C) against thermal load acted on the surface of cooling block (W), also with other	

parameter consider such as mass flow rate and inlet water temperature. The dotted line indicates the simulation results.	81
Figure 4.17: Fabricated cooling block with the cover for heat transfer between cooling block and water.	83
Figure 4.18: Left shown the fabricated side angle bar and right shown mounted cooling block on the angle bar.	83
Figure 4.19: Leaking test performed for the cooling block.	84
Figure 4.20: Side view of CPV system with the whole cooling system	84
Figure 4.21: Leaking test performed for the manifold	85
Figure 4.22: Main frame with the biggest size of square aluminium bar.	86
Figure 4.23: Square aluminium bar with L bar fixed on it and also triangular plate for mirror tilting purpose	86
Figure 4.24: Arrows show the main frame square aluminium bar for supporting the mirror tilting system.	87
Figure 4.25: Completed main frame with mirror being set on it.	87
Figure 4.26: The corridor used as a place for fabrication of main frame.	89
Figure 4.27: With the help of our classmate, the main frame is being moved or rotated for further work.	90
Figure 4.28: References made used for mirror tilting purpose.	90
Figure 4.29: Situation where all the group member involved in doing mirror tilting	91
Figure 4.30: Over burnt of the sand paper	92
Figure 4.31: The darken area of burnt mark on the sand paper measured with the result of 19cm × 19cm.	93
Figure 4.32: Result of Experiment conducted for 1 hour and 15minutes, from 11am to 12:15pm	96

Figure 4.33: Result of Experiment conducted for 4.5 hours continuously from 11am to 3.30pm	97
Figure 4.34: Heat Rejection Rate VS Temperature Different at radiator fan speed of 3m/s and area of 2.2m²	99
Figure 4.35: Solar cell conversion efficiency VS change in temperature	100
Figure 4.36: Solar cell conversion efficiency VS change in temperature and speed of fan	100

LIST OF SYMBOLS / ABBREVIATIONS

CPV	Concentrated Photovoltaic
PV	Photovoltaic
HCPV	High Concentration Photovoltaic
I-V	Current Voltage
$A_{\text{convection}}$	the total surface area involved in the heat transfer via forced convection (m^2)
$A_{\text{radiation}}$	the total surface area for heat transfer via radiation (m^2)
A_c	cross-sectional area (m^2)
A_r	total area of mirrors which reflect the solar flux to the target of NIDC (m^2)
c	heat capacity of water (J /kg K)
D_h	hydraulic diameter (m)
DNI	direct normal irradiance, (W/ m^2)
FF	Fill Factor
h	heat transfer coefficient ($\text{W/ m}^2 \text{K}$)
I_{sc}	short circuit current (A)
k	turbulent kinetic energy (m^2/s^2)
ka	thermal conductivity of air (W/ m K)
$k_{\text{DBC-alumina}}$	thermal conductivity of alumina layer in direct bond copper (DBC) substrate (W/ m K)
$k_{\text{arctic silver}}$	thermal conductivity of arctic silver thermal adhesive (W/ m K)
k_{CPV}	thermal conductivity of CPV cell (W/ m K)
k_{copper}	thermal conductivity of copper cooling block (W/ m K)
k_{solder}	thermal conductivity of solder (W/ m K)
$k_{\text{DBC-copper}}$	thermal conductivity of copper layer in direct bond copper (DBC) substrate (W/ m K)

k_w	thermal conductivity of water (W/ m K)
L	length parallel to the water flow direction in cooling block
L_m	length of mirror
\dot{m}	mass flow rate of water (kg/ s)
Nu_a	Nusselt number of forced convection within radiator and air
Nu_w	Nusselt number of forced convection within cooling block and water
P	perimeter (m)
p	pressure (N /m ²)
P_{in}	solar power input (W)
$P_{CPV, in}$	solar power input to single cell module (W)
$P_{CPV, out}$	electricity power output by single cell module (W)
Pr_a	Prandtl number (based on air temperature)
Pr_w	Prandtl number (based on water temperature)
Pr_s	Prandtl number (based on radiator surface temperature)
$\dot{Q}_{convection}$	Convection heat transfer rate (W)
\dot{Q}_c	Heat conduction of the cooling block base (W)
\dot{Q}_{fc}	Rate of heat transfer by forced convection in the cooling block (W)
\dot{Q}_{in}	Input Power of solar (Thermal load acted on the center of the cooling block) (W)
\dot{Q}_{out}	heat rejection rate (W)
$\dot{Q}_{radiation}$	radiation heat transfer rate (W)
$R_{alumina}$	thermal resistance of substrate alumina in Direct Bond Copper (K/W)
R_{arctic}	silver thermal resistance of arctic silver adhesive (K/W)
R_{CPV}	thermal resistance of CPV cell (K/W)
R_{copper}	thermal resistance of copper cooling block (K/W)
R_{solder}	thermal resistance of solder (K/W)
$R_{sub-copper}$	thermal resistance of substrate copper layer in Direct Bond Copper (K/W)
R_{tot}	total thermal resistance (K/W)
Re_D	Reynolds number of forced convection within radiator and air

Re_L	Reynolds number of forced convection within cooling block and water T temperature ($^{\circ}C$)
T_{amb}	ambient temperature ($^{\circ}C$)
T_{cal}	cooling block's temperature in calculation ($^{\circ}C$)
T_{CPV}	CPV cell temperature ($^{\circ}C$)
T_s	average surface temperature of radiator ($^{\circ}C$)
T_{sim}	cooling block's temperature in simulation ($^{\circ}C$)
u_i, u_j	velocity components (m/ s)
u_l	laminar dynamic viscosity (N s/ m^2)
u_t	turbulent dynamic viscosity (N s/ m^2)
v_a	wind speed (m /s)
v_w	water flow speed (m /s)
V	voltage (V)
V_{oc}	open circuit voltage (V)
W_m	width of mirror
x_i, x_j	coordinates (m)
ΔT	temperature difference ($^{\circ}C$)
ε_t	turbulent energy dissipation rate (m^2/s^2)
ε	surface emissivity
l_a	dynamic viscosity of air (N s/ m^2)
l_w	dynamic viscosity of water (N s/ m^2)
g	the efficiency of direct conversion from solar energy to thermal energy
q	fluid density (kg/ m^3)
q_a	air density (kg/ m^3)
q_w	water density (kg/ m^3)
r	Stefan–Boltzmann constant ($W m^2K^4$)
r_k, r_s	turbulent constant
r_l	laminar Prandtl number
r_t	turbulent Prandtl number
a	air
amb	ambient
c	cross-section

cal	calculation
D	diameter
e	turbulent energy dissipation rate
h	hydraulic
i	i-direction
j	j-direction
k	turbulent kinetic energy
L	parallel length
l	laminar
r	reflective area
s	surface
sim	simulation
t	turbulent
w	water

CHAPTER 1

INTRODUCTION

1.1 Background

1.1.1 Natural Energy on Earth

Energy exists in many forms. The examples are heat, light, chemical energy, and electrical energy. The ability to bring about change or to do work is energy. Only by changing from one form to another, the total amount of energy and matter in the Universe remains constant. According to the first Law of thermodynamics, energy can be changed from one form to another, but it cannot be created or destroyed. (Farabee 2001) The sun, wind, water and earth are the main sources of natural energy. A source of clean and renewable electricity can be provided by these natural energy sources. It even can be used for other purposes. For instance, providing heating for our home or business.

Among those natural energy sources, we are interested in the solar energy source that will be studied in our final year project. Solar energy supplied by the Sun to the earth in the form of solar radiation. This source of solar energy can be used for generating electricity and also heating a water supply. There are photons elements that make the generation of electricity available by means of a photovoltaic system (PV) within the Sun rays. Through research, we found that solar energy is the most widely used natural energy source among people. (Whitburn 2012)

1.1.2 Concentrated Photovoltaic System (CPV)

In all photovoltaic (PV) systems, the Sunlight is captured and converted to electricity by using solar cells made of a semiconductor material. Silicon is the most common semiconductor used. For pure silicon itself is a poor semiconductor. So, in order to overcome its disadvantages, the pure silicon needs to be mixed with other elements to let electrons to move much more freely. For instance it can be mixed with phosphorus. The types of the silicon panels used consist of two which is the positively charge panel and the negatively charge panel. There will be a formation of diode when the two types of pieces of silicon are combined into one. It acts as a one-way gate that allows the movement of the electrons to be free in one way. The electrical charge will be created when photons (which is the light particle) hits the specifically prepared surface of a concentrated photovoltaic cell. This charge will then be stored in a battery. Figure 1.1 shows the semiconductor.

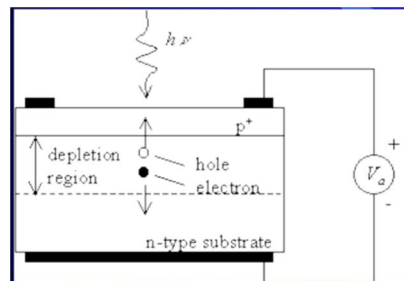


Figure 1.1: Semiconductor with p-n junction (Miñano and Benítez 2008)

About 30% of the available energy can be converted by a single-material PV cell to valuable electrical power. In order to improve the percentage of power conversion, people use different band gaps of multiple cells. Bear in mind that the cells or receivers are more complex so it cost more compare to the original one. There is alternative way to solve the power conversion efficiency problem. We can focus Sunlight on the cell by using the solar concentrator, which is a device that allows the collection of Sunlight from a large area and focusing it on a smaller receiver or exit. A basic illustration of the generation of electricity by using a solar concentrator to harness the power from the Sun to is shown in figure 1.2.

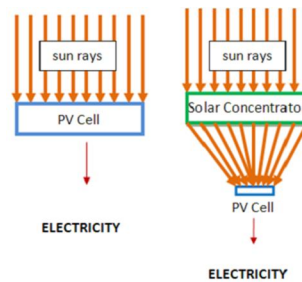


Figure 1.2: Generating electricity from the Sun, with and without a solar concentrator. (Miñano and Benítez 2008)

There are different materials that can be used to manufacture the concentrator, subjecting on the use of the concentrator. With mirror as the most used material, the price of a solar concentrator is greatly cheaper than PV material, if both calculated in unit area. So, with this concentrator, the amount of energy gathered from the Sun is still the same if compared to PV cell. Some of the advantages (Miñano and Benítez 2008) and disadvantages (Mahoney et. al 1993) of using the solar concentrators are summarise below:

a) Advantages:

- The need to depend on silicon cell is reduced
- The intensity of solar irradiance is increased, therefore improving the efficiency of the cell
- Total cost of the whole concentrator photovoltaic system is reduced.

b) Disadvantages:

- This system requires sun tracking in system
- The PV require cooling system.

The CPV modules can be classified according to concentration degree. The number of “Suns” is the expression of concentration degree. For instance, “4X” means that with the photovoltaic material, the intensity of the light that hits on it is 4 times than it would be without concentration. Below shows the classification of different concentration of PV systems:

1) Low Concentration (2-10Suns)

- no cooling system used

- no tracking
 - standard Si cells
- 2) Medium Concentration (10-100Suns)
- no high precision tracking
 - cooling system involved
- 3) High Concentration (>100 Suns)
- High precision tracking
 - Cooling system involved
 - Multijunction cells is used
 - High current densities

In our case, we are dealing with the high concentration CPV (HCPV) system. Heat problem will be introduced with the high concentration ratios. The photovoltaic cells within the receiver unit convert a portion of the energy into electrical power. But as mentioned, photovoltaic is likely to lose some power conversion efficiency. Only a small portion of the incoming Sunlight that is concentrated onto the cell that will be converted into electrical energy. The remainder of the received energy will be converted into thermal energy in the cell. This will induce the rise in temperature in the junction except the heat is well dissipated to the environment. So, it is concerned that the cells is kept as cool as possible due to the relationship of cell efficiencies reduced as temperatures rise. In addition, higher temperatures also make threat to the lasting steadiness of solar cells.

There are 2 types of cooling system which is passive cooling and active cooling. For passive cooling, the cooling of the cells is performed by natural convection. For active cooling, the cooling of the cells is performed by forced convection. Liquid is used as a medium for rapid cooling.

1.1.3 CPV world map

According to the Entech Solar System Research and development company the CPV system has 30 Years of Field-Proven Concentrating Photovoltaic (CPV) Technology around the world (PV insider, 2012).



Figure 1.3: 30 Years of field-proven CPV technology around the world (PV insider, 2012).

In June 22, 2012, the PV Insider has published the edition of year 2012 of the Concentrated Photovoltaic World Map. It is an important guide of CPV installations location around the world. The most updated edition of this world map provides the full analysis of the technology supplier, dimension, and operating status of almost 200 CPV projects internationally. The following figure of 1.4 to 1.6 will show the world map of the CPV system.



Figure 1.4: HCPV plant in USA (PV insider, 2012)



Figure 1.5: HCPV plant in China (PV insider, 2012)

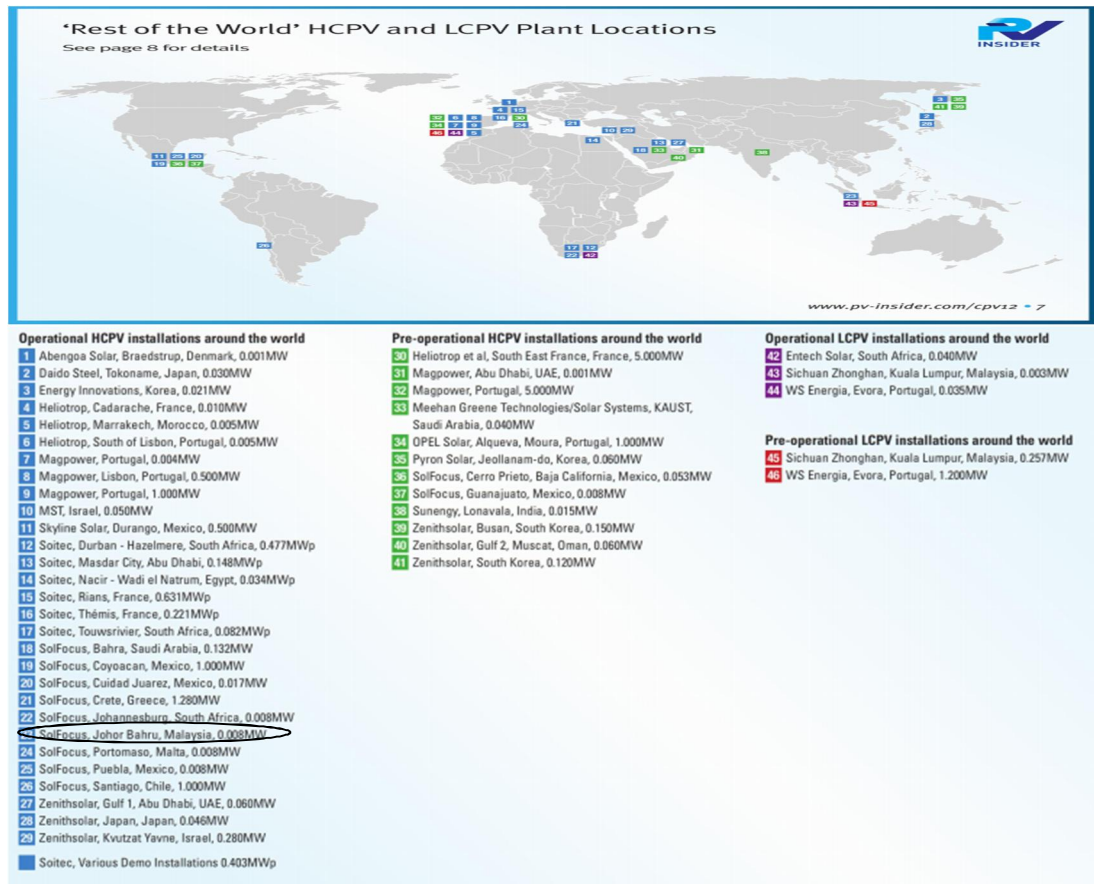


Figure 1.6: HCPV plant in other places (PV insider, 2012)

From all the figure above, we can see that the CPV system development is growing tremendously around the world, especially in USA. Unfortunately, in our country, the usage of CPV system is still not popular. There is only one CPV system as shown in the circle on the figure above.

1.2 Aims and Objectives

The objective of this Final Year Project is to study Concentrator Photovoltaic (CPV) System by:

1. Designing and constructing the hardware of Sun-Tracker for Dish Concentrator System.
2. Designing and constructing the cooling system for Dish Concentrator Receiver Module.
3. Performing data collection and analysis of Dish Concentrator System output.

Since it is a group project, I was assigned with the task of designing and constructing the cooling system for non-imaging dish concentrator system.

CHAPTER 2

LITERATURE REVIEW

2.1 Types of Concentrator Design

Through research, I found out that there are kind a number of developments relating the solar concentrators in different designs. In this section I will only review about the two types of solar concentrator which is the Parabolic Concentrator and the Fresnel Lens Concentrator. One of this concentrator types will be chosen for our receiver design, and with this design, I will develop a suitable cooling system for it.

2.1.1 Parabolic Concentrator

By referring to figure 2.1 below, the parabolic concentrator 2D design drawing is seems to have a parabola shape. This design is favoured by many concentrator designers. It also is commonly used as a reflecting solar concentrator (Muhammad et al. 2010). The special features of this design is that it can concentrate the parallel rays from the Sun wholly to a single focus point, F. The illustration can be seen in figure 2.1. Take note that, to construct the concentrator, it is not necessary to use the whole part of the parabola curve. It is found that only a truncated portion of the parabola has been used in the most of the parabolic concentrator.

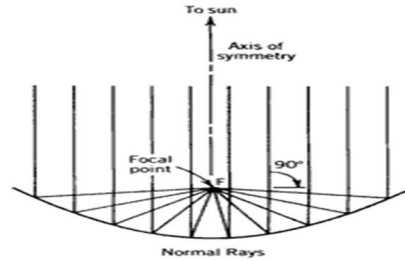


Figure 2.1: The Sun rays are focused at the focal point of the parabola (Stine and Geyer 2009)

Basically, two designs of parabolic concentrator are obtainable. The first one is a parabolic dish. It is designed by revolving the 2D design along the x-axis to produce a parabolic dish. The second design is with a parabolic trough. Typically, huge solar power plant that uses concentrator in concentrating the solar power system will use these two designs that have the reflective characteristic.

To maximise the Sun energy collection, this concentrator design will need a larger field of view. Also, to get a maximum of efficiency, a desirable tracking system is needed. Bear in mind that this concentrator design will not be recommended in a small housing because the tracking system is very costly.

2.1.2 Fresnel Lens

The operation of Fresnel lens concentrator is comparable to the usual lens or mirror. Fresnel lens focuses the Sun ray at one focal point by refracting the rays. Basically, this lens has two divisions which are a flat upper surface and canted facets that are employed at a back surface. According to figure 2.2, the facet is an likeness of the curvature of a lens. Around 100 facets per millimetre could be employed in a good linear Fresnel lens. (Stine and Geyer 2009)

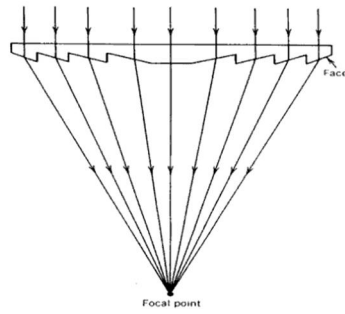


Figure 2.2: Fresnel Lenses (Stine and Geyer 2009)

The approach to use this design of concentrator is arranged the assembly as a point focus Fresnel lens or a line focus Fresnel lens. The Sacramento Municipal Utility District uses the Fresnel lenses concentrators on the 30kW utility grid-connected plant (Sala et. al 2000)

The fresnel lens thinner is thinner if compare to a conventional lens. It also needed a slighter volume of material to fabricate (Kapla 1985). These are the main benefits of Fresnel lens over conventional lens. In addition, the separation of the direct and diffuse light can be done by the Fresnel lens too. With this characteristic, it is mainly suitable to be used in controlling in a building interior's illumination and temperature. The sharpness of the facet will be the drawback of this type of concentrator. The rays might be improperly focused at the receiver if there is more round in shape at the edges of the facets causes by the error in the manufacturing process (Stine and Geyer 2010).

In short both the design of the concentrator is being summarized in table 2.1 below. The table reviews the corresponding of different concentrator, revealing the pros and cons of every design accordingly.

Table 2.1: Summary on the Characteristic of Types of Solar Concentrators.

Concentrator Type	Advantages	Disadvantages
Parabolic Type Concentrator	- High Concentration	- Need a greater viewing field - Require a worthy system of tracking
Fresnel lens	- Thinner in size if compare to normal lens - Require less material if compare to normal lens	-The rays improperly focused at the receiver, causing imperfection on the edges of the facets.

In conclusion, different design has different pro and cons. For suitability and convenience, we have decided to use the mirror and design it to become a parabolic dish shape in our final year project.

2.2 Studies on the Characteristic of the Solar Cell

2.2.1 Current voltage (IV) characteristic of the Solar Cell

It is very important to analyse the combination of current-voltage (I–V) characteristics for the cells that is connected in series in the CPV system. This is because one of the significant parameter used to get information on the overall efficiency and performance of a CPV module and cell under high brilliance condition is the current-voltage measurements. (Current-Voltage Characteristics of High Concentration Photovoltaic Arrays. 2009). The usual current-voltage features, also can be identified as IV curve, of a diode without illumination is presented in green color shown in figure 2.3.

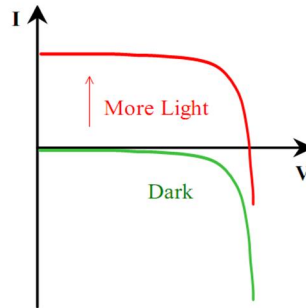


Figure 2.3: As the incident light increases, the development of the solar cell IV curve is shown. (Vorster and Dyk 2004)

The diode's forward bias current turn-on and build-up is shown in the curve. No current will drift through the diode when there is no illumination, except there is exterior current applied. On another hand, the IV curve will move up with incident Sunlight. This shows that external potential drift from the solar cell to a negative load.

The extreme current transported by the solar cell at any light intensity level is the short circuit current, I_{sc} . The short circuit current drift with zero external resistance which causes $V=0$. Across the terminals of the solar cell, the potential that have been developed when the external load resistance is very huge, it is the open circuit voltage, V_{oc} . At both limits, the power provided to the load is zero. At an infinity load resistance value, the power reaches a maximum (P_{max}). Figure 2.4 shows the area of the shaded rectangle represent the maximum power.

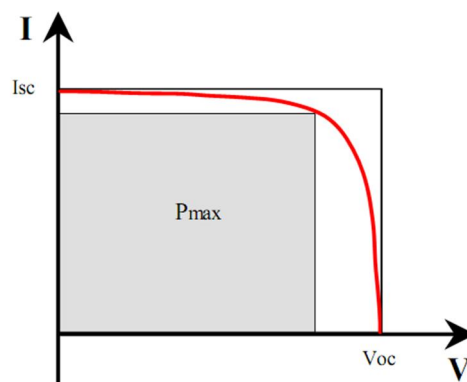


Figure 2.4: The area of the biggest rectangle shown in the IV curve is maximum power of solar cell delivered. (Vorster and Dyk 2004)

A frequently used number that represent the solar cell is the fill factor, FF (Ellingson and Heben 2008). It is described as the ratio of maximum power to the area of the rectangle formed by open circuit voltage and short circuit current.

$$FF = \frac{P_{\max}}{(V_{oc})(I_{sc})} \quad (2.1)$$

where

FF = fill factor

P_{max} = maximum power

V_{oc} = open circuit voltage

I_{sc} = short circuit current

2.2.2 Measurement of the Efficiency for the solar cell

The efficiency of a solar cell is the ratio of the electrical power provided to the load, to the optical power incident on the cell. When the delivered power to the load is at supreme level, and then maximum efficiency is achieved. The solar power on the surface of the earth is the specification of the incident optical power. By using the equation of (2.1), the maximum efficiency (Ellingson and Heben 2008) may be written as:

$$\eta_{\max} = \frac{P_{\max}}{P_{in}} = \frac{(V_{oc})(I_{sc})(FF)}{P_{in}} \quad (2.2)$$

where

P_{max} = maximum power

P_{in} = input power

FF = fill factor

V_{oc} = open circuit voltage

I_{sc} = short circuit current

From the equation, it represent the short circuit current, I_{sc} is directly proportional to the incident optical power, P_{in} . In addition, when the incident power is increased, the output voltage, V_{oc} also rises logarithmically. In short, when there is increase in incident power, the solar cell's total efficiency is likely to rise logarithmically too. Conversely, at high concentration level, the efficiency improvement that can be attained is limited by the thermal effects and electrical losses in the resistance of series for the solar cell. Therefore, at some finite concentration level, the efficiency of practical solar cells is the highest.

2.2.3 Other Parameters of the solar cell

Figure 2.5 represent the simplified corresponding circuit drawing of a solar cell. By referring to the IV curves, information of the the corresponding parallel and series resistances other significant parameters of the solar cell can be extracted.

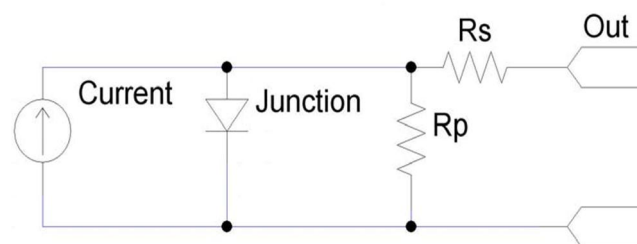


Figure 2.5: Simplified corresponding circuit drawing of a solar cell (Ellingson and Heben 2008)

Usually, parallel resistance R_p (or the shunt resistance R_{sh}) value is way higher than the value of the series resistance R_s . A perfect solar cell will have the R_s value of zero and R_p value of infinite. The slope of the IV curve in that vicinity is an indicator of the value of R_p as the influence of R_s can be ignored near open circuit situations. On the contrary, the slant of the curve of that area is an indicator of the value of R_s as the influence of R_p is insignificant close to short circuit conditions. The optimum efficiency of the solar cell can be evaluated as the proportion of P_{max} to the power

occurrence optical on the solar cell with the condition of the illumination applied to the solar cell during the IV test is representative of the solar radiation it receives in the field.

The IV curve can easily be transformed to a power-resistance curve. Each point on the IV curve links to a load resistance (V_L/I_L) and a power distributed to the load ($V_L \times I_L$). Figure 2.6 represents the maximum power, P_{\max} , that can be distributed to a load by the solar cell and the load resistance value required for optimum power transmission.

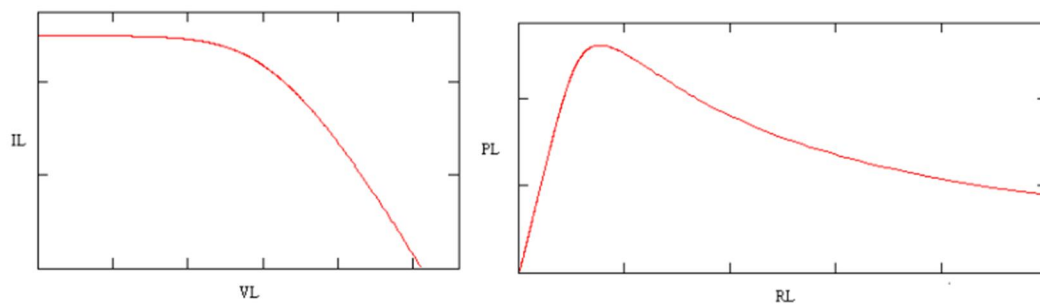


Figure 2.6: On the left is IV curve and on the right is power vs load resistance curve. Two plots can be converted to each other due to same information content. (Ellingson and Heben 2008)

2.2.4 Bypass diode in Solar cell

For bypass diodes need to be installed in each individual cell so that it can have protection on each individual cells from the undesirable results of reverse-biasing, (Vorster and Dyk 2004). By referring to figure 2.7, it represents the current-voltage curves of the irradiance being identified using and not using bypass diodes.

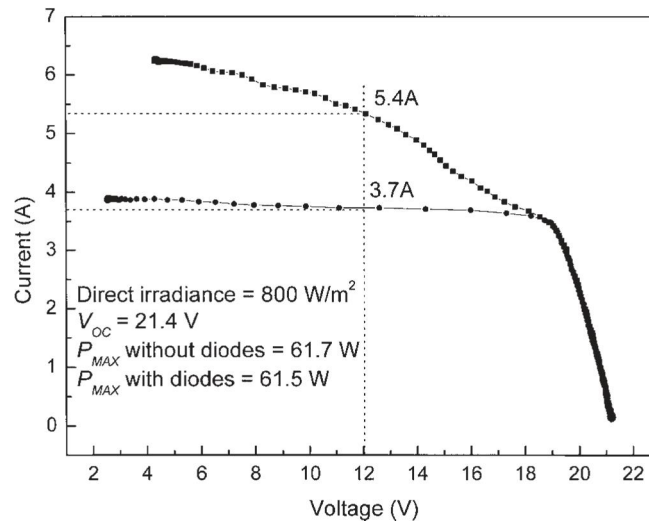


Figure 2.7: Influence of single bypass diodes on behalf of each cell (Vorster and Dyk 2000)

According to figure 2.7, it is obvious that the results of misalignment are reduced by the bypass diodes. In addition, it also has improved the typical feature of the I–V curve of the modules and the irradiance. We can predicate that the module is an entire form and function at greatly lower temperatures when the bypass diodes are tailored at each individual cell with the result of no significant resistive heating occurs, as the mismatched cells are not reverse-biased any more. As refer to figure 2.7, the power generated by the irradiance at a controlled battery charging voltage in between of 12Volts and 14Volts was expressively improved, although the maximum power are having the same value. By referring to figure 2.25, the percentage increase was 46% at 12 V.

2.3 Cooling System for High Concentration Photovoltaic (CPV) System

2.3.1 Concentrator Geometries

At this section, the concentrators are grouped as accordance to their geometry which is the method to assembly the cell. It is important for us to categorize the concentrators accordingly, for different type of concentrator geometry of CPV

system uses different type of cooling method. Another factor to be included is the type of concentrator used because different material will have the different issue of shading (Royne 2005). For example, if it is mirror system, the cells are irradiated front below. This makes a significant matter to deal with shading when we cooling system is being designed. In another way round, if it is a lens system, the cells are basically place below the light source. With this placement, shading effect problem cause by the cooling system won't arise. Through these geometries, best way to cool the system will be determined.

The assembly pattern of individual cells is determined by the supply of the form of the focused Sunlight. We need to take note that the concentrator cells cannot be too huge. This is considering in account of to ohmic losses and thermal behaviour. With the limits mentioned, it is obvious that except for the small point concentrate, whichever a linear assembly of cells or a bidimensional parquet of cells should be implemented. In the following subsection, the grouping of each assembly of the cell will be explained.

2.3.1.1 Point Focus Assembly with Single Cell

The most mutual assembly is the point focus assembly with single cell. A single lens or mirror forms a focus of small extent that can be cast at one cell. We call this assembly as small point-focus concentrators. The proposed way has been used from the initial systems design at 50 times to 60 times, focus Sunlight on Silicon cells sized 2inches in diameter to the current III-V cells up to 5900 times. If there are 50 Suns concentration, there should be an area 50 times the concentrated area available for heat dissipation. Figure 2.8 show that each cell will be having an area approximately equivalent to the concentrator for heat dissipation.

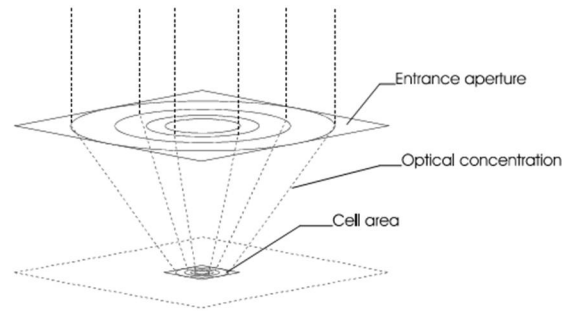


Figure 2.8: Single cell points focus assembly. The obtainable space for heat dissipation is indicated by the dashed line (Royne 2005)

For such as high concentration level, passive cooling method can be implemented in this geometry. Normally, the single cell system uses different types of concentration lenses. Alternative optional is that where the concentrators that is larger in size will conduct the focused light onto single cells with the help of optical fibres.

2.3.1.2 Linear Assembly

This linear assembly system usually focuses the lighting on top of a row of series connected cells by using parabolic troughs type or linearly arranged Fresnel lenses. Usually, a series-parallel interconnection is more favoured, but this connection is much more complicated. The concentration is a constant band of strong solar irradiance. The cells must be attached as a continuous linear strip with no gap, to make sure that it collects all the light at the receiver (Kenny et.al 1999). So, with this arrangement, the cells have less space obtainable for heat dissipation. Figure 2.9 show the linear assembly. Both the sides and the back part of the cell will need to be extended so that more area is available for heat sinking.

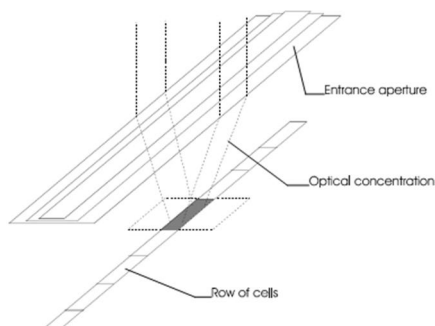


Figure 2.9: Linear assembly. The area available for heat sinking is indicated by the dashed line (Royne 2005)

The linear systems have low geometric concentration and large cell can be used in designing. The real case scenario that uses this type of concentrator is, the Entech Company has installed the prismatic cover for the receiver of Fresnel lens. The geometry of the grid is simpler with this assembly. Figure 2.10 represents the cutaway section of the Entech module.

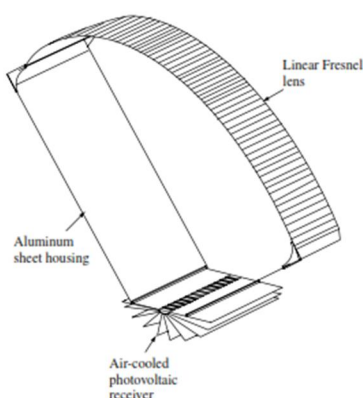


Figure 2.10: Cutaway section of the Entech module (McDanal A, 1984)

2.3.1.3 Large Area Point Focus (Densely Packed) Assembly

This larger point-focus assembly normally uses a large parabolic dish or central tower in the focus is a huge “bidimensional” extent of high irradiance value. The whole focus area must be covered by a multitude of neighbouring cells, densely

packed in order to avoid optical losses. Normally, the receiver is located a little away from the plane of focal. This is to help in increasing the illumination uniformity. To add improvement of the flux homogeneity, secondary concentrators (kaleidoscopes) may be used (Kreske 2002). To reduce optical losses, these cells is essential be escaping interactions on its forward-facing side. Then again, to avoid the light interrupting on the interrelated areas and on the wiring between cells, it's a necessity for the receiver to include the prismatic cover. This densely packed concentrator geometry gives a huge problem in designing the cooling system if compare to the two previous assembly. This is because every single cells only has its end side obtainable for heat dissipation except for the edge cells. The representation of the mentioned geometry is shown in figure 2.11.

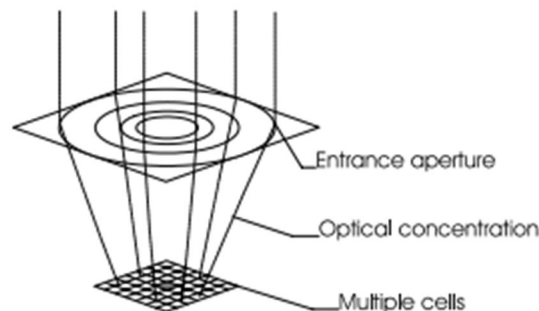


Figure 2.11: Densely Packed assembly. The rear side of the cell is only the area available for heat sinking (Kreske 2002)

This indicates that in standard, the whole heat load is essential to be dissipated in a direction 90 degree to the module's surface. So, passive cooling system can't be used in these arrangements due to the characteristically high concentration levels, high total power, and large receiver area.

2.3.2 Importance of Cooling System Design for a Receiver

Through research, I found out that an individual solar cell can attain a very high temperature which is to the extent of 1200°C. (Cui et al. 2009) This temperature

record is without the present of cooling system at 400 Suns, and in another hand, the temperature drop significantly with an attachment of a metal panel as cooling panel for the system. As mentioned in the introduction, solar cells performance will change according the temperature. The higher the temperature, the power output from the cells will be lower. This is because that the open circuit voltage is extremely dependent on the temperature. Increase in temperature will decrease the voltage, causing lower power output. The effect of rising temperature is represented in the figure 2.12.

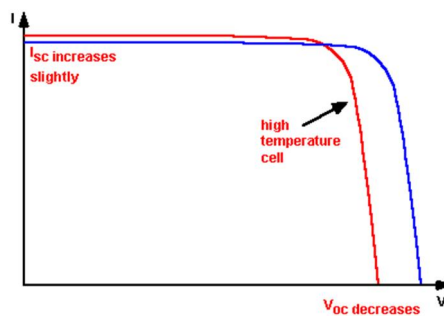


Figure 2.12: The impact of temperature on the current-voltage characteristics of a solar cell. (Honsberg and Bowden 2010)

Therefore, in order to maintain the best performance of the solar cell, a good design of heat dissipation system is a must to have in the Concentrated Photovoltaic (CPV) System with densely packed assembly as in our case. As seen in figure, the cooling area is quite small, so we needed rapid cooling system for the assembly in order to cool the system efficiently. So, only active cooling method can be used in this case because the fluid uses in the design can absorb or release heat and transfer everywhere rapidly. Through the movement of the heated fluid, heat is transported removed in a quick way. In another way, passive cooling that is carried out by natural convection, it means that it does not uses any means of material to transport the heat away quickly, so it does not cool the system down rapidly.

2.3.3 Example of Cooling System for Densely Packed Cells

We plan to design our CPV system as the densely packed cell, so in this section we will review on some of the example of cooling system available for the system. As mentioned in section 2.3.3, passive cooling is not suitable for densely packed cell, and also through findings, there is no research of passive cooling for densely packed cells under concentration founded until today. So, the example mentioned is all about active cooling method.

A monolithic silicon concentrator component with a fully integrated water cooled cold plate (Verlinden et al. 1999). There are about 10 cells in the module and is theoretical act as a "tile" in a greater array. As the flow rate of coolant being optimised at the range of 0.0127 kg/s on an area of 3600 mm², the entire thermal resistance is measured to be 2.3×10^{-4} Km²/W. (Tilford et al. 1993) further describe the design with an illustration of the module diagrams and some supplementary details.

(Lasich 2002) had patented a water cooling circuit used for densely packed solar cells under high solar concentration. The implementation has the capabilities to remove the solar heat flux up to the range of 500 kW/m² from the PV cells. The solar cell temperature is maintained at 40°C under normal operating conditions. The concept behind this circuit is established on water flowing through parallel channels which is in contact of thermal with the cells. Besides that, the patented cooling circuit likewise serves as one of the supportive assembly for the receiver. A modular construction manner is preferable to provide solutions for variable thermal expansion coefficients problems of numerous materials included and also for ease of maintenance.

One of the PV system company name Solar Systems Pty. Ltd. has testified some important outcomes from their parabolic dish photovoltaic systems placed in White Cliffs, Australia (Faiman 2002) using the above described patent for cooling the cells. With rapid water flow rate, measuring at 0.56 kg/ s over an area of 57600 mm² by using 86W electrical pumping power, they are able to uphold the cell temperature at an average value of 38.52 °C, thus achieving cell efficiency of about

24.0% using the HEDA312 Point-Contact solar cells from SunPower. An overall useful energy efficiency of about 70% can be achieved with the condition of the whole thermal energy dissipated were used. This shows the advantages of active cooling system if someone is able to find the uses for the waste heat.

(Horne 1993) had patented a system where a paraboloidal dish concentrated the light onto the PV cells which is attached in a special way. This design can be refer to figure 2.13.

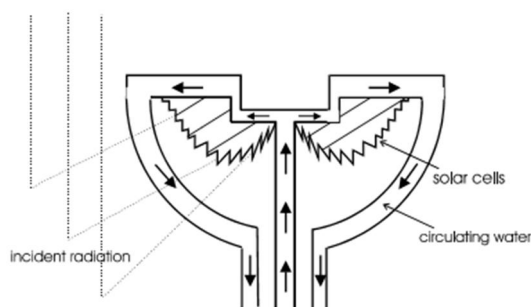


Figure 2.13: Horne's suggested Cooling method for dense module (Horne 1993)

Instead of mounting them horizontally, they were fixed upright on a set of rings, designed to cover the solar receiving area without shading. For water is channelled to the receiver through a central pipe. Then the water has separately flows behindhand the cells and cool the cell before the water is channelled through a glass "case" between the concentrator and the cells back down. When this method is applied, the water cools down the cells and performed as a filter by absorbing a substantial quantity of UV radiation from reaching the cells. In general, cover glass or lenses are used to protect the cells from UV radiation. According to the Horne's case, the water absorbs part of the radiation, causing in the improvement in the cell effectiveness and a lower down the amount of heat generation due to the power conversion in the cells. The Horne's design also integrates a phase-change material in the contact of thermal with the cells, which is used to avoid the cell being damaged at "most horrible case situation" of high temperatures.

Another similar idea had been patented by Koehler, which is to immerse the cells in the continuous flowing coolant liquid. The heat is transferred from both cell

planes (top and bottom). With this design, the coolant also functions to be acted as a filter in absorbing some of the entering low-energy radiation before the energy spreads to the cells. By selecting the accurate coolant and regulating the pressure, local boiling on the PV cells can be controlled, and provide a identical temperature delivery across the PV surface and a greater heat transfer coefficient.

In short, for the densely packed cells geometric, it seems that active cooling method is the only practicable way to realize the cooling system. The high heat flux that makes a low connection resistance from cell to cooling system is enormously significant at high concentrations. Other possible challenges that may be faced in designing the cooling system in order to achieve a low thermal resistance and low pumping power requirement with a simple, reliable and inexpensive system.

2.3.4 Element to be Considered in CPV cooling system design.

There are a few important factors that need to be considered when designing the cooling system for PV cells. First and foremost is the factor of cell temperature. As mentioned in the introduction, the photovoltaic cell efficiency decreases with increasing temperature. Cells may have permanent degradation if the temperature exceeds a definite limit as set by the cell manufacturer (Horne, W.E. 1993). Therefore, it is recommended to follow suit on the operating conditions specified by the cell manufacturers. For instance, we need to know the degradation coefficient of temperature and the temperature of maximum operating for the cell.

Other factor such as uniformity of temperature distribution needs to be considered too. The cell efficiency is identified to be reduced due to non-uniform temperatures through the cell (Mathur 1984). In a photovoltaic module, a number of cells that are connected seriesly and electrically in which some of these series may also have parallel connections. Series connections causes the output voltage to be increased and the current at a given power output is being decreased. Therefore the ohmic losses are being reduced too. Though, the cell that gives the smallest output will edge the current when cells are in series connection. This problem is identified

as current mismatching as mentioned in section 2.2.4. Due to the decreasing of cell efficiency with the increasing in temperature, the efficiency of the whole string of the cell will be restricted at the highest temperature. This issue can be solved by using the bypass diodes as mentioned previously, or by making sure that there is a uniform temperature distributed at each of the series connection.

In addition, the consistency and simplicity of the cooling system needs to be deeply considered. Less complicate and low upkeep solution is required to attain a minimum of operational costs. Toxic materials are not recommended as it may cause healthiness and ecological concerns. Another important characteristic is reliability of the system because when failure occurs, the PV cells might be destructed. The cooling system must be implemented to overcome the "most horrible case situations". For instance, we need to take into consideration of the power outages, tracking irregularities and electrical errors within modules (Horne 1993).

Furthermore, usability of thermal energy is another factor to be considered. There is a substantial rise in the overall conversion efficiency for receiver. It is caused by the usage of the removed energy of thermal from cooling. (Faiman 2002). Because of this, it is desired to invent a cooling system that transports water at as high a temperature as likely. In addition, to make sure that there is no heat loss through a subordinate heat exchanger and an open-loop cooling circuit will be the added advantage to the system.

Moreover we also need to take into the consideration of the pumping power. Meanwhile the power mandatory of whichever active module of the cooling circuit is a sponging loss (Faiman 2002), the pumping power should be kept to a minimum value.

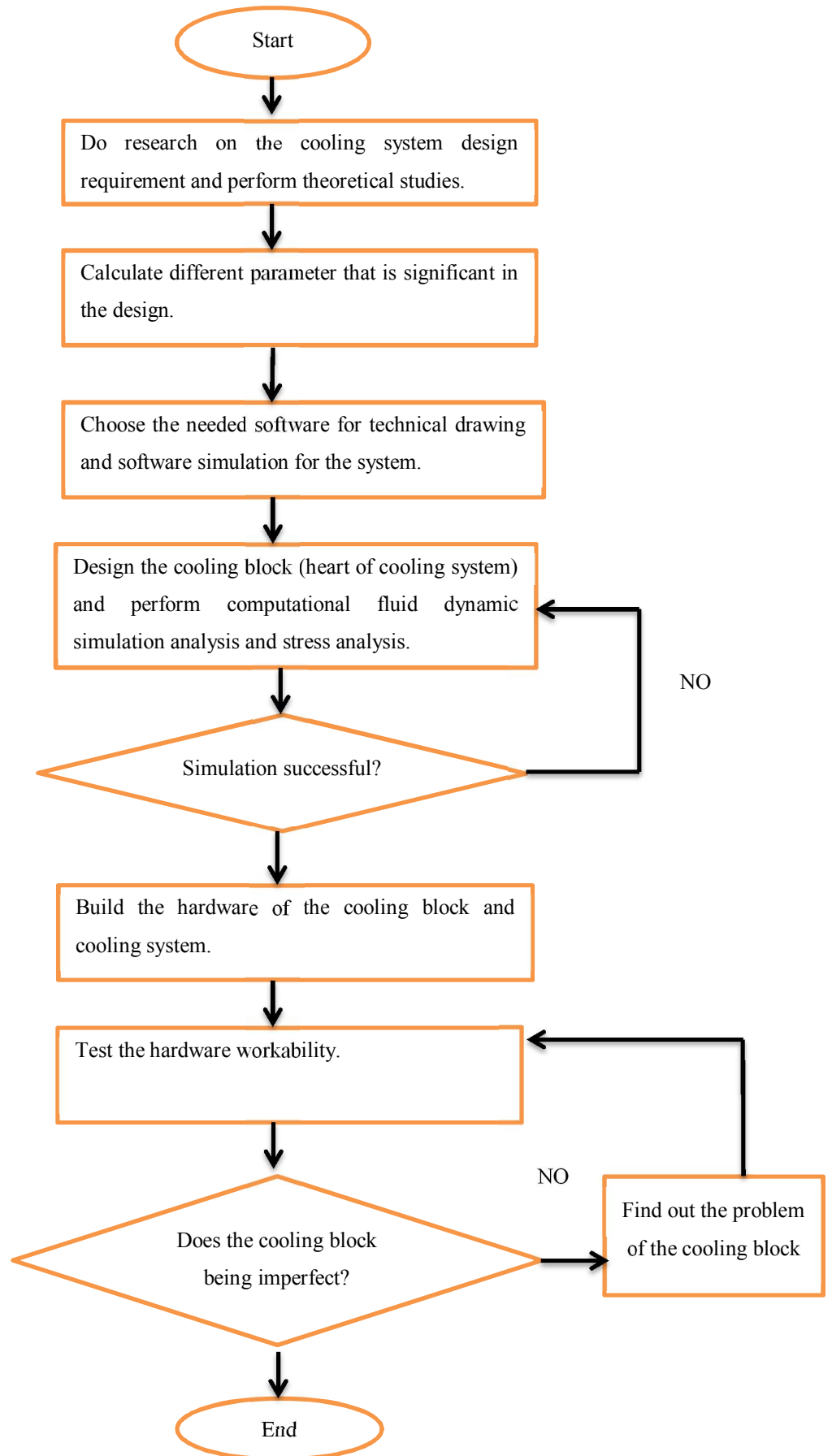
The last factor is the efficiency of material. Materials usage must be retained at minimum to lower down the price, mass and embodied energy concerns, without affecting its reliability. This factor is very important to make sure that the design does not go out of budget.

CHAPTER 3

METHODOLOGY

3.1 Design of the Cooling System for Dish Shape Concentrator Photovoltaic Receiver Module

In this project, I have been assigned to design and construct the cooling system for the concentrator photovoltaic receiver module. The purpose of the cooling system is to maintain the most efficient operating temperature of the solar cell and remove excess heat from the system. Next page shown is the design process of the cooling system.



3.1.1 Main Component Used for the Cooling System

From the literature review, it shows that I have done research on the factor needed to be considered when we are designing the cooling system and different example of cooling option for the system. Active cooling method is used for our dense array CPV system. There are numerous challenges for me in designing the system in order to achieve a low thermal resistance for a low pumping power requirement with a simple, reliable and inexpensive system.

Through discussion with my supervisor and some of the coordinator assigned by the supervisor, we have decided to reuse the existing automotive radiator to be the main element to perform heat dissipation in the cooling system being designed. The reason is that the automotive radiator has high heat rejection characteristic, and it requires a lower power consumption compare to other heat exchanger alternative. So, I will perform theoretical study on the heat rejection perform by the automotive radiator, decide the important design parameter of the cooling system and design of the new cooling block for the CPV system with total reflective area of 3.84m^2 , and 64 of solar cell to be mounted on the cooling block.

For the existing automotive radiator, the system is made up of a radiator used by Proton Wira 1500c.c which means it has the capacity of 1.5-liter for water filling to dissipate heat. The radiator type if the cross flow type. Figure 3.1 shows the working principle of cross flow type radiator. This type of heat rejection radiator is the most common used device among modern vehicles. The coolant travels horizontally with the header tanks on each side. The header tank fitted with the radiator cap is the outlet tank.

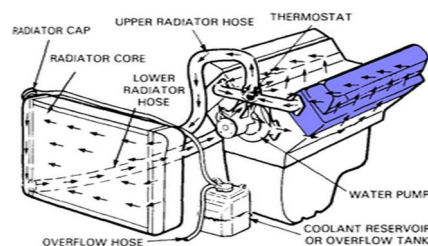


Figure 3.1: Cross flow type of automotive radiator (Boe 2011)

In addition it has a fan that can be used to force air through the radiator's densely packed fins. The casing of the radiator is made of aluminium alloy that is light in weight and has high heat conductivity. The radiator's fin is made of copper. Copper is having a higher conductivity for increased of heat dissipation. An important parameter which is the air flow with variable wind speed with maximum limit of 3m/s can be created by the Direct Current fan with 50.6 W of rated power that is mounted to the automotive radiator. The DC fan is having a 280 mm diameter. Figure 3.2 show the cooling system's automotive radiator.

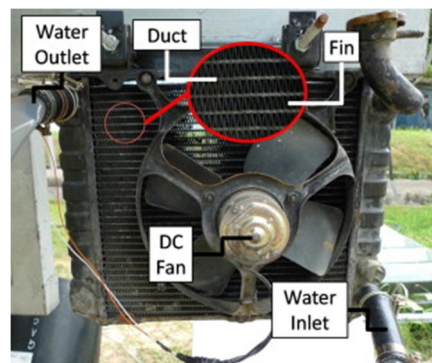


Figure 3.2: The cooling system's automotive radiator with the model "Proton Wira 1500 c.c." with 1.5-liter water capacity. It is used as the main component for the rejection of heat in the cooling system. (Chong and Tan 2012)

The cooling system works on the principles of heat transfer. Heat will always transfer from a hotter to a cooler object. Heat transfer in three ways which is

- a) Conduction - Heat transfer between two solid objects.
- b) Convection - Heat transfer by the circulation of parts of a liquid or gas.
- c) Radiation - Heat transfer by converting heat energy to radiant energy.

When the cooling block transfers heat to the coolant, it is done by convection. Convection also occurs when the hot radiator parts transfer heat to the cooler air surrounding the radiator. For further understanding working principle of the automotive radiator, theoretical study of it will be performing in section 3.1.2.

3.1.2 Theoretical Study of Automotive Radiator

To design a good cooling system, we have to understand the working principle of parts of the system. The purpose of this theoretical study is to fully recognize factor that will affect the rate of heat rejection of the automotive radiator. The specification of the radiator is shown at table below (Chong and Tan 2012):

Table 3.1: Specification of the automotive radiator

Parameter	value
Total surface area	3.8m ²
Surface area covered by fan	2.2m ²
Cross-sectional area	6.914 × 10 ⁻⁵ m ²
Perimeter of the radiator tube	0.0723m
Emissivity of the radiator	0.98
Wind speed available	1m/s to 3m/s

The surface area covered by a fan to perform heat rejection is used for convection calculation whereas the total surface area is used to perform radiation calculation. No conduction calculation will be performed since the rate is negligible. The addition of heat dissipated by the both forced convection and radiation is the total heat removed via the automotive radiator. The equation for the heat transfer rate via forced convection is shown as below:

$$\dot{Q}_{convection} = hA_{convection}\Delta T \quad (3.1)$$

where

h = heat transfer coefficient of forced convection

A = total surface area involved in the heat transfer via forced conversion

ΔT = temperature difference between heat transfer area and fluid.

For coefficient of heat transfer for forced convection equation is:

$$h = \frac{Nu_a k_a}{D_h} \quad (3.2)$$

where

k_a = the thermal conductivity of air which depends on the ambient temperature,
 Nu_a = Nusselt number in the case of forced convection between the radiator surface and air.

D_h = hydraulic diameter

For the hydraulic diameter is defined as the effective diameter of a non-circular tubes in the first approximation (Holman 2011):

$$D_h \equiv \frac{4A_c}{P} \quad (3.3)$$

where

A_c = cross-sectional area

P = perimeter of the radiator tube

The diameter is needed to be used in executing the parameters of Reynolds number, Re_D and Nusselt number, Nu_a . The design of the inner tube of the radiator causes it to be justified as a situation of cross flow on a non-circular tube because it consist of an arrangement of 33 non-circular tubes and being organized in parallel from uppermost to bottommost and across the parallel tubes is where the wind flow through produced by fan. Therefore, the Reynolds number (Rhodes 1989) is determined with equation shown:

$$Re_D = \frac{\rho_a v_a D_h}{\mu_a} \quad (3.4)$$

where

ρ_a = air density

v_a = wind speed

μ_a = dynamic viscosity of air.

The Nusselt number of motorised radiator for the case of cross flow on non-circular tubes can be expressed as (Zukauskas 1972):

$$Nu_a = C Re_D^m Pr_a^n \left(\frac{Pr_a}{Pr_s} \right)^{1/4}$$

$$\left[\begin{array}{l} 0.7 \leq Pr_a \leq 500 \\ 1 \leq Re_D \leq 10^6 \end{array} \right]$$
(3.5)

Where

$$n = 0.37 \text{ for } Pr_a \leq 10$$

$$m = 0.5$$

$$C = 0.51 \text{ (} Re_D \text{ in the range of } 40\text{--}1000\text{)}$$

Note that the density and dynamic viscosity is different reliant on on the ambient temperature rated from 32°C to 52°C. and the parameter such as (ρ_a , μ_a , Pr_a , k_a) are valued according to the air temperature through the radiator which is equal to the ambient temperature of 32 degree, except that Pr_s is valued according to the surface temperature of the radiator. (Chong and Tan 2012).

For the equation of the transfer rate of heat by radiation is shown as below:

$$\dot{Q}_{radiation} = \varepsilon \sigma A_{radiation} (T_s^4 - T_{amb}^4)$$
(3.6)

Where

ε = the emissivity of the radiator surface

σ = Stefan–Boltzmann constant $5.67 \times 10^{-8} \text{ Wm}^{-2} \text{ K}^{-4}$.

$A_{radiation}$ = the total surface area for heat transfer via radiation.

T_s = average temperature of radiative surface

T_{amb} = the ambient temperature

The specification of the automotive radiator such as the fan surface area and wind speed are changed to determine the relationship of rate of heat rejection and different in temperature. Since the surface area is 2.2m^2 , I try to vary it to range of near value such as 1.8m^2 and 2.6m^2 . The few tables below show the calculated

parameter result for the heat rejection rate and heat rejection rate at different temperature. For the wind speed will be vary from 2m/s to 3m/s.

Table 3.2: Calculated Parameter Result For The Heat Rejection Rate

ΔT with V =2m/s	Re_D	Nu_a	h	ΔT with V =3m/s	Re_D	Nu_a	h
5	468.44	9.7080	67.7623	5	702.62	11.8895	82.9935
10	468.44	9.7086	67.7698	10	702.62	11.8925	83.0143
15	468.44	9.7128	67.7995	15	702.62	11.8954	83.0347
20	468.44	9.7153	67.8163	20	702.62	11.8984	83.0553

Calculated results for heat rejection rate at different temperature different:

For area of 1.8m² with wind speed of 2m/s:

Temperature different ΔT , (°C)	Heat rejection rate, W
5	609.86
10	1219.86
15	1830.59
20	2442.47

For area of 2.2m² with wind speed of 2m/s:

Temperature different ΔT , (°C)	Heat rejection rate, W
5	745.38
10	1490.94
15	2237.39
20	2984.96

For area of 2.6m^2 with wind speed of 2m/s :

Temperature different ΔT , ($^{\circ}\text{C}$)	Heat rejection rate, W
5	880.91
10	1762.02
15	2644.19
20	3527.68

For area of 1.8m^2 with wind speed of 3m/s :

Temperature different ΔT , ($^{\circ}\text{C}$)	Heat rejection rate, W
5	746.94
10	1494.26
15	2241.94
20	2989.99

For area of 2.2m^2 with wind speed of 3m/s

Temperature different ΔT , ($^{\circ}\text{C}$)	Heat rejection rate, W
5	912.93
10	1826.32
15	2740.15
20	3654.43

For area of 2.6m^2 with wind speed of 3m/s

Temperature different ΔT , ($^{\circ}\text{C}$)	Heat rejection rate, W
5	1078.91
10	2158.38
15	3238.36
20	4318.87

For total surface area of 3.8m^2

Temperature different ΔT , ($^{\circ}\text{C}$)	Heat rejection rate for radiation, W
5	0.1743
10	0.4356
15	0.8089
20	1.3224

The representation of the results of the plot is shown in figure 3.3. It can be observed that, the rate of heat dissipation of the radiator has a linear relationship with the temperature different between automotive radiator and ambient. In addition, the greater the change in temperature, the higher the rejection rate for all the cases. Thus this has proven the relationship stated in Eqs. (3.1) and Eqs. (3.6). Furthermore, it is also noticeable that increase in wind speed and surface area for heat transfer causes the slope of the graph to be stiffer. In short the results stated that the faster the speed of wind with larger surface area of heat transfer area cause the coefficient of heat transfer to be higher. So, in conclusion, since the area of heat rejection is fixed, so I have chosen 3m/s of fan speed for the cooling system to ensure better heat rejection performance.

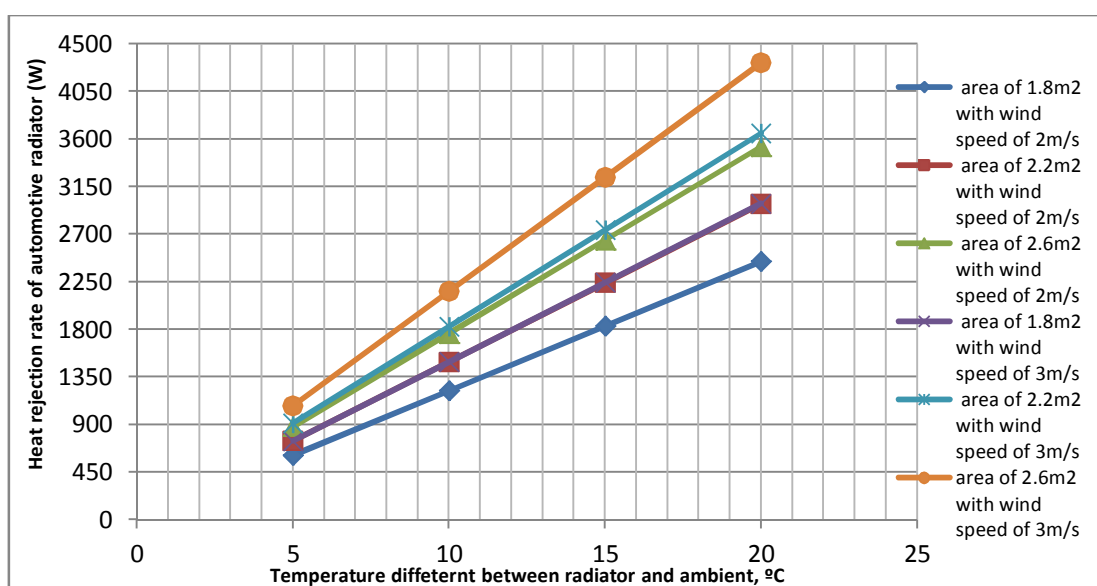


Figure 3.3: Graph of rate of heat rejection of automotive radiator VS different in temperature among radiator and ambient, with different speed of wind and area of heat being transfer

3.1.3 Cooling block design for the Densely Packed Concentrated Photovoltaic (CPV) Receiver Module

There are two factor need to be consider in choosing the material of cooling block which is the thermal conductivity and the material's weight. Thermal conductivity with high value is needed for rapid cooling; the block must be light in weight so that it provide minimum load to the CPV system and does not add burden to the driving system.

To fulfil the goal of rapid cooling, the chosen material must be appropriate in order for the heat exchangers (the cooling block) to maximise its performance. The material chosen to be used in designing the cooling block is copper. This is because that cooper is excellent in heat conduction if compare to other common metal. With this high thermal conductivity characteristic, it allows heat to pass through it quickly. Table 3.3 shows the comparison of thermal conductivity of some common metals.

Table 3.3: Some Common Metals Thermal Conductivity

Metal	Thermal conductivity (W/m K)
Silver	429.00
Copper	399.80
Gold	316.72
Aluminium	235.38
Yellow brass	120.00
Cast iron	80.19
Stainless steel	14.02

In addition, due to the high corrosion resistance characteristic of copper, it is less prone to chemical reaction to the surrounding. This specification is important because the cooling block involves fluids in transferring heat, and the water might contain impurities that will corrode the material. Even though stainless steel is also having a high corrosion resistance, but the thermal conductivity of stainless steel is 30 times less than copper. The cover material used for the cooling block is

aluminium because aluminium has a light weight characteristic and high corrosion resistance.

3.1.4 Technical Design of the Cooling Block

The cooling block designed need to enlarge the surface area in interaction through the cooling medium (water) enclosing it. Basically, finned water heat exchangers design are most commonly used for rapid liquid cooling systems in the CPV system, So I will be using the fin design for the cooling block. There are two design factors for the fin model which is the fin efficiency and fin arrangement.

The ratio of actual heat transfer rate from the fin to the ideal heat transfer rate from the fin is the fin efficiency.

$$\eta_{fin} = \frac{q_{fin}}{q_{fin,max}} = \frac{\text{Actual heat transfer rate from the fin}}{\text{Ideal heat transfer rate from the fin if the entire fin were at base temperature}} \quad (3.7)$$

$$\eta_f = \frac{\tanh(mL_c)}{mL_c} \quad (3.8)$$

$$mL_c = \sqrt{\frac{2h_f}{kt_f}} L_f \quad (3.9)$$

Where

h_f = convection coefficient of the fin

k = thermal conductivity of the fin material

L_f = fin height

t_f = fin thickness

According to the equation, it is noticeable that the efficiency of fin is increased by having the fin aspect ratio to be decreased. The fin aspect ratio is the fin height and fin thickness. In addition, the conductivity of thermal the material also contributes to

the fin efficiency. We have chosen the best material for the cooling block with good thermal conductivity, we will also consider in designing the dimension of the fin to improve fin efficiency. The results of the calculated fin efficiency for the final decided dimension of the cooling block will be review in the results and discussions part.

For the fin arrangement, straight fin designed is used. Generally, the cooling block transfer heat better, with more surface area; though it is not accurate as always. A pin fin heat sink's theory is to try to pack as much surface area into a given capacity as possible, as well. It works well in any orientation. (Kordyban, T., 1998) Through research it is found out that the heat exchange of straight fin is better than the pin fin in force convection flow design (Kordyban, T., 1998). Since the cooling block will not be oriented in different position (only moving up or down according to the CPV system moving up and down), so straight fin arrangement is the most suitable design for the cooling block.

We have decided to place an 8×8 solar cell assembly on the cooling block. The dimension of a single cell assembly is represented at figure 3.4:

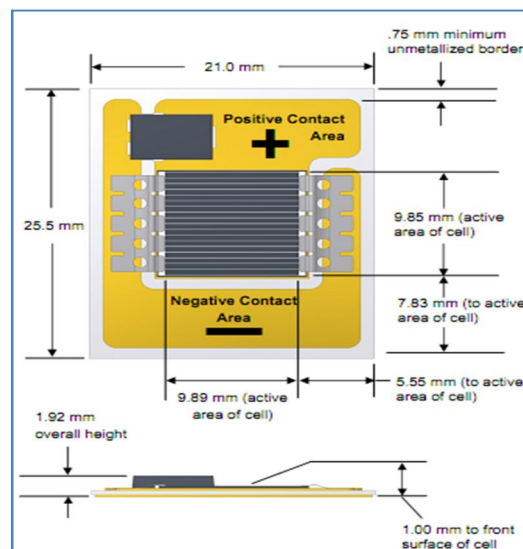


Figure 3.4: The physical drawing of CDO 100, C3MJ cell assembly. (Emcore 2010)

The full detail of the solar cell assembly can be referred to appendix A.

The calculation of the area needed for the cooling block is shown as below:

Minimum length of the cooling block = $21\text{mm} \times 8 = 168\text{mm} = 0.168\text{m}$

Minimum height of the cooling block = $25.5\text{mm} \times 8 = 204\text{mm} = 0.204\text{m}$

Area = length \times height = $0.168\text{m} \times 0.204\text{m} = 0.0343\text{m}^2$

According to the calculation and other simulation results shown in chapter 4, I have decided to set the dimension of the cooling block to be $245\text{mm} \times 245\text{mm}$ ($0.245\text{m} \times 0.245\text{m}$), with the inner cooling region area to be $200\text{mm} \times 204\text{mm}$ ($0.200\text{m} \times 0.204\text{m}$). The height of the cooling block is designed to be 16mm . The multiple water channel dimension is $200\text{mm} \times 0.196\text{mm} \times 10\text{mm}$, which this dimension contribute to a large surface area of 0.20m^2 . The surface area is calculated according to the equation shown below:

$$\text{Total Surface area} = 32 \times (\text{total perimeter of the fin} \times \text{height of the fin}) \quad (3.10)$$

With this large surface area, the cooling block can have a high heat transfer rate. There are 8 symmetry water channel (each for inlet and outlet flow) designed for the cooling block, and each channel contain 3 fin straight with length of 196mm and width of 3mm . Furthermore, this pattern of will permit the flow of water through the channel by means of fast speed because there is increment in the coefficient of heat transfer by the straight and narrow guides design. In addition, each water channel fin is designed not to fully extend to each end of the area. With this design, if one channel fail to have water flow, other channel's water are still be able to flow to the particular part preventing the area to be overheated. Each side of the block is drilled will 5 through hole for cover up purpose, and a 3mm deep square fillet is made for o-ring placement, to prevent the leaking of water. The other detail design dimension is shown in appendix B.

3.1.5 Theoretical Study On The Cooling Block

The purpose of this theoretical study is to fully recognize factor that will affect the rate of heat rejection of the cooling block. The cooling block's center

temperature will be our goal of calculation analysis, with different parameter being manipulate such as the water's mass flow rate, inlet water temperature and the thermal load acted on the cooling block. There are few assumption need to be made for the analysis. Figure 3.5 represents the illustration of the heat transfer in the cooling block.

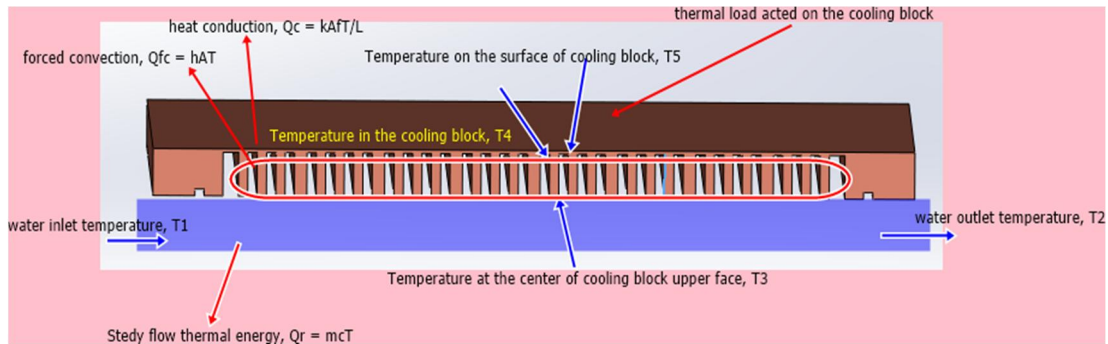


Figure 3.5: Illustration of the heat transfer in the cooling block

Assume that in ideal case and no heat lost to the surrounding, so the equilibrium state of heat transfer can be assume to be:

$$\dot{Q}_{in} = \dot{Q}_r = \dot{Q}_{fc} = \dot{Q}_c \quad (3.11)$$

Where

\dot{Q}_{in} = Input Power of solar (Thermal load acted on the center of the cooling block)

\dot{Q}_r = steady flow thermal energy

\dot{Q}_{fc} = rate of heat transfer by forced convection in the cooling block

\dot{Q}_c = heat conduction of the cooling block base

For the equation of input power is the product of Direct Normal Irradiance (DNI) at the total reflective area of our CPV system. It is stated that the standard value for solar constant is 1367 W/m^2 (Sala et al. 2008). However, this standard value does not take into account the losses such as reflective losses, as well as weather, buildings, trees and so forth. A well-established approximation for solar irradiance incident on Earth's surface is 1000 W/m^2 . Yet, to get this amount of solar constant, the condition of weather is that, it is Sunny and clear days. A value of 750 W/m^2 is

much more realistic, given the data collected at San Diego State University Real-time Environmental Monitoring and Observation Technology. (Sala et al. 2008). For the solar irradiance can be direct, diffuse or reflected radiation. When solar radiation is travelling on a straight line down to the surface of the earth from the Sun, it is the direct solar radiation. The DNI in our equation is the maximum value of direct radiation received per unit area of the mirror that the CPV received when the CPV system's mirror is tilted to position that the Sun's rays are focussing them at a 90° angle. For this quantity is of specific attention to concentrate our CPV system. Take note that in this study we do not take into account of the efficiency loss of direct conversion from thermal energy to electrical energy for the power input.

The input power can be expressed as:

$$Q_{in} = DNI \times A_{CPV} \quad (3.12)$$

where

A_{CPV} = total reflective area of the CPV system

The equation of total reflective area of the CPV system is expressed as:

$$A_{CPV} = L_m \times W_m \times 96 \quad (3.13)$$

where

L_m = Length of mirror

W_m = Width of the mirror

Next, we assume that the cooling fluid is an incompressible fluid has already achieved steady state condition, no change in latent energy and no thermal energy generation. (Incropera et al. 2007) The equation for steady flow thermal energy is:

$$Q_r = \dot{m}c(T_2 - T_1) \quad (3.14)$$

where

Q_r = steady flow thermal energy of the radiator

\dot{m} = mass flow rate

c = specific heat capacity of water

T_2 = water outlet temperature

T_1 = water inlet temperature

For the parameter for forced convection used in this study is same as the theoretical calculation of the automotive radiator. There is slight different which is, water is used in the cooling block's forced convection instead of air. Equation of rate of heat transfer via forced convection stated at Eq. 3.1 is applied in this section too. So, from Eq. (3.1), the cooling block's forced convection is:

$$Q_{fc} = hA_f(T_4 - T_3) \quad (3.15)$$

Where

h = heat transfer coefficient of forced convection between cooling block and water

A_f = total fin surface area involved in the heat transfer via forced conversion

T_4 = temperature of heat transfer area in the cooling block

T_3 = Temperature of the fluid

T_3 can be obtained by averaging T_1 and T_2 which is:

$$T_3 = (T_1 + T_2)/2 \quad (3.16)$$

It is assumed that the characteristic of water flow in the cooling block is related to that of a finite plate flow with a finite length (Chong and Tan 2012). So, the equation of Reynolds number for finite plate flow is represented in Eq. (3.17):

$$Re_L = \frac{\rho_w v_w L}{\mu_w} \quad (3.17)$$

where

L = length parallel to the water flow direction in cooling block

ρ_w = the water density

v_w = the water speed

μ_w = dynamic viscosity of water.

The equation for velocity of the water is determined as:

$$v_w = \dot{m} / \rho_w A_c \quad (3.18)$$

where

$$A_c = \text{cross sectional area in total of the fin for water flow} = 8.88 \times 10^{-4}$$

In the situation of forced convection between cooling block and water, the equation of Nusselt number is the Nusselt number of cooling block for the cooling block and water's in between forced convection is expressed as:

$$Nu_w = 0.453 Re_L^{1/2} Pr_w^{1/3} \quad (3.19)$$

Where

$$Pr_w = \text{Prandtl number reliant on the temperature of water.}$$

The equation of coefficient of heat transfer for forced convection between cooling block and water is:

$$h = \frac{Nu_w k_w}{L} \quad (3.20)$$

where

$$k_w = \text{thermal conductivity of water.}$$

As for the heat conduction, it is a steady state, one dimensional conduction. So the equation can be written as:

$$Q_c = \frac{k_c A_f}{L} (T_5 + T_4) \quad (3.21)$$

where

$$k_c = \text{Thermal conductivity of cooling block}$$

$$A_f = \text{total surface area of fin included in the transfer of heat by forced conversion}$$

L = Length of heat conduction (Different between inner layer of cooling block and outer layer of cooling block)

T_5 = cooling block's center temperature

The parameter of the cooling block such as the mass flow rate, water inlet temperature and solar constant are changed to determine the relationship of that parameter and the rate of heat rejection of the cooling block. The mass flow rate used is 0.43kg/s and 0.53kg/s, water inlet temperature will be vary from 32°C to 52 °C and the solar constant will be from 600W/m² to 1000 W/m². The results calculated will be shown in the results and discussion section and will be used to plot graph of heat rejection analysis. In addition, the results will also be used to compare with the simulated CFD results.

3.1.6 Software Simulation Studies for the Cooling Block Design

A series of software analysis such as Computational Fluid Dynamic (CFD) and Stress analysis will be performed for the cooling block. CFD analysis is to identify the effects of water inlet temperature, mass flow rate and thermal load acted on the cooling block, on the heat rejection performance of the cooling block. On another hand, the stress analysis is used to identify the performance of the cooling block under pressure and load.

During the CFD simulation, few input needed to be concern such as the material assignment, flow boundary condition, thermal load, tetrahedral meshing method and surface contact of the block object. There are three parts of the drawing is being assembly to run the CFD simulation which is the cooling block with straight slot fin, water that act as cooling medium and the cover plate. The material assignment is pure cooper for cooling block, water for water assembly and aluminium 6061 for cover plate. The assembly are meshed by using the tetrahedral meshing method with an overall of 48378 finite elements with the different size of spacing. There are 7749 elements included in cooling block, 3604 elements included in the cover plate and 6847 elements included in the water. Since the entire surface

contact between the component need to be well define, we perform surface to surface contact and found out that there are 277 faces in contact for total.

With this assumption, we can start the iteration of simulation. The equation used is the 3 Dimensional include the main equations of mass, momentum, energy, kinetic energy of turbulent and rate of dissipation for turbulent kinetic energy in the steady state. These equation are shown as below: (Versteeg and Malalasekera 1995)

Continuity equation:

$$\frac{\partial \rho \bar{u}_i}{\partial x_i} = 0 \quad (3.22)$$

Momentum equation:

$$\rho \bar{u}_j \frac{\partial \bar{u}_i}{\partial x_j} = -\frac{\partial \bar{p}}{\partial x_i} + \frac{\partial}{\partial x_j} \left[\mu_t \left(\frac{\partial \bar{u}_i}{\partial x_j} + \frac{\partial \bar{u}_j}{\partial x_i} \right) \right] \quad (3.23)$$

Energy equation:

$$\rho \bar{u}_j \frac{\partial \bar{T}}{\partial x_j} = \frac{\partial}{\partial x_j} \left[\left(\frac{\mu_l}{\sigma_l} + \frac{\mu_t}{\sigma_t} \right) \frac{\partial \bar{T}}{\partial x_j} \right] \quad (3.24)$$

Turbulent kinetic energy (k) equation:

$$\rho \bar{u}_j \frac{\partial k}{\partial x_j} = \frac{\partial}{\partial x_j} \left(\frac{\mu_t}{\sigma_k} \frac{\partial k}{\partial x_j} \right) + \mu_t \left(\frac{\partial \bar{u}_i}{\partial x_j} + \frac{\partial \bar{u}_j}{\partial x_i} \right) \frac{\partial \bar{u}_i}{\partial x_j} - k \epsilon \quad (3.25)$$

Turbulent kinetic energy dissipation (ϵ) equation:

$$\rho \bar{u}_j \frac{\partial \epsilon}{\partial x_j} = \frac{\partial}{\partial x_j} \left(\frac{\mu_t}{\sigma_\epsilon} \frac{\partial \epsilon}{\partial x_j} \right) + C_1 \mu_t \frac{\epsilon}{k} \left(\frac{\partial \bar{u}_i}{\partial x_j} + \frac{\partial \bar{u}_j}{\partial x_i} \right) \frac{\partial \bar{u}_i}{\partial x_j} - C_2 \rho \frac{\epsilon^2}{k} \quad (3.26)$$

The k-epsilon turbulent model is applied in the 3 Dimensional modelling of cooling block which is represented according to Eq. (3.11) to Eq. (3.15). It is given that the empirical constants in the equations Eq. (3.11) to Eq. (3.15) are shown as below:

$$C1 = 1.44$$

$$C2 = 1.92$$

$$C1 = 0.09$$

$$rk = 1.0$$

$$re = 1.3$$

Those are the constants for the Standard k-epsilon model. For complete analysis and these entire empirical constants's calculation, we can refer to the work of (Rodi, W. 1980). With every manipulation of the parameter mentioned, 60 computational simulations were executed for graph plotting. Thus, we can obtain the temperature at the center of cooling block. The obtained result will be shown in appendix C.

For the stress analysis, the input needs to be concern is the material assignment, pressure apply to the load, fixture and tetrahedral meshing method. Both the block and the cover is used for stress analysis and a standard of 100000N/m² of pressure which is the atmospheric pressure is apply to each component, and a gravitational force of 9.81m/s² is considered too. The main result need to be extracted from the stress analysis is the maximum displacement and the maximum stress. For the maximum displacement should not exceeded 1mm, so that the component will not deform; for the maximum stress cannot be more than the component yield strength so that the component will not have failure and broken in parts.

In addition, during the software analysis, the cooling block dimension is change accordingly to determine the effect of dimension on the results so that I can verify that the design for cooling block is usable. The detail analysis on both the simulation will be review in the results and discussion part. For the full software generated report of finalize parameter and dimension, please refer to appendix D.

3.2 Fabrication of the Hardware of the Concentrated Photovoltaic (CPV) Frame

Due the limitation of one person in fabricating such a huge frame (2.045m × 2.135m), I have been assigned to work out with my group mates to complete the CPV frame. For my role, I have fabricated different height of the aluminium bar for holding the

mirrors, generated the idea for the mirror tilting method and help out in the fabrication of the overall frame.

3.2.1 Process Planning of The Main Frame Parts Fabrication.

Basically, for the whole frame fabrication, the process is being summarized as below:

- ✓ Measure and cut all the component needed into different dimension
- ✓ Fabricate the L bar onto the different height of the mirror supporter aluminium square bars.
- ✓ Fabricate the mirror supporter aluminum square bars onto another cutting angle aluminium square bar to be placed onto the main frame.
- ✓ Fabricate the triangular aluminum plates onto the mirror supporter aluminium square bars.
- ✓ Fabricate the overall frame, uses customized triangular aluminium plate to place at each of the corner of the main frame, to connect the main frame and the “X” bar in the middle for supporting purpose.
- ✓ With that ready frame, fabricate the main frame support square aluminium bar with cutting angle onto the main frame.
- ✓ Fabricate the target holder and the cooling block holder.
- ✓ Place the mirror onto the main frame and perform mirror tilting.

Below are the descriptions of the certain processes on how the main frame is done:

Process	Description
Cutting	All the aluminium bars are being cut using a semi-automatic gas cutting machine.
Filling and Finishing	Used to remove excessive material on the aluminium bars and aluminium plates.
Hammering	Used to make center mark for hole drilling accuracy, with the help of center punch.
Clamping	Used to make sure the component did not slip away during the drilling process.

Drilling	Used to drill thousands of holes on the aluminium bars and aluminium plates for riveting purpose.
Riveting	Used to join plates and aluminium bars, and also connect all the aluminium bars

3.2.2 Fabrication Process of the Mirror Supporter for the Concentrated Photovoltaic (CPV) Frame

Firstly, according to the software design, there should 22 group of different height of aluminium bar need to be cut. The dimension of the aluminium square bar chosen is with the diameter of 25.4mm and 1.19mm thickness as shown in figure below, and with the weight of 0.315kg/m. This dimension is being referred to the Company of Kamco Aluminium SDN BHD's aluminium square bar datasheet. This datasheet can be seen in appendix E.

The measuring tape is used as a tool to measure the length of the bar; horizontal band saw is used to cut the bar into different length. Due to the accuracy of the Solidworks software, the measurement of the bar is in 3 decimal places, in mm. In our workshop, we do not have such long length equipment to measure up to this precision, so we round the number off to whole number or with 0.5mm added. Table 3.1 below shows the different measurement of height of the aluminium bar.

Table 3.4: Rounded Off Measurement for the Square Aluminium Bar

No	Original Measurement (mm)	Rounded Off Measurement (mm)	Total Length (x4 of measurement)
1	31.664	32.0	128
2	41.612	42.0	168
3	46.436	46.5	186
4	56.384	56.5	226
5	58.796	59.0	236
6	78.693	79.0	316
7	83.517	84.0	336
8	85.928	86.0	344
9	93.465	93.5	374
10	98.289	98.5	394
11	120.597	121.0	484

12	123.009	123.5	494
13	128.124	128.5	514
14	137.781	138.0	552
15	142.906	143.0	572
16	150.142	150.5	602
17	160.090	160.5	642
18	170.039	170.5	682
19	174.862	175.0	702
20	209.531	210.0	840
21	211.943	212.0	848
22	261.384	261.5	1046
sum	2655.192	2671.0	10686

According to table 3.1, 10686mm of the bar is needed. So, we have bought 2 6m (standard length) long bar for the fabrication. In addition, the total percentage different of the original value and the rounded off value is calculated as shown:

Percentage differennt

$$= \frac{\text{Rounded off value} - \text{original value}}{\text{Rounded off value}} \times 100\% = \frac{2671.0 - 2655.192}{2655.192} \times 100\% = 0.594\%$$

Since the percentage different is so small, the rounded off value is acceptable in our case. Moreover, this extra measurement of length can act as the tolerance for the cutting purpose to avoid overcut of material.

In the process of cutting the aluminum square bar, a standard 6m long bar was cut into different length. In order to make sure that there is no wastage of material, the longest total length of the bar need were being cut off first, then followed by the second longest bar and so on. Then those bars with total length were cut into 4 smaller bars with same measurement accordingly. After that, for all the bars that were being cut off, each end side of the bas was being finish properly by using the wood file tool to ensure that when it is fix to frame's bar, there will not be any excessive material that stuck between the bars.

Next the 3mm thick aluminium plates were being fabricated. There are total of 96 triangular plate with the measurement of 130mm × 130mm were being cut. Since the triangular plate is half of a square shape, I have cut out 48 pieces of square

plate with the measurement of 130mm × 130mm and with the square plates, I did a symmetry marking to the plate and cut each of it into 2 triangle shape with the help of the shear cutter machine.

There are three holes needed to be drilled on each of the triangular plate for mirror tilting purpose. The distance needed is 25mm away from each end of the plate. With the help of the vertical ruler machine, the length being mark is straight and precise. Moreover, center marking need to be done to make sure that during the drilling session, the hole being drilled will be accurate. The center marking is done by hammering the plate using center punch. Figure 3.6 show the marking of the triangular plate.

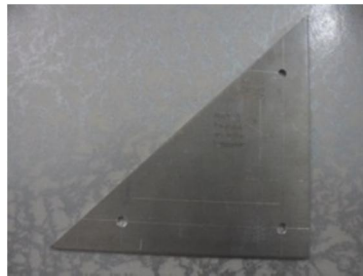


Figure 3.6: The triangular plate with marking and with hole drilled.

The drill hole is M4 size. The maximum tilting angle calculated by my group mate was 16°. I have done the calculation to make sure that the drilled hole is big enough to tilt a maximum angle of 20° (I added 4° as tolerance and so the maximum tilting angle is 20°).

Let the maximum tilting angle = 20°

$$\tan \theta = \frac{\textit{opposite}}{\textit{adjacent}}$$

$$\tan 20^\circ = \frac{\textit{opposite}}{\textit{adjacent}}$$

$$0.3640 = \frac{\textit{opposite}}{\textit{adjacent}}$$

So, the division result should be 0.3640 or more in order to get a tilting angle of 20. For the result calculated is 0.3839. So, with this M4 hole size, the maximum tilting

angle can go up to 21 degree, which is more than enough. The total hole being drilled for the plate is 288 holes. Each of the holes is being finished properly.

The L bar with the size of 25.4mm length and 2mm thickness is being cut to be used for support between the aluminium bar and the triangular plate; and between the aluminium bar and the bar for the main frame. Figure 3.7 show the connected triangular plate with the square aluminium bar that needed the L bar support.

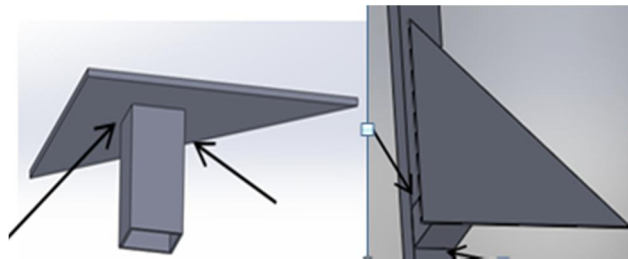


Figure 3.7: Connection that needed the L bar support

This means that each aluminium bar will need 4 L bar for the support of both side of the plate and on the main frame. For there are 88 aluminium bars, the total needed L bar will be $88 \times 4 = 352$ pieces. Each L bar is drilled for 4 holes and rivet with the M4 size rivet to make sure that the connected bar and frame is having strong support. The total hole being drilled is $352 \text{ pieces of L bar} \times 4 \text{ holes} = 1408$ holes. Each of the holes being drilled is being finished properly to ensure that the rivet is being place properly between the gaps. Figure 3.8 show an example of aluminium bar with the four L bar connected to it.



Figure 3.8: Example of aluminium bar with the four L bar connected to it.

There are total of sixteen main frames square bar, with four at each side as refer to figure 3.9. According to figure 3.9, the main frame is made up of a rectangular shape. So, each of the opposite is having the identical square bar for the main frame. Each of the bars will have a cutting angle on each side so that it can be connected to another big bar of the main frame.

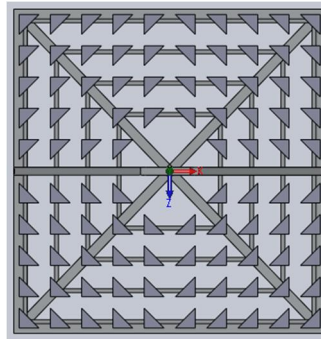


Figure 3.9: Main frame picture showing that each side contain 4 cutting angle square bars for mirror support.

Table 3.5 shows the different measurement of length of the main frame support for square aluminium bar.

Table 3.5: Rounded Off Measurement for the Main Frame Support Square Aluminium Bar

No	Type of square bar (D × T) (mm)	Original Measurement (mm)	Actual Measurement (mm)	Total Length (actual measurement x 2)	Original Cutting angle (°)	Actual Cutting angle (°)
1	1.19 × 25.4	627.50	627.5	1255	43.83	43.85
2	1.19 × 25.4	1054.60	1055.0	2110	43.83	43.85
3	1.57 × 25.4	1481.70	1482.0	2964	43.83	43.85
4	3.18 × 25.4	1906.31	1906.5	3813	43.83	43.85
5	1.19 × 25.4	651.530	652.0	1304	46.17	46.20
6	1.19 × 25.4	1045.11	1045.5	2091	46.17	46.20
7	1.57 × 25.4	1438.70	1439.0	2878	46.17	46.20
8	3.18 × 25.4	1829.98	1830.0	3660	46.17	46.20
sum		10035.4	10037.5	20075	360	360.2

According to table 3.2, 20075mm of the bar is needed. So, we have bought four 6m (standard length) long bar for the fabrication with two of it is with the dimension of 1.19×25.4 , one with 1.57×25.4 and one with 3.18×25.4 . Furthermore, the total percentage different of the original aluminium square bar and the rounded off value is calculated as below and since both the percentage different is so small, the rounded off value is acceptable in our case.

Percentage different for the length measurement

$$= \frac{\text{Rounded off value} - \text{original value}}{\text{Rounded off value}} \times 100\% = \frac{10037.5 - 10035.4}{10035.4} \times 100\% = 0.021\%$$

Percentage different for the cutting angle measurement

$$= \frac{\text{Rounded off value} - \text{original value}}{\text{Rounded off value}} \times 100\% = \frac{360.2 - 360}{360} \times 100\% = 0.056\%$$

Just like the process of cutting the aluminum square bar, a standard 6m long bar was cut into different length. Then those bars with total length were cut into 2 smaller bars with same measurement accordingly. After the aluminum bar is cut according to sizes, angle marking is made on each side of the bar. The horizontal band saw is then used to cut the angle required, according to the mechanical setting that we have made. Finally, for all the bars that were being cut off, each end side of the bar was being finish properly by using the wood file tool. The example of the frame bar support for the mirror with cutting angle is shown at figure 3.10.

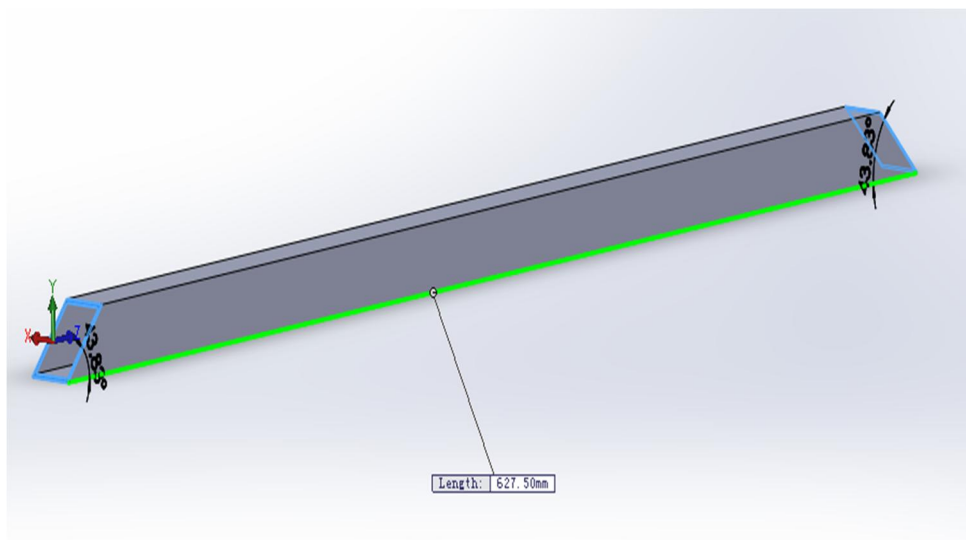


Figure 3.10: Square aluminium bar with angle cutting.

For the overall frame fabrication, customized triangular aluminium plates are used to place at each of the corner of the main frame, to connect the main frame and the “X” bar in the middle for supporting purpose. The M5 rivets are used in the riveting process, this rivet is bigger than the previous rivets used and have a better joint strength. With that ready frame, all the other fabricated main frame support square aluminium bar with angle cutting is then fabricated on the main frame too. Still, we are using customized triangular aluminium square plate to connect all the bars to the main frame.

3.3 Design and Fabrication of the Mirror Tilting System

The reflective material used in our project is flat mirrors. Each mirror has a 200mm × 200mm dimension and 3mm thickness. The total number of the mirror is 96 pieces, and the mirror is arrange in the form of ten columns times ten columns on the main frame as can be refer to figure 3.10.

By referring to the old main frame design, the component used by our senior for the mirror tilting system is pvc piping filled with silicon surrounded the screw fixed on the back part of the mirror. A nut is turned to the end of the screw. A compression spring is attached to the screw and a ring nut is used to control the compression of the spring. Figure 3.11 shows the example of the old mirror tilting system.



Figure 3.11: Old mirror tilting syst

The disadvantage of the old mirror tilting system is that the silicone gel that contain the elasticity characteristic tense to be soften under high temperature and thus affecting the tilting angle of the mirror. In addition, the old tilting material easily disconnect from the back of the mirror due to high heat too. Hence, new mirror tilting system is designed to overcome these problems.

3.3.1 Material Used for the Mirror Tilting Purpose

Through discussion and market research, we have found the glass holder to act as the main component for mirror tilting purpose. Figure 3.12 shows main component of the mirror tilting system.



Figure 3.12: Main component of the mirror tilting system

A M4 screw is place into the hole of the glass holder, then a spring is attached to the screw and a ring nut or hexagon nut is used to control the compression of the spring. Round head screw is used in this case because when it is place into the glass holder, it can be adjusted with a higher degree of freedom. The compression springs that were being custom made is having the spring constant value of 0.95N/mm. Through the help of online spring compression calculation, this spring can withstand a force of 25 (Refer to appendix F). For the nut, ring type nut is used because it is easily to be adjusted compared to the hexagon nut. Yet, hexagon nut still will be used in some of the mirror tilting system due to the limited space of placing the ring nut in between the space main frame and triangular plate. We have planned on using the epoxy adhesive for bonding between the component and the back part of the mirror.

The epoxy has the super-strong gap filling function. To test the usability of the design, few glass holders was bought and tested on an old mirror. We had done few testing on the bonding way. Figure 3.13 below show the testing of the new mirror tilting system.

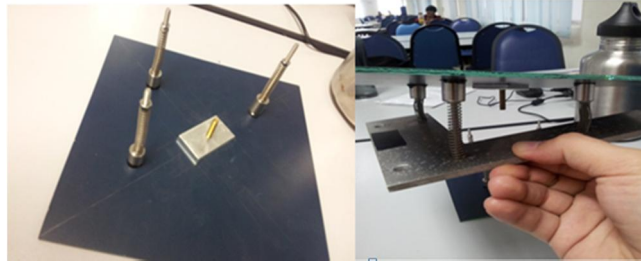


Figure 3.13: Testing on the main component of the mirror tilting system

We have tried to apply silicon glue into the hole of the hollow circle aluminium component; fully fill the hole to increase the surface contact between the component and the mirror and also for ease of easy mirror tilting purpose. The result was bad as in the component is easily being separated from the mirror after a small force was applied to it. This is because when we do full filling for the hole the silicon glue causes the flat surface to be non-even because of the bad filling method as shown in figure. Figure 3.14 shows the comparison between filled silicon component and non-filled silicon component. Furthermore, some of the silicon does not stick with the epoxy material.



Figure 3.14: fully filled silicon with bad finishing causes uneven surface

Finally, for the last test, we have removed part of the silicon filling. So for this time, the component is being filled with 4/5 of silicon glue. This method is used because when we compress the component onto the back part of the mirror with applied epoxy, the epoxy will be filling the remaining 1/5 of the empty hole and with this, the surface area of contact is being increased. As for the result, the tested bonding strength is very high and. As for short, this method is being used in the mirror tilting system. In, figure 3.15 show the 3D outlook of the structure of the mirror tilting system.

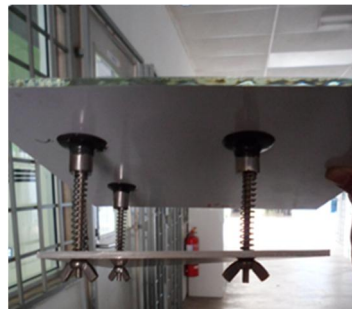


Figure 3.15: 3D outlook of the structure of the mirror tilting system.

With the design concept proposed, we can set the compression of each mirror along the row and column directions. A standard of three contact points of screw–spring assemblies are present in the mirror tilting system. The mirror can be tilted freely to concentrated Sunlight onto the target by turning or releasing the ring nut of the flexible mirror tilting system by means of manual work.

There are other condition need to be considered when creating the bonding of the component and the mirror which is the mixing ratio of the epoxy and way of placing the component on the mirror. The mixing ratio of the black and white epoxy must be 1:1. There were several time that the bonding failed is due to the mixing ratio of the epoxy. If we mix the black paste too much, the epoxy is difficult to be harden and thus causing the bonding to be soft and easily separated from the mirror. On another way round, if we mix the white paste too much, it is easily being hardened but there is no much of holding strength for bonding purpose and this cause the component to be easily separated from the mirror too. As for the method of placing the component on the mirror, we should apply epoxy on the aluminium

component first, then place in contact to the mirror and component is being turned forth and back to make sure that the epoxy fill the hole and have better bonding strength.

After then, the mirrors are then being place onto the main frame. Figure 3.16 shows the all the 96 mirror was being place onto the main frame. Over the past few weeks, the mirror tilting system's bonding has proved to be strong and able to be used for long period tilting operation.



Figure 3.16: Mirror being placed onto the main frame.

3.4 Setup of Experiment

As mentioned in section 3.2 the non-imaging planar concentrator fabrication is done by us. With this prototype, we can perform real life testing to determine the solar flux distribution and the performance of the cooling block. In addition, on-site testing with added on solar cell is also carried out to determine how the heat rejection or the system affects the conversion of efficiency of the CPV module. With those results collected, the results then can be used to compare with the theoretical study results of the cooling system.

3.4.1 Non Imaging Dish Concentrator

Before doing the experiment, we have use the software program to simulate the solar flux distribution according to the design of the NIDC prototype via the ray tracing method (Chong et al. 2010). The NIDC prototype contains 96 flat mirrors with a focal distance of 1.7m. Figure 3.17 and 3.18 below shows the simulated result in 3 Dimensional and 2 Dimensional graphs plotting consequently. The solar flux profile contains flat top area in the central part and has a solar concentration ratio at maximum value which is 84 Suns. It is the uniform illumination area. The computer-generated result shows that $18\text{ cm} \times 18\text{ cm}$ in the uniform illumination area.

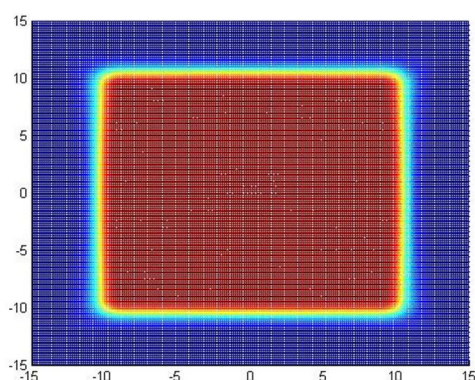


Figure 3.17: Results of solar flux distribution for NIDC prototype shown in 2-D form. The total flux distribution area is $18\text{cm} \times 18\text{cm}$

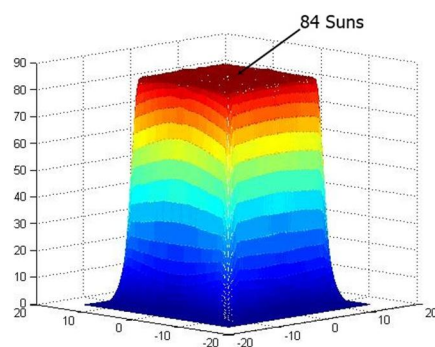


Figure 3.18: Results of solar flux distribution for NIDC prototype shown in 3-D form. The total number of Suns is 84.

To verify the simulation result, experiment has been carried out. The experiment starts by concentrating Sunlight onto the copper cooling block with focal length of 1.7m. The prototype is capable to produce a good uniformity of solar illumination with the 96 flat type mirrors and a total reflective area of 3.82m^2 is form. The Sun tracking system is done my group mates. By using the Microsoft Visual Basic.net that was established, a Windows-based program implemented to control the Sun-tracking mechanism in relative to the day number of the year, the local time, time zone, latitude and longitude of the CPV frame installation. Figure 3.19 shows the prototype of the NIDC located at latitude of 32N and longitude of 107.7E in the campus.



Figure 3.19: The prototype of the NIDC positioned at latitude of 32N and longitude of 107.7E in the campus.

We have exposed a black colour type of sand paper to the concentrated Sunlight for a few second to determine the distribution of solar flux at the center of cooling block. We have performed the experiment for 3 times to get the desired result. Figure 3.20 show the situation where all the group member involve in the experiment. And figure 3.21 shows the experiment situation where the sand paper is being burned.



Figure 3.20: Situation where all the group member performing the NIDC experiment



Figure 3.21: Situation the Sunlight focuses on the cooling block causes the sand paper to be burned

The results of the experiment will be discussed in the chapter 4.

3.4.2 Experimental setup To Test the Cooling System

The setup of the cooling system is as shown in figure 3.22, with one side of the pipe water connected to the radiator and another side connected to the water reservoir that store cooled water. Then the three other pipes are used to connect between water pump and the water reservoir, between cooling block and water pump and lastly between radiator and cooling block.

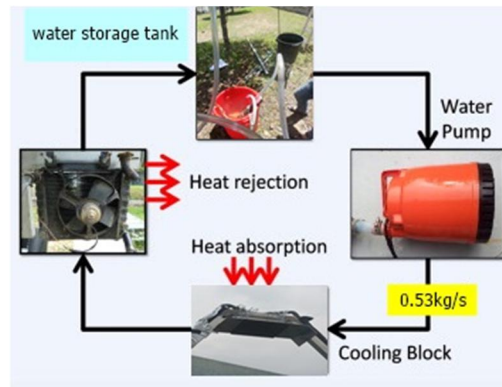


Figure 3.22: The schematic diagram shows the entire component for the automotive radiator cooling system.

The water pump is used to pump the water to the cooling block with the mass flow rate of 0.53kg/s (determine by on-site experiment) and it also make sure that a there is a constant water speed inside the automotive radiator cooling system. Also, the radiator's fan speed is adjusted to be 3m/s to ensure better heat rejection performance of the system. The storage tank is the beginning and finish point of the circulation of water for the cooling system. It is also used to store the submersible water pump for the water pump need to be in the water all the time to avoid pump failure.

In order to determine the mass flow rate of the water accurately, we have construct a simple on-site experiment to measure the mass flow rate of the water. Figure 3.23 shows the on-site experiment performed to measure the water mass flow rate.



Figure 3.23: The on-site experiment performed to measure the water mass flow rate.

The on-site experiment procedure to control the mass flow rate is:

1. A submersible water pump with a rated power of 100W has been ready and run the cooling cycle.
2. The pump control valve is turned to desired flow rate.
3. An empty container is ready to be used to contain the outlet water by the cooling system in a count of 10 second.
4. A stop watch is prepared to count the time for water filling of the container.
5. After 10second, the outlet water pipe is removed from the container and the container is being weighed with an electronic device for the mass of the water.
6. If the mass being weighed is not the desired mass, repeat step 2 onwards.
7. The experiment is repeated for 10 times to get the mass flow rate, and the result of the mass being determine is tabulated in table 3.6.

Table 3.6: Mass result of number of experiment

No	Mass (kg)
1	5.32
2	5.28
3	5.30
4	5.34
5	5.30
6	5.33
7	5.33
8	5.27
9	5.35
10	5.30
Average mass	5.31

For the mass flow rate is in ratio of mass to second (kg/s). So the average mass is divided by the 10 second and with this the mass flow rate got in the experiment is 0.53 kg/s. It is assumed that the fluid inside the cooling block is having incompressible flow at the steady-state.

By referring to figure 3.19 too, with the water pump being switch on, the water from the storage tank is then being channelled to the copper cooling block positioned at the aim of the solar concentrator with a distance of 2.2 m relative to the storage tank. As water passes through the cooling block, it absorbs heat from the concentrated Sun, cooling the block. At the same time, the water temperature will increase in the heat absorption process. After the water leaves the cooling block, it passes through the parallel aluminium ducts in the automotive radiator evenly and heat rejection occurs at this process. The fan of the radiator performs heat rejection by forced convection and cool down the water. Then, water is passes back to the water reservoir for a new cycle to be started again. Table 3.7 is the summary of the specification in whole experimental setup.

Table 3.7: Summary of the specification in whole experimental setup.

Radiator	
Radiator capacity	1.5-liter
Total surface area	3.8 m ²
Heat transfer area covered by fan	2.2 m ²
Cross section area of radiator ducts, A_c	$6.914 \times 10^{-5} \text{m}^2$
Perimeter of radiator ducts, P	0.0773 m
Air flow boundary diameter (Fan's diameter)	0.28 m
Wind speed created by fan, v_a	3m/s
Reynolds number of air across radiator, Re_D	702.62
Nusselt number of air, Nu_a	12
Heat transfer coefficient of air, h	83 W/ m ² K
Range of temperature for radiator surface, T_s	From 32 °C to 52 °C
Conductivity of radiator fin	387 W /m K
Conductivity of radiator ducts	170W / m K
Rated power of fan	50.6 W
Cooling block	
Dimension	0.245m×0.245m×0.016m
Number of slot-fins	32
Total surface area of each slot-fin	0.006272 m ²
Total heat transfer surface area	0.20 m ²

Conductivity	401 W/m K
Water mass flow rate	0.583 kg/s
Reynolds number of water, Re_L	152110
Nusselt number of water, Nu_w	307
Heat transfer coefficient of water, h	968.23 W/ m ² K
Non-imaging planar concentrator	
Total reflective area, A_r	3.82m ²
Focal distance	1.70 m
Latitude	3.2N
Longitude	107.7E
Rated power of water pump	100 W

In addition, a single solar cell (Emcore 2010) that is being commercialized will be mounted on the cooling block. The purpose of the solar cell is for us to know the effect of the heat rejection of the cooling system to the efficiency of conversion for the CPV module. Figure below show the cell mounted to cooling block in the experiment. The datasheet of the solar cell will be provided at appendix A.



Figure 3.24: Commercialized solar cell mounted to the cooling block

During the experiment, there are few important parameter need to be measured from time to time such as the DNI, ambient temperature, humidity of the air, inlet and outlet water temperature, cooling block's center temperature, open

circuit voltage and short circuit current of the solar cell. The experiment has been conducted for 4.5 hours from morning to later afternoon.

3.4.3 Experimental Analysis on the Heat Rejection Rate and Efficiency of Conversion of CPV module

In section 3.4, the setup of the experiment is being explained in detailed. There are some calculation needed to be executed to determine the heat rejection rate of the radiator, power input of the solar, efficiency of the electrical conversion of the CPV module and the cooling block's temperature.

For Eq. (3.14) can be applied to calculate the rate of heat rejection for the radiator. For the power input of the solar, Eq. (3.12) can be applied but with the consideration for the direct conversion efficiency of the solar energy to thermal energy with the value of 0.8 (Chong and Tan 2012), which is the loss of reflection for the mirror. So, Eq. (3.12) can be rewrite as:

$$\mathbf{P}_{in} = \eta \times \text{DNI} \times A_r \quad (3.27)$$

Where

η = direct conversion efficiency of the solar energy to thermal energy

For the efficiency of the electrical conversion of the CPV module can be determined by using the Eq. (3.28)

$$\eta_{CPV} = (\mathbf{P}_{CPV, out} / \mathbf{P}_{CPV, in}) \times 100\% \quad (3.28)$$

where

$\mathbf{P}_{CPV, in}$ = Power input of solar that the CPV module has received

$\mathbf{P}_{CPV, out}$ = Generation of electrical power output by the CPV module

For the Power input of solar that the CPV module has received and the generation of electrical power output by the CPV module can be enumerated using the following equations:

$$P_{CPV,in} = \eta \times DNI \times A_r \times (A_{CPV}/A_{image}) \quad (3.29)$$

where

A_{CPV} = CPV's cell sum of active area = 0.0001m²

A_{image} = Sum of image area of the concentrated Sunlight directed on the cooling block = 0.04m²

$$P_{CPV,out} = V_{oc} \times I_{sc} \times \text{CPV module's fill factor} \quad (3.30)$$

where

V_{oc} = CPV module's open circuit voltage being measured

I_{sc} = CPV module's short circuit current being measured

CPV module's fill factor = 0.87 (Emcore 2010)

For the CPV cell's temperature can be enumerated by using the equation Eq. (3.31):

$$T_{CPV} = P_{CPV,in} \times R_{tot} \times (1/A_{CPV}) \times (1 - \eta_{CPV}) + T_{CB} \quad (3.31)$$

T_{CB} = is the temperature of cooling block

R_{tot} = total thermal resistance from cooling block to CPV cell

The total thermal resistance from cooling block to CPV cell consist of the following materials: copper (cooling block), arctic silver thermal adhesive, copper layer in direct bond copper (DBC) substrate, alumina layer in DBC substrate, copper layer in DBC substrate, solder material and CPV cell that can be calculated as:

$$R_{CPV} = R_{solder} + R_{DBC-copper} + R_{DBC-alumina} + R_{arctic\ silver} + R_{copper} \quad (3.32)$$

where

$$R_{CPV} = l_{CPV} / k_{CPV}$$

$$R_{solder} = l_{solder} / k_{solder}$$

$$R_{DBC-copper} = l_{DBC-copper} / k_{DBC-copper}$$

$$R_{DBC-alumina} = l_{DBC-alumina} / k_{DBC-alumina}$$

$$R_{arcticsilver} = l_{arcticsilver} / k_{arcticsilver}$$

$$R_{copper} = l_{copper} / k_{copper}$$

where

l_{CPV} , l_{solder} , $l_{DBC-copper}$, $l_{DBC-alumina}$, $l_{arctic silver}$, and l_{copper} = different material's thicknesses

Table 3.8 shows the thermal conductivity value for different material and the different material's thickness. (Luque and Andreev (2007)).

Table 3.8: Thermal conductivity value for different material and the different material's thickness

Material	Thermal conductivity (W/m K)	Thickness (mm)
CPV	55	0.12
Solder	29	0.15
DBC-copper	400	0.3
DBC-alumina	24	0.635
arctic silver	7.5	0.1
copper	400	5

CHAPTER 4

RESULTS AND DISCUSSIONS

4.1 Results for The Cooling Block Design, Analysis and Fabrication

4.1.1 Stress Analysis

The Solidworks software has been used in technical drawing and the stress simulation analysis. Figures below show the final drawing result of the cooling block by using the Solidworks software:

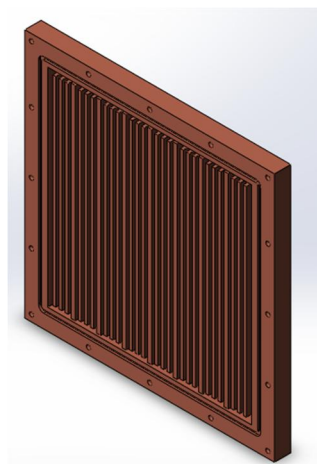


Figure 4.1: Cooling block drawn by using Solidworks software with the dimension of 245mm × 245mm × 16mm

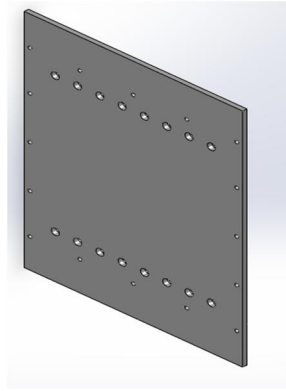


Figure 4.2: Aluminium cover drawn by using Solidworks software with the dimension of 245mm × 315mm × 5mm

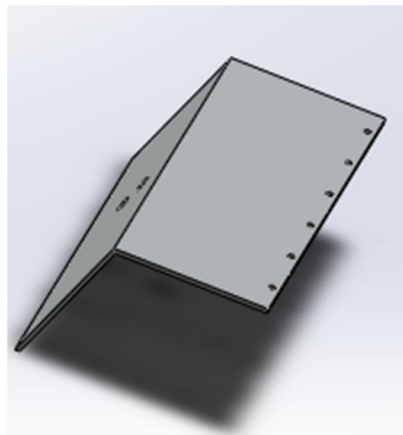


Figure 4.3: Angle bar for cooling block mounting drawn by using Solidworks software with the thickness of 3mm and angle of 113 degree

Before deciding the final dimension, few changes has been made to the drawing to determine the best dimension for the cooling block. Since the length and width of the cooling block is fixed with a fixed extrusion of fin with 10mm height. I have tried to change the height of it to determine how the height affects the stress and deflection of the block. Figure 4.4 to 4.6 shows the different of maximum stress of the block, figure 4.7 to 4.9 shows the different of maximum displacement of the block.

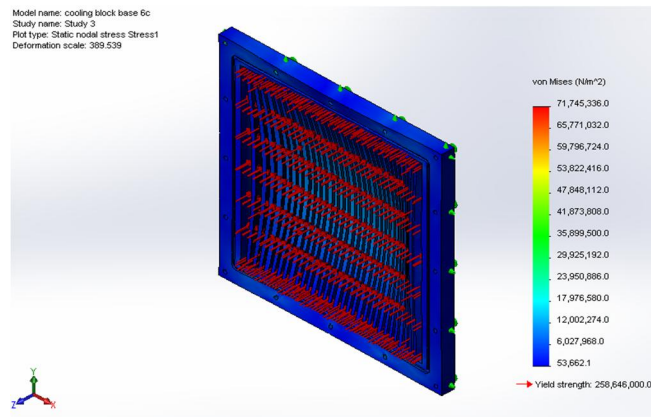


Figure 4.4: Maximum stress analysis result for the 14mm height cooling block

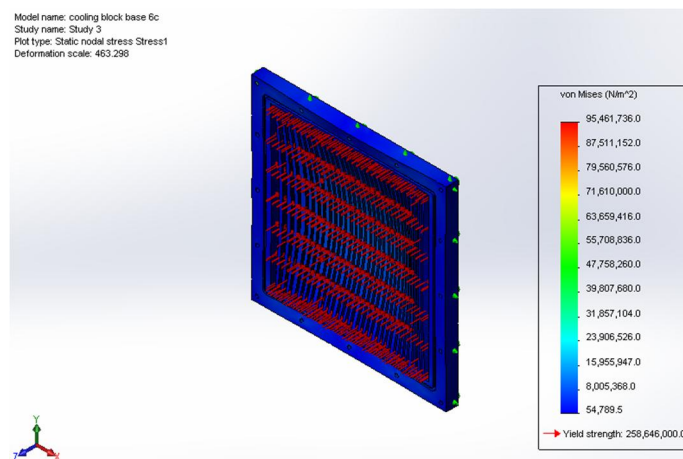


Figure 4.5: Maximum stress analysis result for the 15mm height cooling block

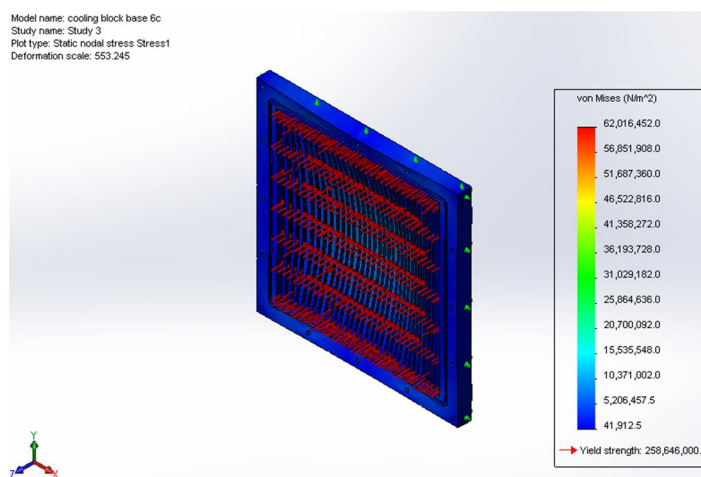


Figure 4.6: Maximum stress analysis result for the 16mm height cooling block

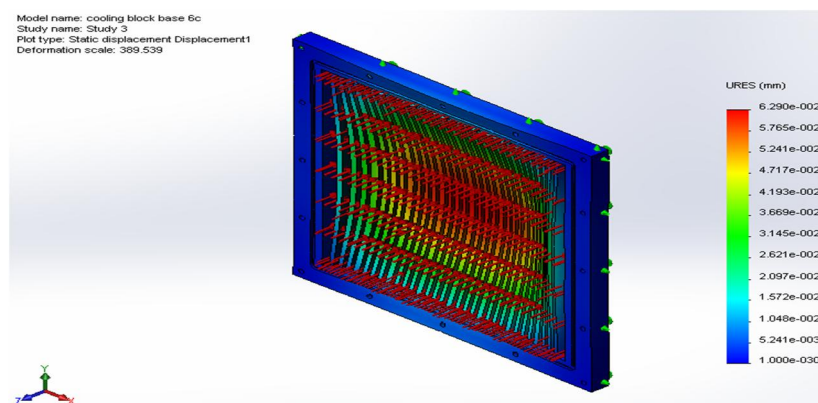


Figure 4.7: Maximum displacement analysis result for the 14mm height cooling block

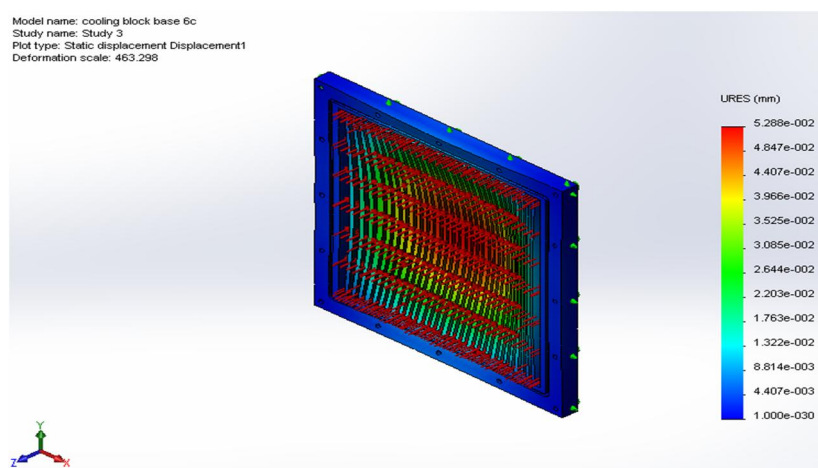


Figure 4.8: Maximum displacement analysis result for the 15mm height cooling block

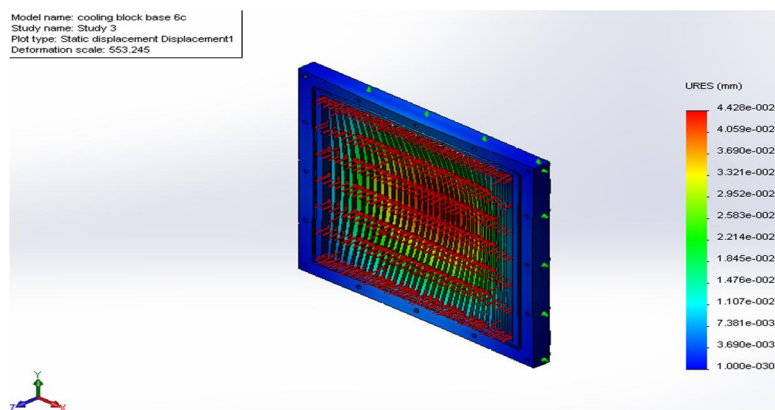


Figure 4.9: Maximum displacement analysis result for the 16mm height cooling block

From the figures of maximum stress, the yield strength of the cooling block is 258,646,000 N/m². It is noticeable that the 16mm height have the least maximum stress which is 62,016,452 N/m². Next, for the maximum displacement, the 16mm cooling block is having the least displacement which is 4.428×10^{-2} mm. The displacement of the cooling block should be as less as possible so that deflection does not occur for the cooling block. With this results, it can be say that the increase in the height of the block reduce the chance for the block to be deformed and have failure. Since 16mm height is more than enough to resists the deformation, hence this dimension is acceptable.

In addition, for the cover, its side is extended to 315mm for mounting of wing plate at the target. With the dimension of 245mm × 315mm × 5mm, the simulation results of stress and displacement is shown at figure 4.10 and 4.11.

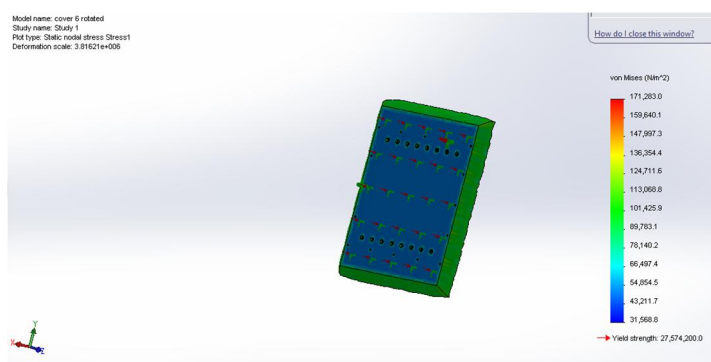


Figure 4.10: Maximum stress analysis result for the cooling block cover

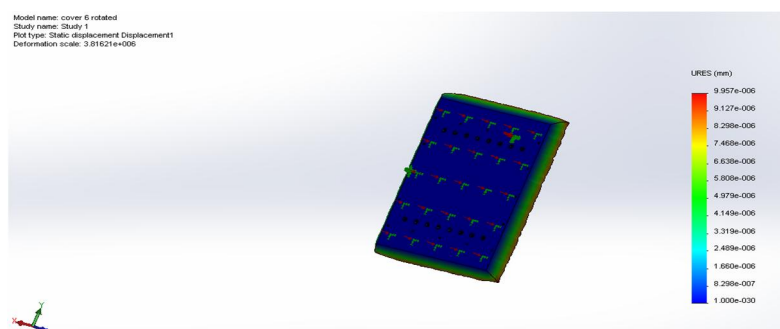


Figure 4.11: Maximum displacement analysis result for the cooling block cover

From both the figure 4.10 and 4.11, the maximum stress of the plate is 171,283N/m² which does not exceeded the yield strength of 27,574, 200 N/m² and the maximum displacement of the cover plate is 9.957×10^{-6} mm. This excellent simulation result concludes that the plate will not be easily deformed, since the cover plate is mounted to the cooling block base.

Lastly, the stress simulation for the angle bar for plate mounting is being analysed. Figure 4.12 and 4.13 show the result of stress and displacement analysis.

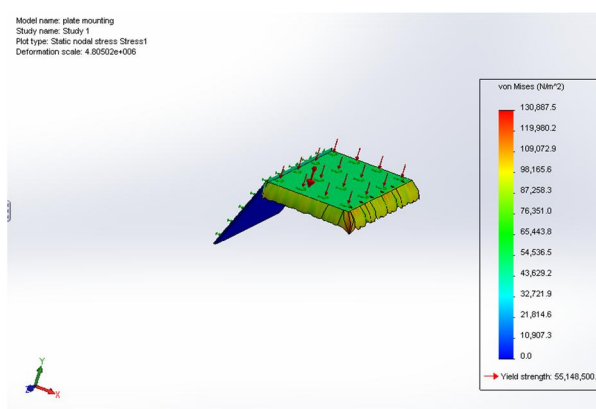


Figure 4.12: Maximum stress analysis result for the angle bar of the cooling block

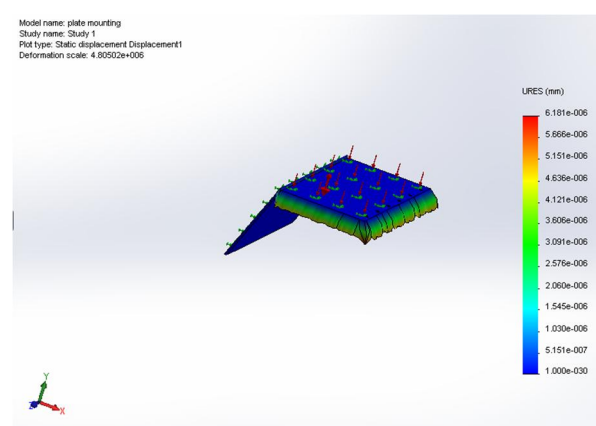


Figure 4.13: Maximum displacement analysis result for the angle bar of the cooling block

From both the figure 4.12 and 4.13, the maximum stress of the angle bar is $130,887\text{N/m}^2$ which does not exceeded the yield strength of $55,148,500\text{ N/m}^2$ and the maximum displacement of the angle bar is $6.181 \times 10^{-6}\text{mm}$. This simulation result concludes that the bar will not be easily deformed too.

4.1.2 Result of Calculated Fin Efficiency

For the final dimension of cooling block is decided, the fin efficiency is then being calculated by using Eq. (3.7) to Eq. (3.7). Figure 4.14 below shows the guide to determine the length, L and width, w of the fin.

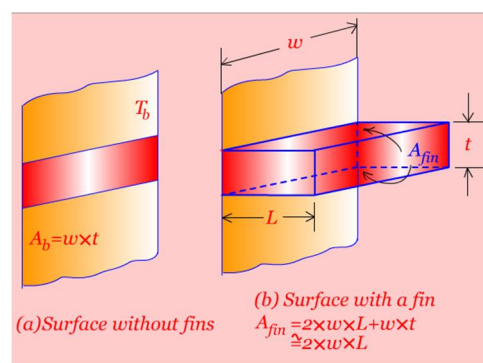


Figure 4.14: Guide to assign fin length and fin height

For the fin length of my design is 0.013m , width is 0.196m and thickness is 0.003mm . With the calculated convection coefficient of the fin is $h = 968.23\text{W/m}^2\text{ K}$ and the thermal conductivity of copper is $401\text{ W/m}^2\text{ K}$ the value of mL_c calculated is 0.02857 , and the fin efficiency is 94.92% . This means that if all the fin were at base temperature, the actual rate of heat transfer from the fin is 94.92% of the ideal rate of heat transfer from the fin. With this high fin efficiency, the cooling block can perform heat transfer with high efficiency.

It is stated that a significant attention in the design of finned surfaces is the choice of proper fin length, L (Sheshu, 2011). Basically, the longer the fin length, heat transfer area will be larger and there is higher heat transfer rate from the fin.

Even though increasing length resulted in increasing rate of heat transfer but it will decrease the fin efficiency due to the decrement of fin temperature with length.

Normally the efficiency of most fins used in practice is above 90% and the if the efficiency to drop below 90% cause by the fin length, it will not be acceptable and cannot be acceptable in economical means. This scenario must be prevented. In addition, the larger the fin, the bigger the mass of it and it will cause load to the cooling block, and also causes the larger friction of fluid. Thus, increase in length of the fin exceeded a definite value can't be acceptable except for the additional paybacks compensate the additional mass to the CPV system and the costing. In short, the fin dimension proposed is acceptable, with the high fin efficiency of 94.92% which is above the percentage value stated (90%) by the design industry.

4.1.3 Computational Fluid Dynamic (CFD) Analysis Results

As mentioned in the methodology, the parameter for simulation is determined to run the CFD analysis. Table below shows the important parameter used to carry out the CFD analysis.

Table 4.1: Parameter Used To Carry Out the CFD Analysis

Parameter	Value
Flow boundary condition	0.43kg/s or 0.53kg/s for inlet and outlet, assume ideal flow rate
Ambient temperature	32 degree, 42 degree and 52 degree
Thermal load	2304W, 2688W, 3072Watt, 3456W, 3840W
tetrahedral meshing	123203 finite elements with the 5mm spacing in size.
surface contact	277 faces contact

Figure 4.15 show the full assembly of cooling block being used for simulation. The full results (60 simulations) of CFD analysis are placed at the appendix C. The extracted information of the CFD analysis is then used to compare with the calculated cooling block's center temperature for heat rejection analysis.

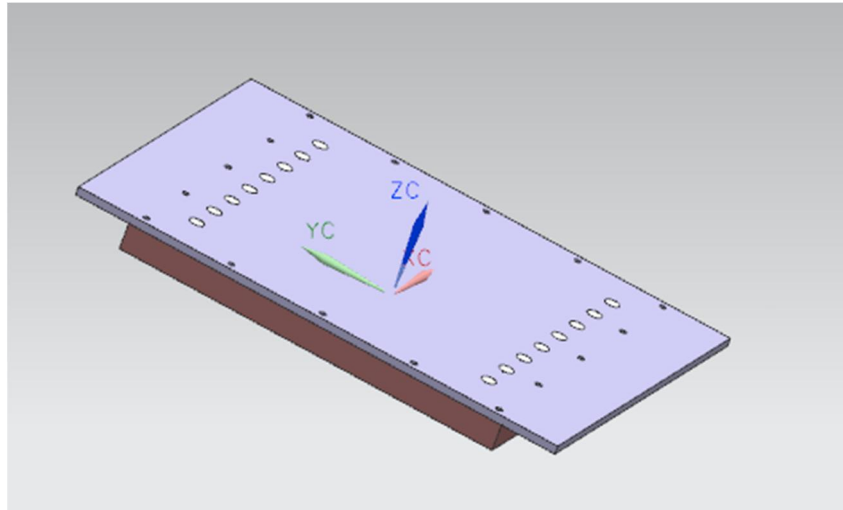


Figure 4.15: Figure of full assembly of cooling block used for thermal-load simulation

4.1.4 Comparison between theoretical study and simulated results of the Cooling block

Table 4.2 and Table 4.3 is the theoretical parameter calculated to determine the heat rejection rate at each phase for conduction, convection and radiation.

Table 4.2: Parameters calculated for heat rejection analysis at different temperature

Parameter	Value		
	32C	42C	52C
Viscosity, μ_f	769×10^{-6} Ns/m ²	631×10^{-6} Ns/m ²	528×10^{-6} Ns/m ²
Prandtl Number, Pr_w	5.2	4.16	3.42
Thermal Conductivity, k_w	0.620W/mK	0.631 W/mK	0.645 W/mK

Table 4.3 Thermal load calculated for heat rejection analysis at solar constant

Solar Constant, W/m ²	Thermal Load
600	2304
700	2688
800	3072
900	3456
1000	3840

The results of the temperature of the calculated and simulated cooling block's center temperature are shown according to the tables below:

0.43kg/s, 32 °C		
Thermal Load (W)	Calculated Temperature, °C	Simulated Temperature °C
600W	35.86	38.85
700W	38.17	40.01
800W	40.49	41.15
900W	42.80	42.20
1000W	45.11	43.50

0.43kg/s, 42 °C		
Thermal Load (W)	Calculated Temperature, °C	Simulated Temperature °C
600W	45.32	48.90
700W	47.54	49.90
800W	49.76	51.14
900W	51.98	52.16
1000W	54.20	53.29

0.43kg/s, 52 °C		
Thermal Load (W)	Calculated Temperature, °C	Simulated Temperature °C
600W	54.75	58.87

700W	56.88	59.78
800W	59.00	61.20
900W	61.13	62.14
1000W	63.25	63.47

0.53kg/s, 32 °C		
Thermal Load (W)	Calculated Temperature, °C	Simulated Temperature °C
600W	34.43	38.05
700W	36.50	38.99
800W	38.58	40.03
900W	40.65	40.95
1000W	42.72	42.05

0.53kg/s, 42 °C		
Thermal Load (W)	Calculated Temperature, °C	Simulated Temperature °C
600W	43.94	47.43
700W	45.93	48.78
800W	47.92	49.88
900W	49.91	50.90
1000W	51.90	52.12

0.53kg/s, 52 °C		
Thermal Load (W)	Calculated Temperature, °C	Simulated Temperature °C
600W	53.43	57.97
700W	55.34	59.04
800W	57.24	60.05
900W	59.15	60.94
1000W	61.05	62.07

Figure 4.16 shows temperature at the center of cooling block ($^{\circ}\text{C}$) against thermal load acted on the surface of cooling block (W), also with other parameter consider such as mass flow rate and water inlet temperature.

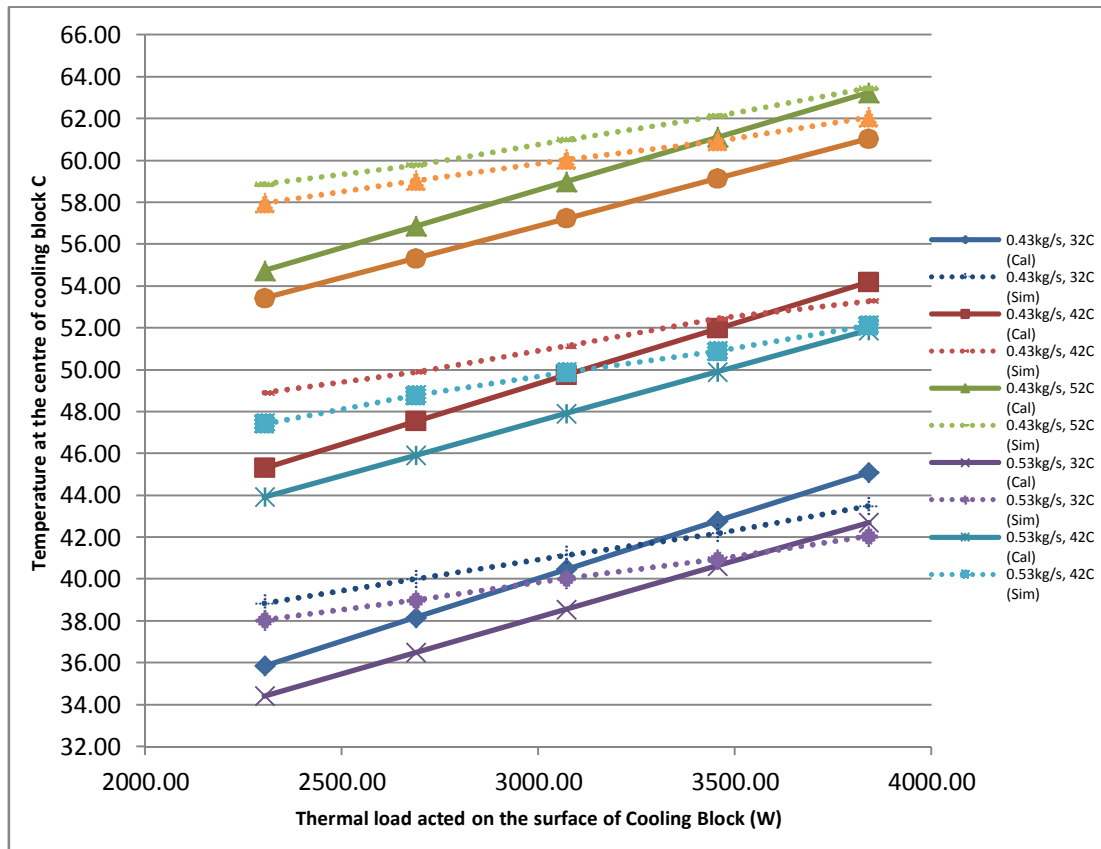


Figure 4.16: Graph of temperature at the center of cooling block ($^{\circ}\text{C}$) against thermal load acted on the surface of cooling block (W), also with other parameter consider such as mass flow rate and inlet water temperature. The dotted line indicates the simulation results.

According to the results of plotted graph, both the calculated and simulated results shown that when the mass flow rate increases, the temperature of the cooling block decreases at any rate of thermal load acted on the cooling block surface. According to Eq. (3.18), the higher the mass flow rate, the higher the water flow velocity. This means that with the increase of speed of water, the heat transfer coefficient of convection between the cooling block and water is higher too. With this, more heat can be transfer away from the cooling block.

Furthermore, it is observed that at any particular value of thermal load acted on the surface of the cooling block, cooling block's center temperature raises when the water inlet temperature increases. The reason for the raise of temperature at any thermal load is that the higher inlet water temperature transfers extra thermal energy if compare to those lower water inlet temperature. With this thermal energy, it causes the reduction in difference of temperature between cooling block and water and thus, the thermal resistance for dissipation of heat from cooling block to water is increased too. In short, the higher temperature the higher the thermal resistance and hence heat transfer performance is reduced.

In addition, it is noticed that there is different between the calculated results and the simulated results. It is seen that the trend of temperature different between the calculated result and simulated results is always around 8°C. The simulated results are lower than the calculated results. The average percentage different calculated based on Eq. (4.1) is 3.10%.

$$\text{Percentage difference} = \frac{T_{\text{simulated}} - T_{\text{calculated}}}{T_{\text{calculated}}} \quad (4.1)$$

Where

$T_{\text{simulated}}$ = simulation result of the cooling block's center temperature.

$T_{\text{calculated}}$ = calculated result of the cooling block's center temperature block.

There is such a value of percentage difference between calculated and simulated value is that there might be error occur during the time of simulation. The CFD simulation results are never 100% trustworthy because the input data may involve too many estimating or roughness and the accuracy results might be limited by the available computing power. Also, the results might be affected by the acknowledged error such as discretization error (approximation of PDEs by algebraic equation), iterative convergence error and round-off error due to the finite precision of the computer arithmetic. There might be also the unacknowledged error such as usage error where the parameter value, models or boundary condition insert have different with the calculated value.

4.1.5 Fabrication Results of the cooling block

The cooling block designed as mentioned in section 3.1.4 is mounted on the CPV system. Figures below shows the fabricated cooling block used for cooling. For all the water inlet is sealed with the gasket to prevent water leaking. Then 3mm o-ring is place at the extruded area of the cooling block and the block is covered tightly with the aluminium cover plate by screw. Then the cooling block is taken to test the leaking and the result shows no leaking for the cooling block.

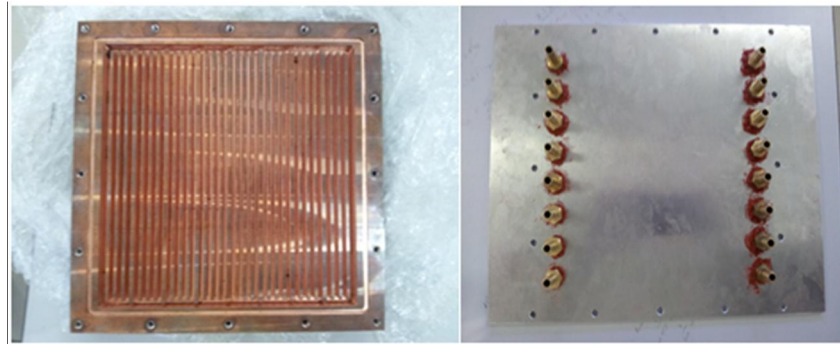


Figure 4.17: Fabricated cooling block with the cover for heat transfer between cooling block and water.

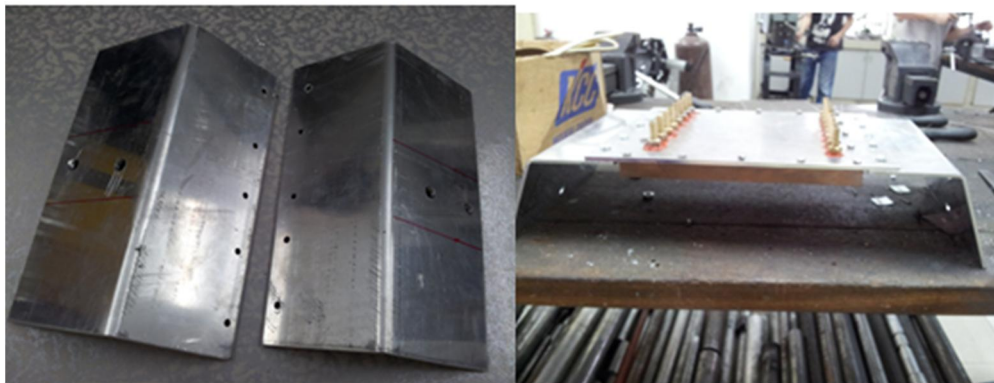


Figure 4.18: Left shown the fabricated side angle bar and right shown mounted cooling block on the angle bar.



Figure 4.19: Leaking test performed for the cooling block.

4.2 Fabrication Results of the whole cooling system

After the main frame is placed on the base frame, the cooling system designed by me is then invented on the main frame. Figure 4.20 shows the CPV system with the whole cooling system. The component of the cooling system include automotive radiator, cooling block, water pump, storage tank (1 main tank and 1 backup tank), water channel piping, manifold, heat insulator and manifold.



Figure 4.20: Side view of CPV system with the whole cooling system

The manifold is used to control the channel of water distributed into the inlet pipe head of the cooling block, and then channel out water from the outlet pipe head of the cooling block. This self-made manifold is made up using PVC piping. It is done by drilling 4 holes each at the one side of the PVC pipe and the end of the pipe is closed by filling with simen material. Then the leaking test is performed on the manifold, and the result shows no leaking for the cooling block. Figure 4.21 shows the leaking test performed on the manifold.



Figure 4.21: Leaking test performed for the manifold

Noticed that we have use the air conditioner type of insulation foam cover the water flow piping, and then the piping is added with another layer of aluminium foil. This is to avoid direct Sunlight acted on the piping that will cause the water in the piping to be heated. If the water is heated, it will affect the results collection analysis. The water container is also been place at a place with no direct Sunlight so that the water in the tank won't be heated too. The cooling system has been used for weeks for mirror tilting purpose, and experiment purpose.

Moreover, due to the environment of the site, it causes the water piping to be dirty and muddy. When the water is mix with the dirt, it will contain a lot of impurities. If too much of impure water is channelled to the cooling block, it might have causes the impurities to be blocked between the fin in the copper block and thus this reduce the performance of the cooling block. So we have to make sure that the water piping is always clean, and change the water of the cooling system from time to time.

This cooling system implemented is being on from time to time during the mirror tilting process and experiment period to make sure that the cooling block and solar cell is not over heated.

4.3 Fabrication result for the Hardware of the Concentrated Photovoltaic (CPV) Frame

4.3.1 Fabrication Result of the Mirror Supporter for the Concentrated Photovoltaic (CPV) Frame

After around 3 months of fabrication period, the hardware of the frame has been completed. Figures 4.21 show the result of fabrication.

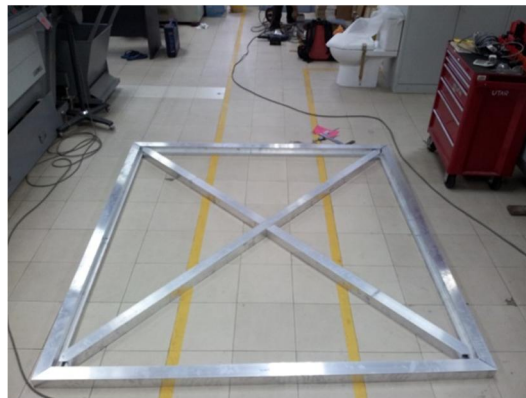


Figure 4.22: Main frame with the biggest size of square aluminium bar.



Figure 4.23: Square aluminium bar with L bar fixed on it and also triangular plate for mirror tilting purpose



Figure 4.24: Arrows show the main frame square aluminium bar for supporting the mirror tilting system.



Figure 4.25: Completed main frame with mirror being set on it.

Throughout the whole fabrication process, many experience had been learn. There is few precaution steps need to be taken in order to make a good fabrication. Precaution steps were taken during the following processes:

a) Measuring and cutting:

- ✓ During the measuring process, we should give tolerance to the measurement. This is because during the cutting process, the cutting machine used might have overcut or undercut the material. For undercut material, we can file it to the desired measurement but for overcut material, it will be wasted. So, with the tolerance made, we can avoid the overcut problem and save the material used.

b) Grinding and filling:

- ✓ During this process, we have to make sure that we finish the surface properly. No extra cutting chips should be left over at the cutted bar or the drilled holed.

c) Center marking and Drilling:

- ✓ An indentation need to be made first before the drilling process is took place. The indentation will guide the drilling process. The indentation is made first to avoid slipping which may cause serious injuries. During the center marking process, we should make sure that center marking that we are making is at the right position. The center punch should be hold at 90° to the material needed to be drilled. For the usage of drilling machine, the fixture must be held firmly or screwed tightly on the drilling platform to minimize the defect of drilling and to avoid slipping. This is same as apply to the drilling gun used.

d) Rivetting:

- ✓ For proper installation, the rivets should be inspected. The gripping between the two materials should be good to make sure that after riveting, there is no gap in between the material.

Other than that, during the whole frame fabrication process, we need to make sure that the triangular plates are aligned in rows and columns. In real fabrication situation, we might miss aligned the position of the square bar on the frame and causes the triangular plate to be out of alignment. With this error, the mirror being installed might be clashing with each other.

Throughout the fabrication process, I've encountered several problems. First of all is the filling process whereby I did not wear any gloves. As a result, there are some blisters and bruises on the palm of my hand. Another problem encountered was Bracket rust easily. I need to file again to remove the rust which consume much of my time.

During the center marking process, sometimes I did not hold the center punch directly perpendicular, instead, there is a bit slanted. So, some of the drilled hole is a

bit out of measurement. Besides that, during the drilling process, the drill gun sized used is not appropriate, causing me to need more strength to drill the hole. In the workshop, there is only one big drill gun available, so we have to use that drill gun to drill all the holes.

In addition, some of the plate did not hold join properly with the aluminium bar during the riveting process. The cause of it is the work is not firmly together and rivets shank swelled. The work need to be clamped properly for riveting process and new rivet new to be replaced in this cased.

Moreover, after the main frame rack is being fabricated, it has consumed a big space. The workshop did not allow us to continue our fabrication work in the workshop and hence we were forced to move the frame to other open are to continue our work. For this case, we need to find the new electricity supply for hole drilling purpose and also we found an empty corridor to continue our work. The corridor space was limited, causing us too difficult to move the main frame around. Figure below show the space of the new working are.

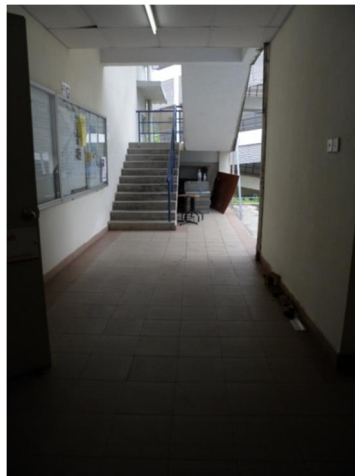


Figure 4.26: The corridor used as a place for fabrication of main frame.

There is no doubt that the complete fabrication of the main frame is very heavy (around 150kg). So, a lot of man force is needed when we need to turn around the frame or to move the frame to the base frame. Figure below show that with the help of our classmate, the main frame is being moved.



Figure 4.27: With the help of our classmate, the main frame is being moved or rotated for further work.

4.3.2 Problem Encounter During On site Prototype Setup

After the main frame of the CPV system is mounted on the base frame, we perform on-site testing on the control system and mirror tilting to ensure that the CPV system can be automatically track the Sunlight or manually being moved, mirror tilting is to make sure that all the 96 pieces of mirror focus the Sunlight onto the solar cell at the right place. An aluminium bar is drilled with hole to make sure that the Sun light is hitting the solar panel at 90 degree which is the Direct Normal Irradiance (DNI). Figure shows the references made used for mirror tilting purpose.



Figure 4.28: References made used for mirror tilting purpose.

This is one of the hardest parts in the setting up of the CPV system for data collection, for we always need Sunny and clear sky to do mirror tilting. Not always there is a good sunny day with clear Sun. Most of the times we are having hot weather but the heavily cloudy sky has cover up the Sun, causes no reference for the mirror tilting system, thus we need to stop our work to wait for the right weather to work again. Also, we have to stop working when the sky turns dark and rain. In addition, even there is sunlight with less cloud, but there might me diffuse radiation. We called it overcast day. The particles and molecules within the atmosphere causes scattering to the sunlight upon reaching the surface of the earth. Almost all of the solar radiation from the Sun is diffusion radiation during extremely overcast day. We are unable to perform mirror tilting on these days. This situation consume most of our time in setting up the CPV system.

In addition, we need to stand under the extremely hot weather perform mirror tilting and on-site testing. All the mirror reflection causes a lot of reflective image on the cooling block. So, we have to use cloth to cover up part of the mirror so that we will not mess up the image of the mirror being tilted. Due to the elevation of the CPV system to track the Sun, one part of the frame might be very high up and causes hard time for us to reach that part for mirror tilting. Figure 4.29 shows the situation where all the group member involved in doing mirror tilting.



Figure 4.29: Situation where all the group member involved in doing mirror tilting

Furthermore, even though the control system being implemented has pass the software simulation, but problem will still occur during on-site testing. One of the problems that we have faced is that the CPV manual control system stops functioning. After my group mate has performed checking and debugging, we found out that part of the hardware of the controller has short circuited. Also, sometimes, due to all day long software inspection on the tracking system, the coding will show bug and the whole system need to be reset again to get the correct results.

4.4 Result for the NIDC Experiment

During the first and second experiment performed we have fail to get the desired results because we have left the sand paper to be exposed under focused Sun light and results in the over burn of the sand paper. Figure shows the fail experimental result.



Figure 4.30: Over burnt of the sand paper

In the final experiment, we have successfully obtained the desired result. As refer to figure 4.31, it is observed that the sand paper is having a different degree of burn marks. Figure also shows the measured total area burnt mark on the sand paper.

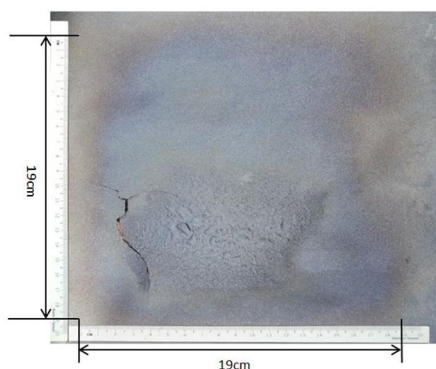


Figure 4.31: The darken area of burnt mark on the sand paper measured with the result of $19\text{cm} \times 19\text{cm}$.

In comparison with the simulated result in part 3.4.1, the dimension of the actual measurement is close to the simulated result provided by my group mates as shown in figure 3.17 previously. The different between simulated result and experimental result is 1cm. There is $19\text{cm} \times 19\text{cm}$ in the darken area of burnt mark. With this result, it is proven that the NIDC is performing as the way we want it, which has the 84 Sun concentration and 1.7m of focal length. So, we can proceed to other data collection experiment.

4.5 Result on the On Site Testing Of the Cooling System and Power Conversion Efficiency of the CPV module

Firstly, we have conducted the experiment for 1 hour and 15 minutes from 11am to 12:15pm. Data is collected for every 5 minutes. Then, the experiment is continued with data collection at every 15 minutes interval to determine the long term stability of the cooling system and the changes in the cooling block temperature. In addition we also have conducted the experiment to compare the cell conversion efficiency result in the situation of fan on and fan off.

Table 4.4 to 4.7 shows the result of calculated parameter by using the data collected from the on-site experiment.

Table 4.4: Solar Power Input, Heat Rejection Rate, Cooling Block Temperature and from 11am to 12:15pm at every 5 minutes of interval

Time (minutes)	Solar Power Input (W)	Heat Rejection Rate (W)	Cooling Block Temperature (°C)
0	1965.77	2003.40	40.90
5	2002.86	2226.00	44.30
10	2002.86	2226.00	44.50
15	2077.04	2671.20	47.70
20	2114.13	2893.80	46.90
25	2114.13	2003.40	50.90
30	2151.22	2448.60	49.50
35	2151.22	3116.40	51.90
40	2188.31	2448.60	49.50
45	2188.31	2226.00	50.00
50	2225.40	1558.20	50.30
55	2225.40	2448.60	50.70
60	2188.31	2448.60	53.20
65	2151.22	2226.00	53.50
70	2188.31	1780.80	51.40
75	2188.31	1780.80	52.00

Table 4.5: Solar Power Input, Heat Rejection Rate, Cooling Block Temperature recorded from 11:00am to 3:30pm at every 15 minutes of interval

Time	Solar Power Input (W)	Heat Rejection Rate (W)	Cooling Block Temperature (°C)
11:00	1965.77	2003.4	40.90
11:15	2077.04	2671.2	47.70
11:30	2151.22	2448.6	49.50
11:45	2188.31	2226.0	50.00
12:00	2188.31	2448.6	53.20
12:15	2188.31	1780.8	52.00
12:30	2151.22	2003.4	55.80

12:45	2151.22	2448.6	53.00
13:00	2114.13	2003.4	54.10
13:15	2151.22	1780.8	54.70
13:30	2151.22	2003.4	60.00
13:45	2151.22	2003.4	59.00
14:00	2077.04	2671.2	54.20
14:15	2114.13	2226.0	54.30
14:30	853.07	2448.6	51.00
14:45	815.98	1780.8	48.00
15:00	778.89	2003.4	44.00
15:15	667.62	1780.8	40.00
15:30	630.53	1780.8	38.00

Table 4.6: Conversion Efficiency comparison with fan

Cell Temperature (°C)	Conversion Efficiency (with fan) %
42.90	32.52
49.82	32.47
51.66	33.42
52.18	34.08
55.38	33.96
54.19	33.84
57.94	33.97
55.16	33.52
56.14	36.28
56.97	30.24

Table 4.7: Conversion Efficiency comparison without fan

Cell Temperature (°C)	Conversion Efficiency (without fan) %
43.9	32.35
47.0	31.43
49.3	33.20
53.5	32.97
57.7	29.64
60.2	29.43
65.7	26.59
70.5	22.68
75.5	21.00
75.5	22.89

The Result of Experiment conducted for 1 hour and 15minutes, from 11am to 12:15pm to show the relationship between Solar input power, cooling block temperature and heat rejection rate of radiator is being shown in figure 4.32.

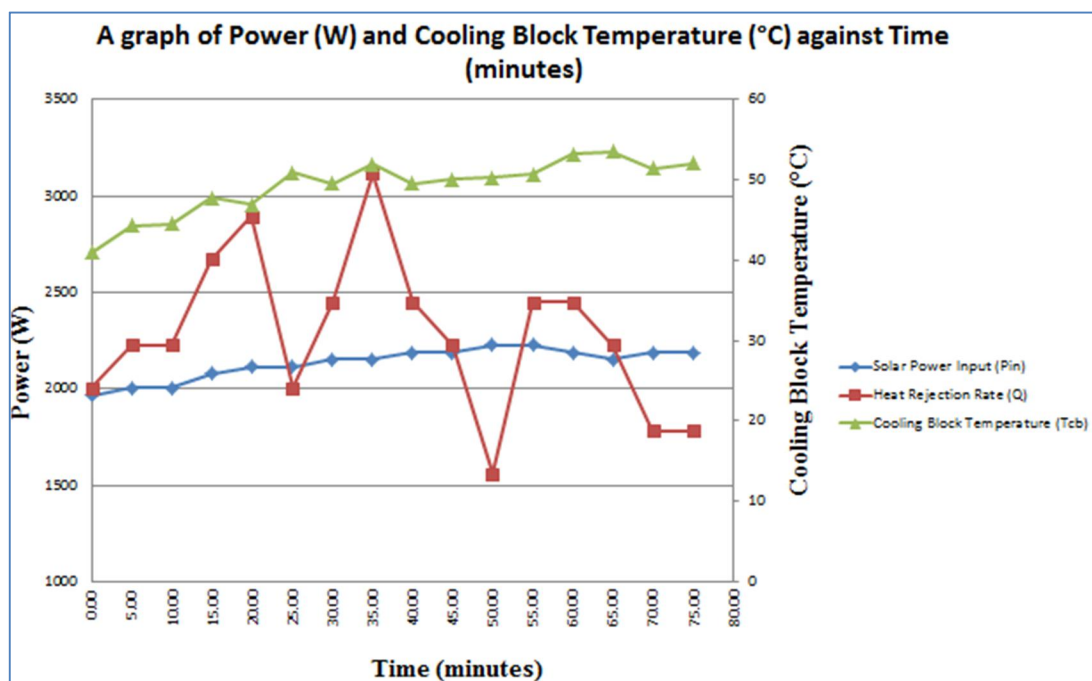


Figure 4.32: Result of Experiment conducted for 1 hour and 15minutes, from 11am to 12:15pm

According to the result in figure 4.32, it can be seen that the solar power input is having a constant range of value which is around 2000W to 2300W. The temperature of the cooling block is at a range from 40 °C to 52 °C. The temperature of the cooling block rise with the solar power input. As there is more input, so more power is generated and thus produced more heat to the cooling block. The heat rejection starts to rise from the beginning until the experiment has been conducted for 20 minutes.

After 20 minutes, the heat rejection rate has a tremendously rise and drop in between 25 minutes and 50 minutes. In this period of time, it is observed that the automotive radiator is still able to reject the heat being absorbed by the cooling block, so it reaches the thermal equilibrium after some time. The highest rate of rejection of the radiator is 3116W. With this high heat rejection rate, it is able to equalize the input of solar power, provided that there different in temperature of 15°C or higher between the radiator and ambient temperature.

The Result of Experiment conducted for 4.5 hours, from 11am to 3:30pm to show the relationship between Solar input power, cooling block temperature and heat rejection rate of radiator is being shown in figure 4.33.

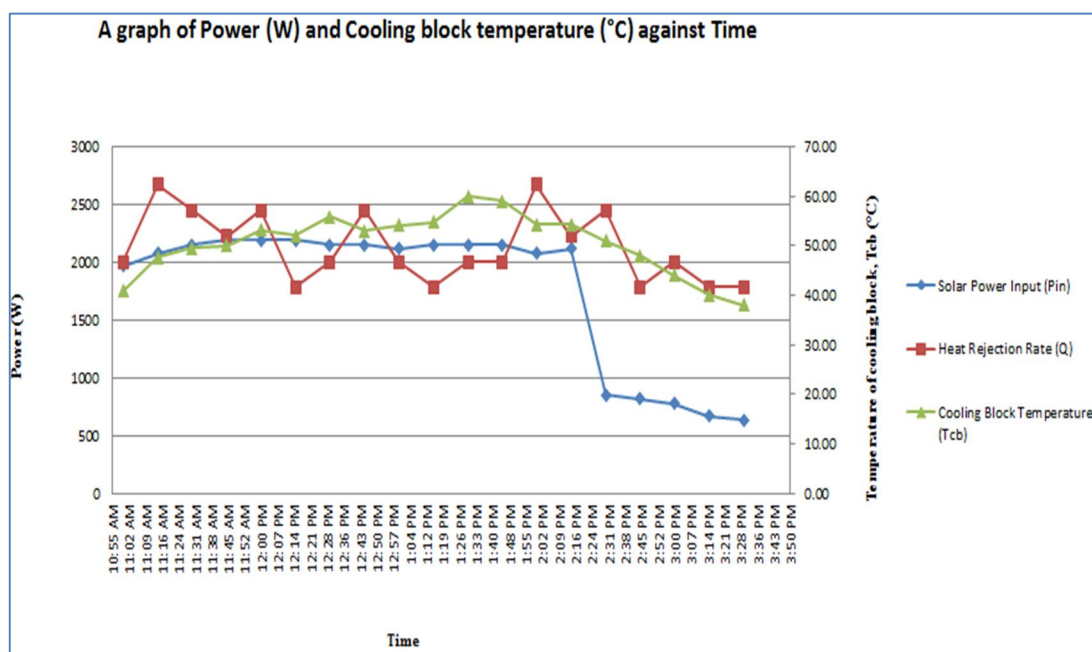


Figure 4.33: Result of Experiment conducted for 4.5 hours continuously from 11am to 3.30pm

According to the graph results of figure 4.33, from 11am to 1:45pm, the heat rejection rate of the radiator is average between value of 1800W to 2671W, and it rejects almost the same amount of heat of the solar power input at some point. So, the radiator can be said to achieve the thermal equilibrium in between this period of time and the heat transfer rate is almost ideal. The input of solar power is at an average value 2000W to 2200W from 11am to 2.15pm. It is notice that after 2.15pm, the solar power input has been reduce tremendously. This is due to the weather started to change and the sky starts to be cloudy. When there is decrease in solar power, it affects the cooling block's temperature and also the rate of heat rejection of the radiator. Temperature of the cooling block starts to be reduced and the water temperature different is reduces and thus causing the heat rejection rate to be reduced too.

The highest heat rejection rate throughout this whole second experiment is 2671W, which is higher than the average solar power input. The heat rejection rate is not ideal because there might be other source of heat lost such as conduction of heat, convection of heat in nature and also radiation. Throughout this four and a half hour, the temperature of the cooling block can be maintained below 60 degree and we can conclude that the cooling block's temperature is able to maintain the stability of temperature from the trend of graph plotted. Thus this cooling system designed is effective for the CPV system.

In addition figure 4.34 compare the different between the theoretical result and the experimental result of the heat rejection rate of the radiator.

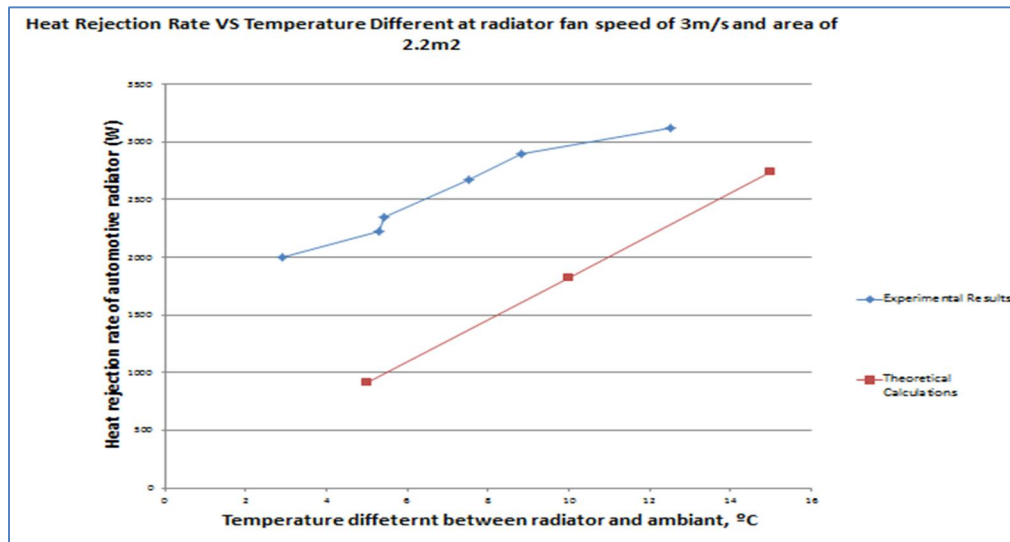


Figure 4.34: Heat Rejection Rate VS Temperature Different at radiator fan speed of 3m/s and area of 2.2m²

From the results, it is seen that the experimental results are always higher than the theoretical value calculated for the heat rejection rate of the radiator. This is because as mentioned above, there might be other heat lost sources such as conduction of heat, convection of heat in nature and also radiation. The percentage different calculated between the theoretical value and calculated value is 5.34% which is in the acceptable range of percentage. This means that the experimental result is 5.34% higher than the calculated results.

Next, the relationship between of cell conversion efficiency of cooling block and cell temperature is being plot as shown in figure 4.35.

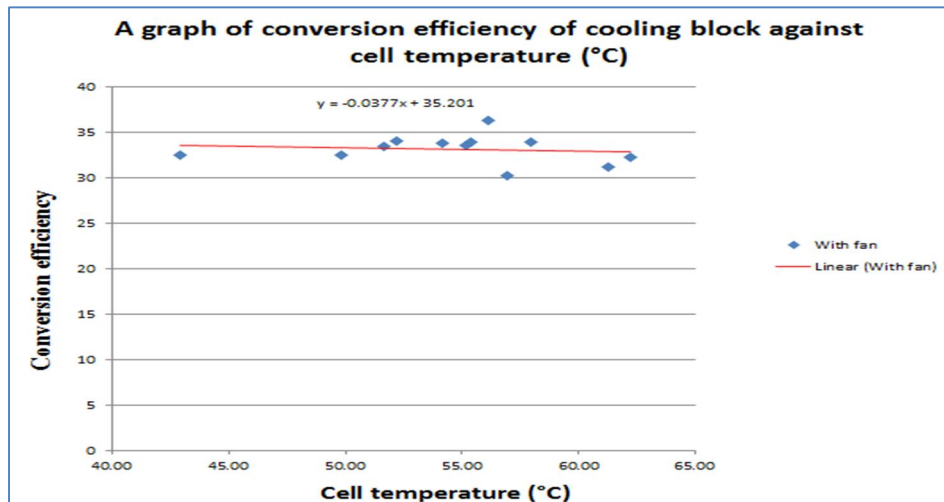


Figure 4.35: Solar cell conversion efficiency VS change in temperature

From the results, it can be seen that the relationship of the cell conversion efficiency and cell temperature has a linear relationship. This means that when the temperature of the cell is increased, the cell conversion rate decreases. From the graph, the cell conversion of efficiency is reduced by 3.77% with every decrement of 1 degree celcius. The maximum conversion efficiency for the cell is 36%. This result is reasonable as compare to the datasheet of the solar cell.

Finally, the relationship between of cell conversion efficiency of cooling block, speed of radiator fan and cell temperature is being plot as shown in figure 4.36.

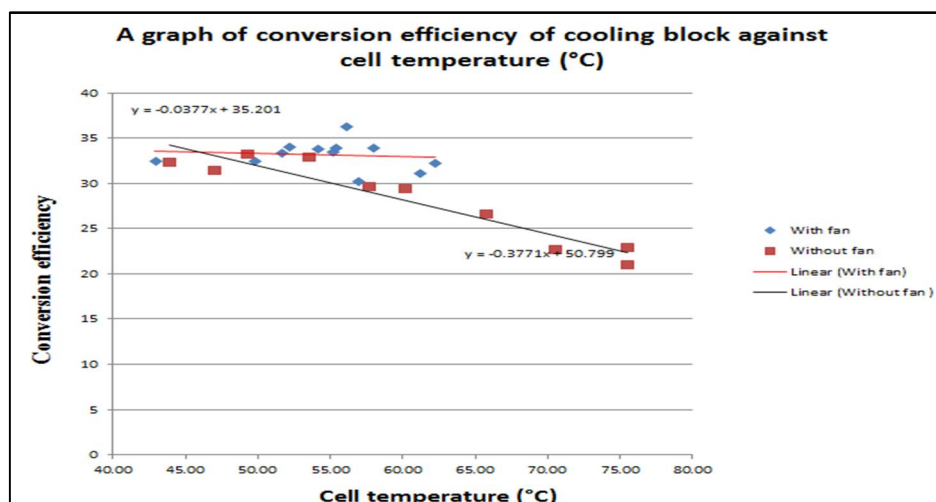


Figure 4.36: Solar cell conversion efficiency VS change in temperature and speed of fan

During the experiment, it is recorded that the cooling block's temperature increases tremendously when the fan of radiator is switched off. We conducted the experiment only for a short period of time to avoid the temperature of solar cell exceeded the maximum operating temperature. This will cause the defect in solar cell.

According to the comparison graph of cell conversion efficiency, there is a tremendous change cell conversion efficiency over a period of time. Initially, the conversion rate is normal but when the cell temperature is above 50 °C, the conversion become inefficient. From the graph, the cell conversion of efficiency is reduced by 37.77% with every decrement of 1 degree Celsius. The minimum conversion of efficiency is 22.89% at 75 °C. This shown that the radiator fan play an important role in heat rejection process and also causes the drastic change in the rate of conversion of cell efficiency.

In addition, calculation based on fan off and off of conversion efficiency is carried out to determined how the efficiency of cooling system affect the net electrical power output produced bythe CPV system. Table below shows the comparison between the case of cooling system with fan and without fan that produces the net electrical output.

Table 4.8: Comparison of the net electrical output between the case of cooling system with fan and without fan

	With fan	Without fan
Temperature of solar cell	49.82	65.70
Solar power input with DNI = 690.51W/m ²	2077W	2077W
Cell conversion efficiency, %	32.47	26.59
Electrical Power output produced by CPV	674.40W	552.27W
Net electrical power output	674.40 -150.6W = 523.80W	552.27W- 100W = 452.27W

*Note that power consumption of water pump is 100 W and power consumption of radiator fan is 50.6W.

The different in the net electrical power outputs is 71.53W. This means that the cooling system with fan produces 71.53W of power more than the cooling system without fan. Therefore, we can conclude that cooling system's efficiency is very important in generating high net electrical power output. The better the efficiency of the cooling system, the higher the net electrical power output generated.

As according to figure 4.35, for the overall system, the highest net electrical output power is 595.78W, with the input of solar cell is 2188.31W and the conversion efficiency is at 34.08%.

CHAPTER 5

CONCLUSION AND RECOMMENDATIONS

5.1 Conclusion

In conclusion, the aim and objective of this project has been achieved. I have successfully design and construct the cooling system for concentrator photovoltaic receiver module and completed hardware fabrication of the CPV system with my team mates.

Theoretical study has been performed for the automotive radiator and it is determined that with the wind speed of 3m/s and mass flow rate of 0.53kg/s, the rate of heat rejection is the highest.

In addition, for the cooling block design, the stress analysis and CFD simulation and has been carried out to verify the simulated result of the cooling block under stress and to study its performance. The simulated results have been compared with the experimental result. In order to confirm the theoretical study of the cooling system, on site experiment has been carried out for data collection.

Three different experiments have been carried out to determine the performance of the CPV system. The NIDC prototype has around 84 Suns of concentration and total reflective area of 3.82m². The rate of heat rejection is measured as 5.34% deviated from the calculated result. The experiment shows that the cooling block can maintain the temperature range from 32 to 55 degree Celcius, which means that the cooling block operates at good condition.

Furthermore, the relationship between the electrical conversion efficiency of the CPV module and the cell temperature is also determined. From the results tabulated, we can see that there is a linear relationship of CPV module and the CPV cell temperature (increases 3.77% with every decrement of 1 degree Celsius in the temperature of the cell). The maximum conversion efficiency for the cell is 36% and the minimum conversion of efficiency is 22.89% at 75 °C. The radiator fan play an important role in heat rejection process and also causes the drastic change in the rate of conversion of cell efficiency. For the overall system, the highest net electrical output power is 595.78W, with the input of solar power is 2188.31W and the conversion efficiency is at 34.08%.

5.2 Recommendation for Future Work

Since it is proven in the theoretical study that, the increase in the surface area of the automotive radiator will increase the heat rejection rate, the future researcher can use a larger radiator in future research, provided that the power rating of the radiator is at an acceptable range. The larger radiator contains more fins and has a larger water capacity for the cooling system.

In addition, due to the funding limit, we have to make simple water manifold to channel the water. For future project and research purpose, if we want a more accurate and controlled of water channelled, a conventional aluminium manifold with flow meter can be used to replace the current self-made manifold to ensure more uniform water flow and we can control the exact amount of water flow rate to the cooling block.

Furthermore, for the current storage tank is only a plastic container and it is temporary place at the site, water has to be changed from time to time (to ensure clean water supply). To improve the water channel system, the future researcher can realize a permanent water storage tank with filter function. The proposed system needs the permission of UTAR to allow the water piping to be channelled to the site so that the water source can be directly channel to the water storage tank. Filter is

used to filter out water impurities so that the cooling block is clean from blockage for all time.

REFERENCES

- ANJA RØYNE, 2005. COOLING DEVICES FOR DENSELY PACKED, HIGH CONCENTRATION PV ARRAYS. [Online]. Available at <http://folk.uio.no/anjaroy/PVCooling.pdf>. [Accessed 17 June 2012]
- A. R. Mahoney, J.E. Cannon and J.R. Woodworth, 1993. Accelerated UV-aging of Acrylic Materials used in PV Concentrator Systems. In Proceedings in the 2 3rd IEEE Photovoltaic Specialists Conference, Louisville, Kentucky, USA, 1993.
- Chong K. K. and Tan W. C., 2012. Study of automotive radiator cooling system for dense-array concentration photovoltaic system, [E-journal] pp. 2-12. Available through Universiti Tunku Abdul Rahman Library website <http://library.utar.edu.my/>. [Accessed 1 August 2012].
- Christiana Honsberg and Stuart Bowden, 2010. The effect of temperature on the IV characteristics of a solar cell. [Electronic Print]. Available at <http://pvcadm.pveducation.org/CELLOPER/TEMP.HTM>. [Accessed 17 August 2012]
- David Faiman. 2002. Large Area Concentrators, , The Path to Ultra-High Efficient Photovoltaics, Second Workshop, JRC ISPRA.
- Horne, W.E. 1993. Solar energy system. Patent no. US5269851.
- F. Muhammad-Sukki et al., 2012. Solar Concentrator. [Online]. Available at <http://www.cscjournals.org/csc/manuscript/Journals/IJAS/volume1/Issue1/IJAS-8.pdf> [Accessed 17 June 2012]
- Rodi, W., 1980. Turbulence models for environmental flows. In: Knollmann, W. (Ed.), Prediction Methods for Turbulent Flows. Hemisphere Publ. Corp., London, pp. 259–350.

- G.M. Kaplan. 1985. A Understanding Solar Concentrators Technical Paper #30. Volunteers in Technical Assistance (VITA)
CURRENT-VOLTAGE CHARACTERISTICS OF HIGH
CONCENTRATION PHOTOVOLTAIC ARRAYS. 2009 [Online].
Available at
<http://dspace.nmmu.ac.za:8080/jspui/bitstream/10948/639/5/Chpt%202.PDF>
[Accessed 23 July 2012]
- G. Sala, D. Pachón and I. Antón, 2000. “Book 1: Classification of PV Concentrators”, Test, Rating, and Specification of PV Concentrator Components and Systems, C – Rating Project [Online]. Available at <http://www.ies-def.upm.es/ies/CRATING/crating.htm>. [Accessed 19 June 2012]
- Incropera, F.P., Dewitt, D.P., Bergman, T.L., Lavine, A.S., 2007. Fundamental of Heat and Mass Transfer, sixth ed. John Wiley & Sons, Printed in Asia, pp. 9–13 (ISBN-13: 978-0-471-794714).
- J.C. Miñano and P. Benítez, 2008. High Concentration Photovoltaics: Potentials and Challenges. [Online]. Available at <http://www.slideshare.net/sustenergy/high-concentration-photovoltaics-potentials-and-challenges-presentation>
[Accessed 17 June 2012]
- Kreske K. 2002. Optical design of a solar flux homogenizer for concentrator photovoltaics. Appl. Optics 41, 2053-8 Cui, M., Chen, N., Yang, X., et al., 2009. Thermal analysis and test for single concentrator solar cells. Journal of Semiconductors 30 (4),044011(1–4).
- Lasich, J.B. 2002. Cooling circuit for receiver of solar radiation. Patent no. WO02080286.
- Mathur, R.K., Mehrotra, D.R., Mittal, S. and Dhariwal, S.R. 1984. Thermal non uniformities in concentrator solar cells. Solar Cells 11, 175-188.

- McDanal A. 1984. Development of a Stand-Alone Linear Fresnel Lens Photovoltaic Collector Array, Sandia National Laboratories, Albuquerque, NM, SAND84-0556.
- M, J., 2001. LAWS OF THERMODYNAMICS. [Online]. Available at <http://www.emc.maricopa.edu/faculty/farabee/biobk/biobookener1.html> [Accessed 18 June 2012]
- P.Sheshu, 2011. Fin Efficiency [Online]. Available at <http://www.cdeep.iitb.ac.in/nptel/Mechanical/Heat%20and%20Mass%20Transfer/Conduction/Module%203/main/3.4.html> [Accessed 16 October 2012]
- PV Insider.CPV World Map 2012. [Online]. Available at <http://www.pv-insider.com/cpv/documents/CPVWorldMap2012.PDF> [Accessed 25 June 2012]
- Sala, G. 1989. Chp. 8: Cooling of solar cells, in Cells and optics for photovoltaic concentration, ed. Luque, A. Adam Hilger, Bristol, pp. 239-267.
- Sala, G D. Pachón and I. Antón, 2008. DIRECT NORMAL IRRADIANCE FOR RATING C-SYSTEMS [Online]. Available at <http://www.iesdef.upm.es/ies/Crating/artrad.pdf>. [Accessed 25 August 2012]
- Tilford, C.L., Sinton, R.A., Swanson, R.M., Crane, R.A. and Verlinden, P. 1993. Development of a 10 kW reflective dish PV system. 23rd IEEE Photovoltaic Specialists Conference, Louisville, pp. 1222-1227.
- Verlinden, P., Sinton, R.A., Swanson, R.M. and Crane, R.A. 1991. Single-wafer integrated 140 W silicon concentrator module. 22nd IEEE Photovoltaic Specialists Conference, Las Vegas, pp. 739-743.
- W.B. Stine and M. Geyer, 2009. Power from the Sun. [Online]. Available at <http://www.powerfromthesun.net/index.htm>. [Accessed 17 June 2012]

Whitburn, G. 2012. 13 Fundamental Advantages and Disadvantages of Solar Energy. [Online]. Available at <http://exploringgreentechnology.com/solar-energy/advantages-and-disadvantages-of-solar-energy/> [Accessed 17 June 2012]

Zukauskas, A., 1972. Heat transfer from tubes in cross flow. In: Hartnett, Irvine, T.F., Jr. (Eds.), . In: Advances in Heat Transfer, vol. 8. Academic Press, New York.

Versteeg, H.K., Malalasekera, W., 1995. Computational Fluid Dynamics. Longman Group.

APPENDICES

APPENDIX A: Datasheet of Solar Cell Used

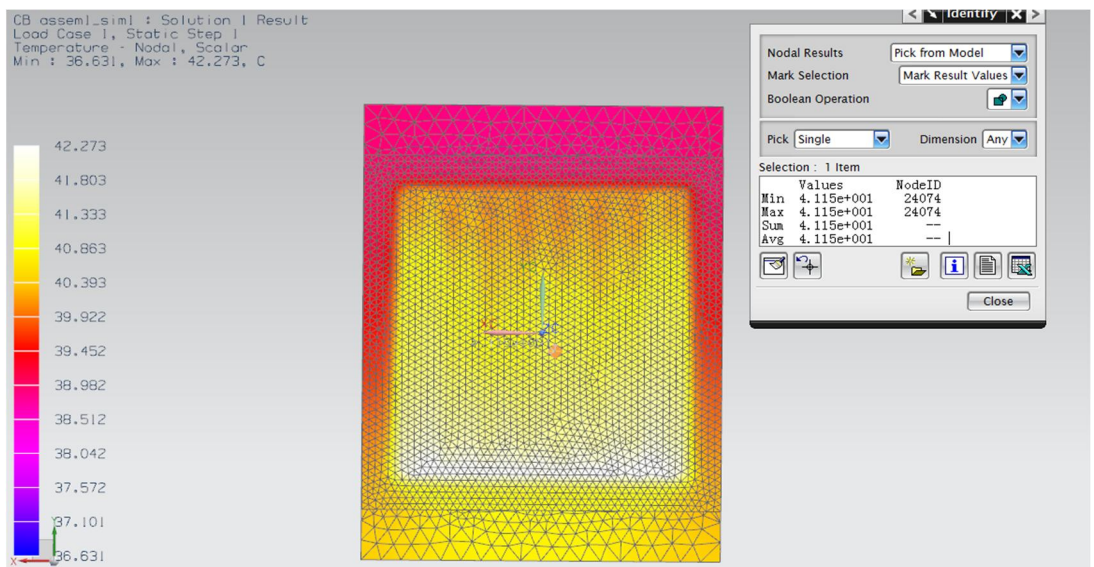
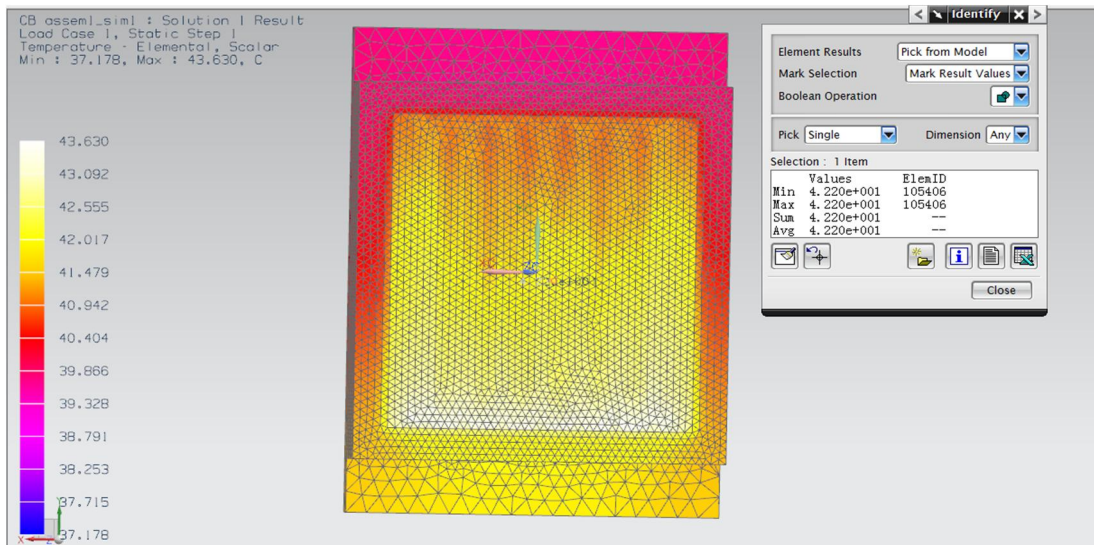
Please refer to the following page for the full datasheet of solar cell.

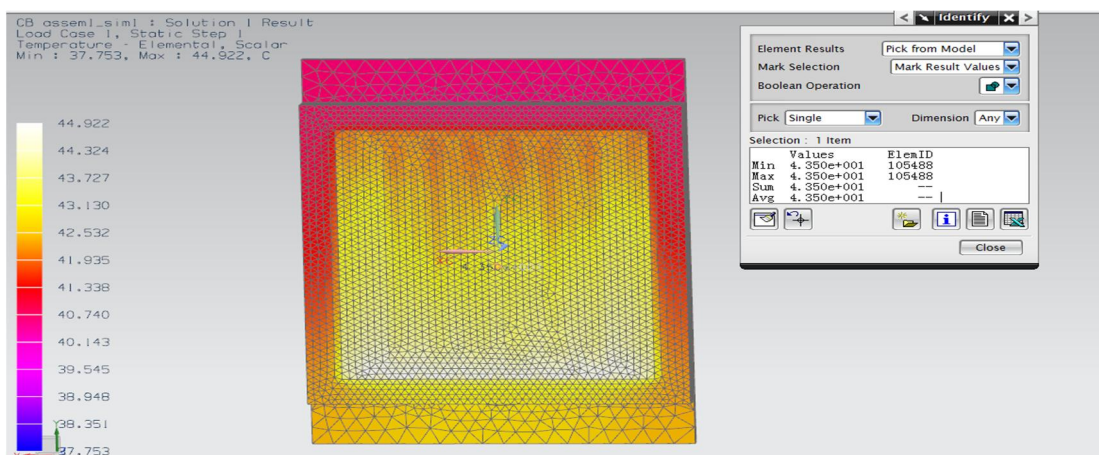
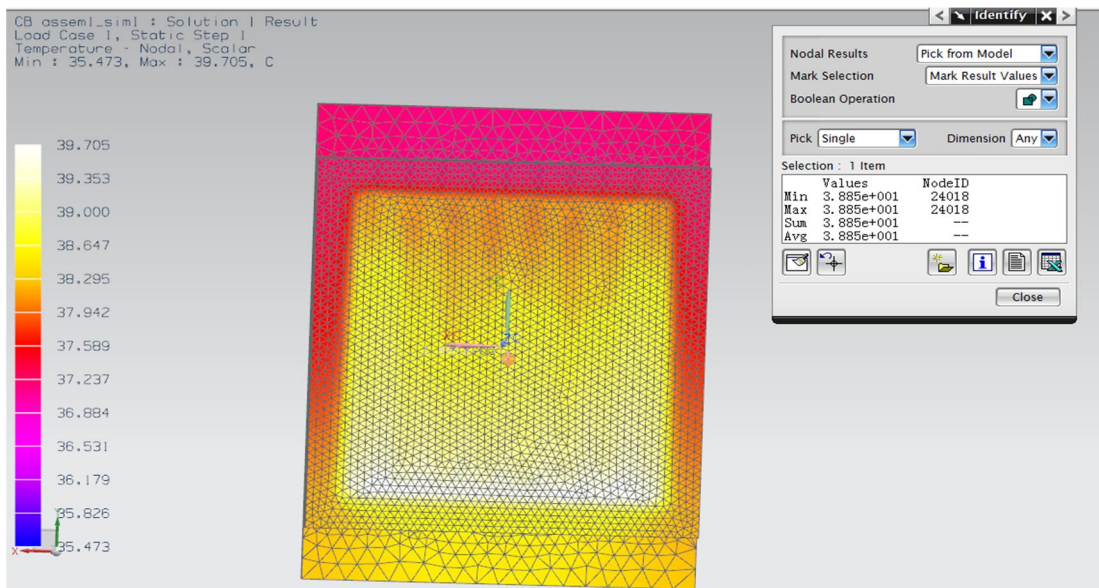
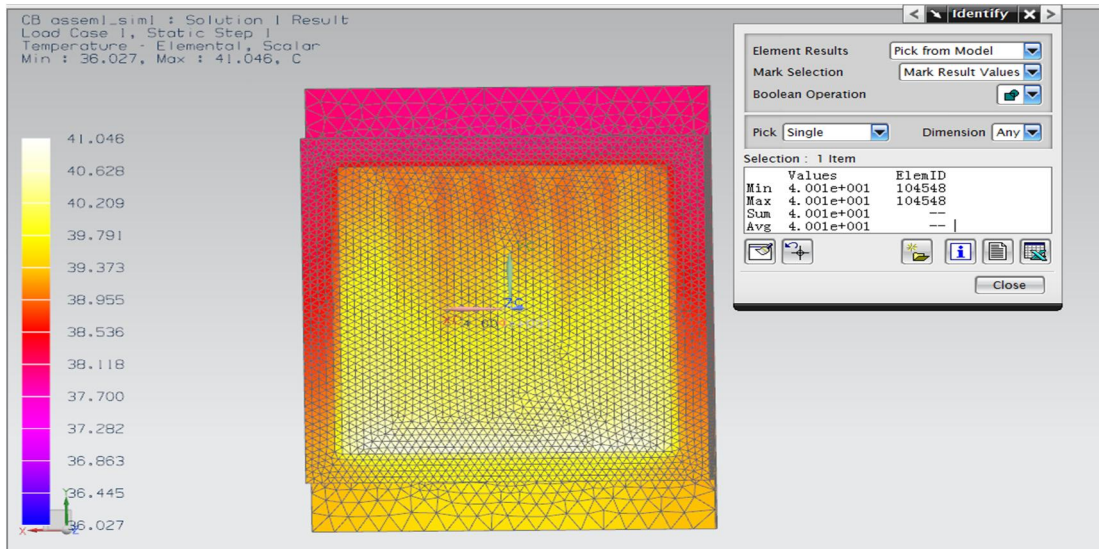
APPENDIX B: Full Dimension Listing For The Cooling Block Design

Please refer to the following page for the full dimension listing for the cooling block design.

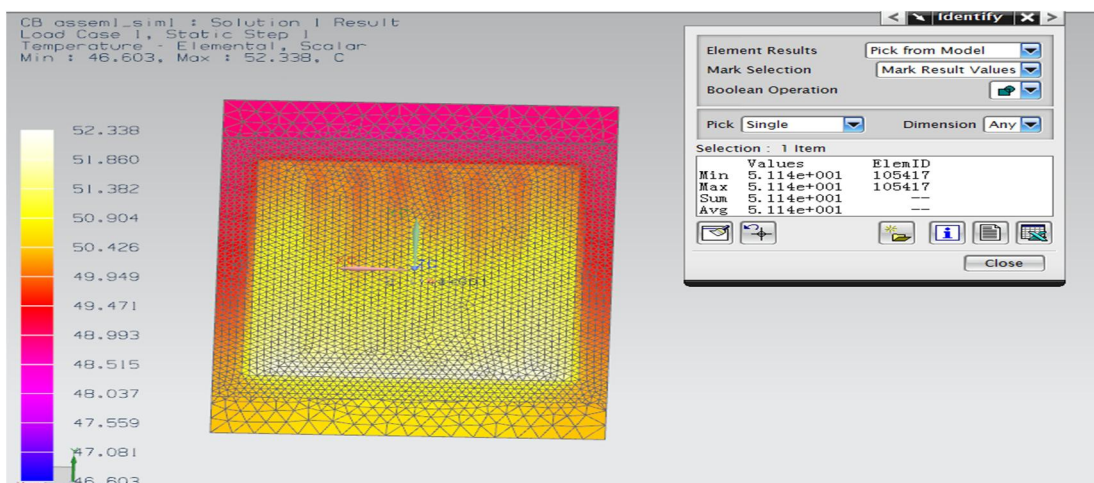
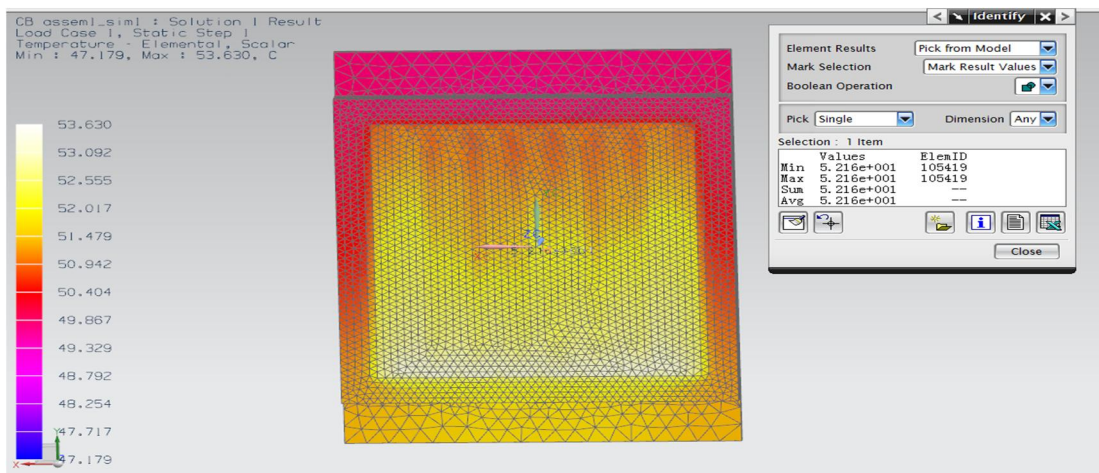
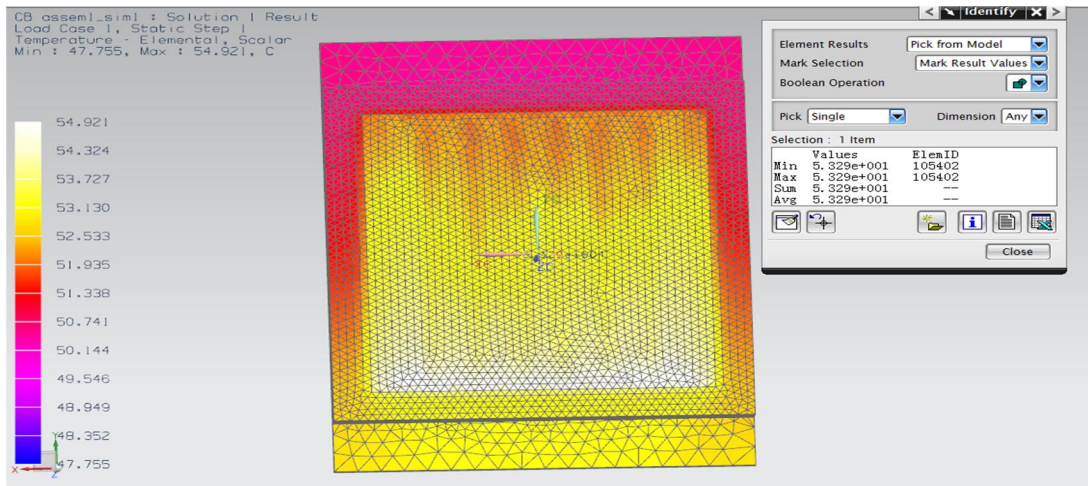
APPENDIX C: Results of CFD Simulation Generated by NX Software

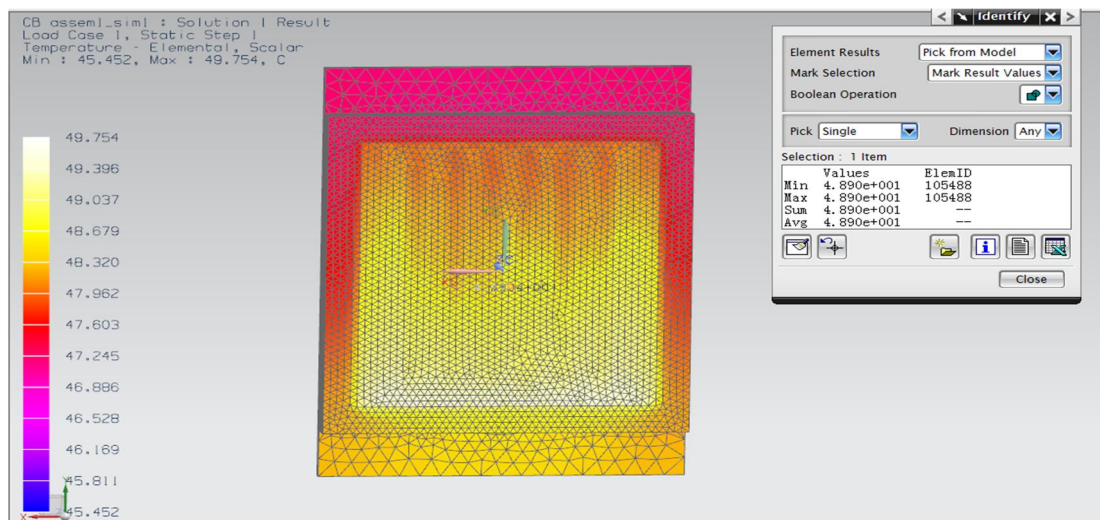
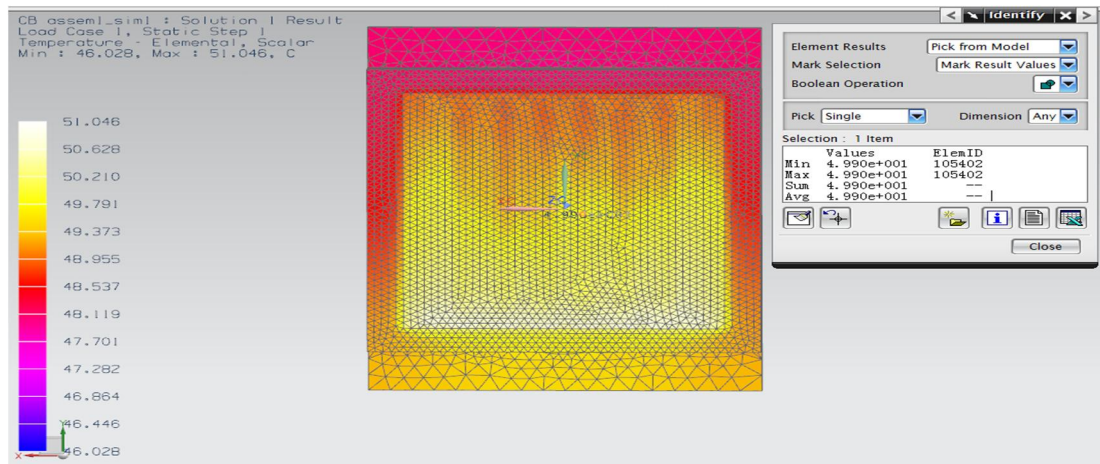
The following figures show the CFD simulation results for 0.43kg/s mass flow rate with water inlet temperature of 32°C at thermal load value from 600 W to 1000W:



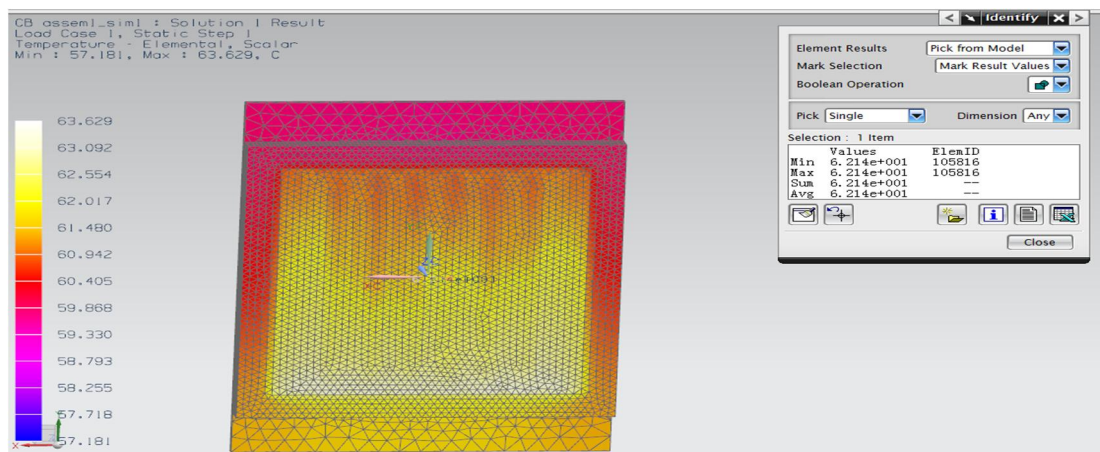


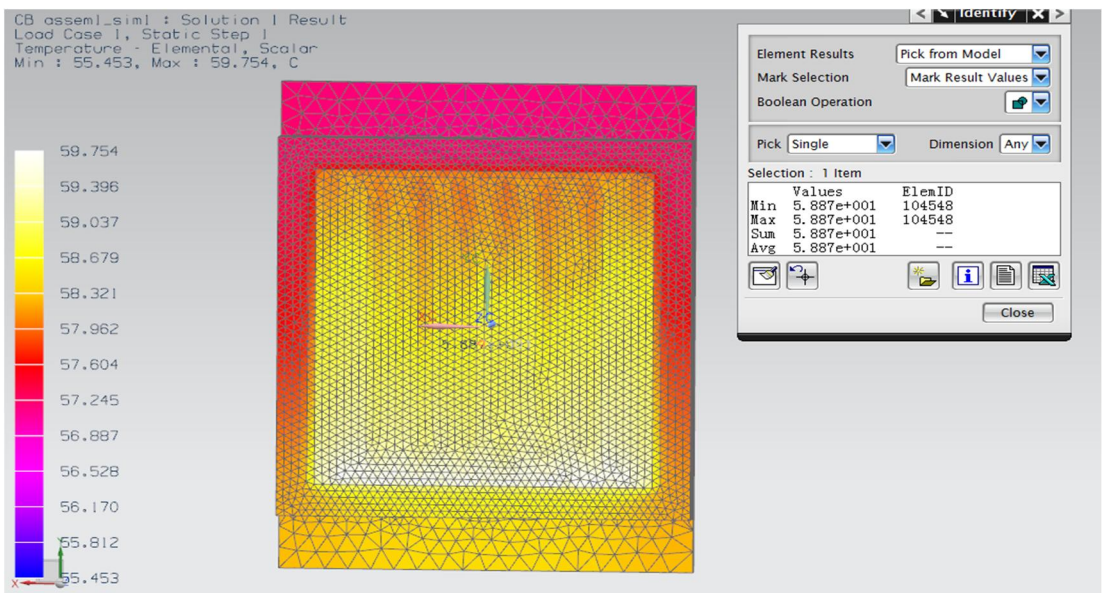
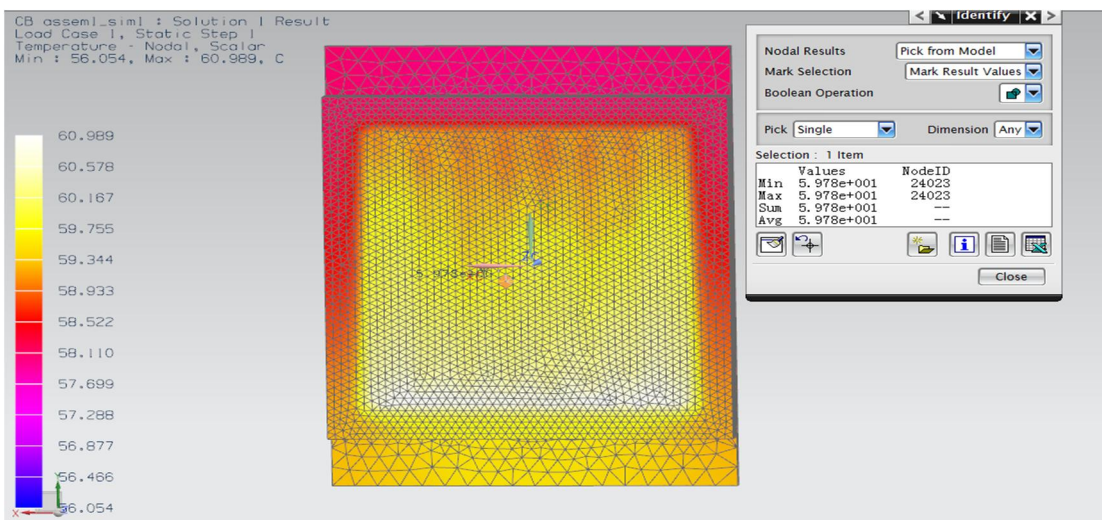
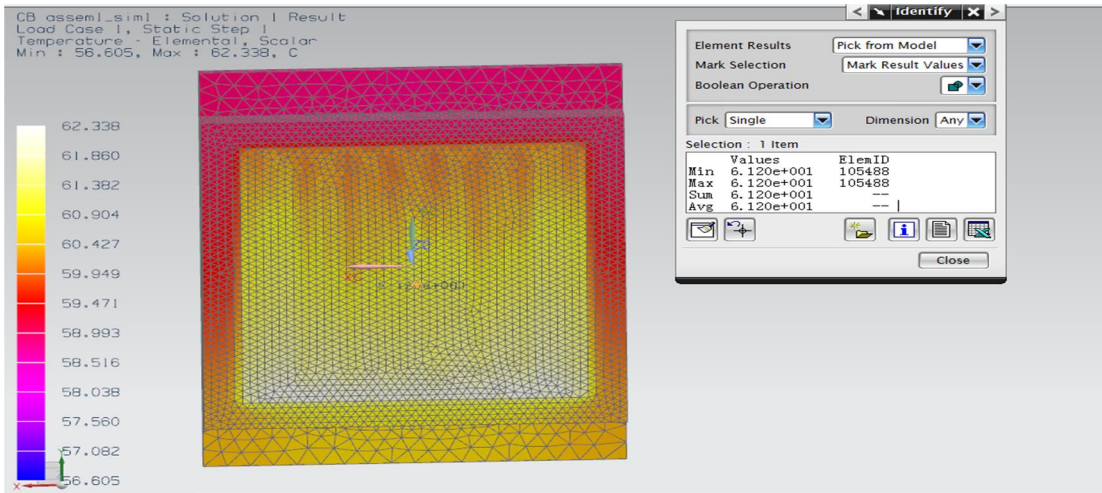
The following figures show the CFD simulation results for 0.43kg/s mass flow rate with water inlet temperature of 42 °C at thermal load value from 600 W to 1000W :

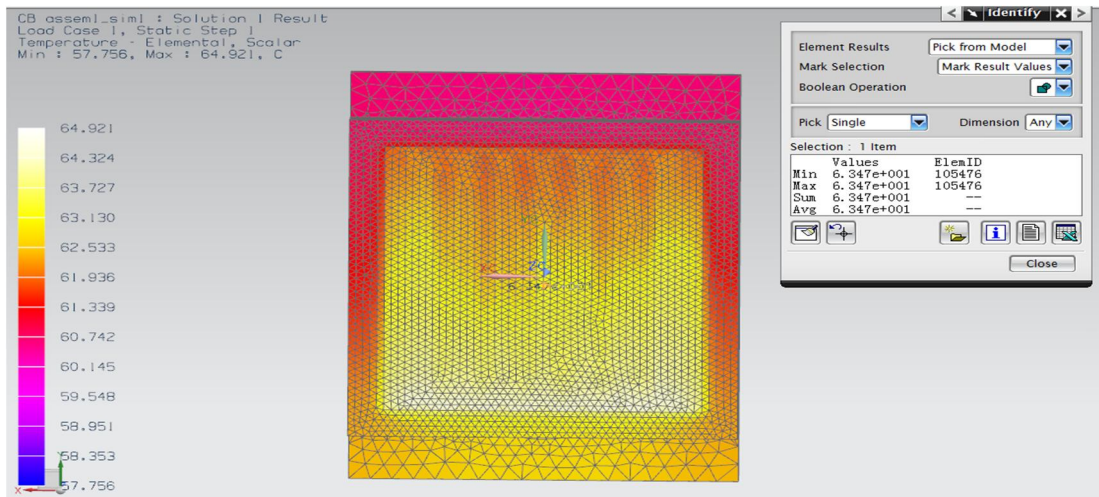




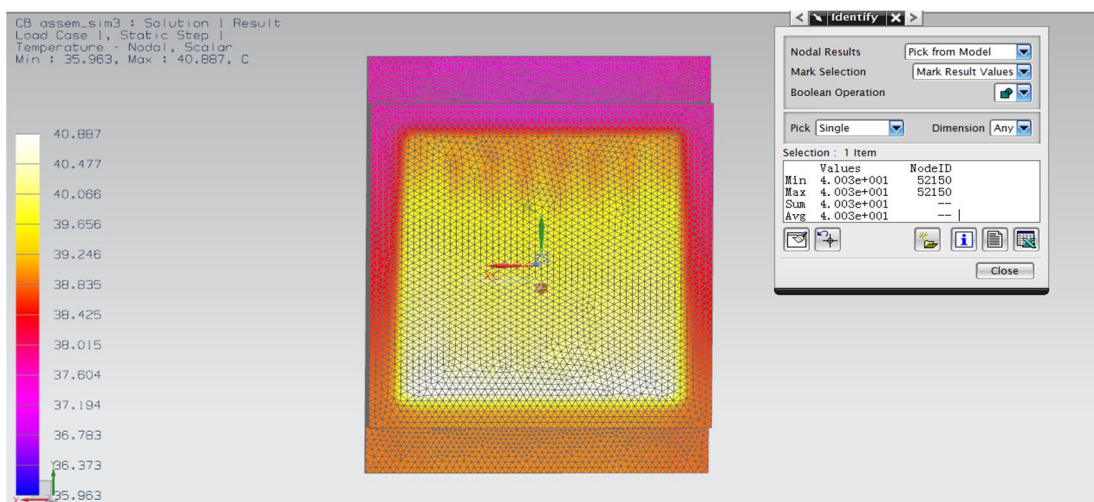
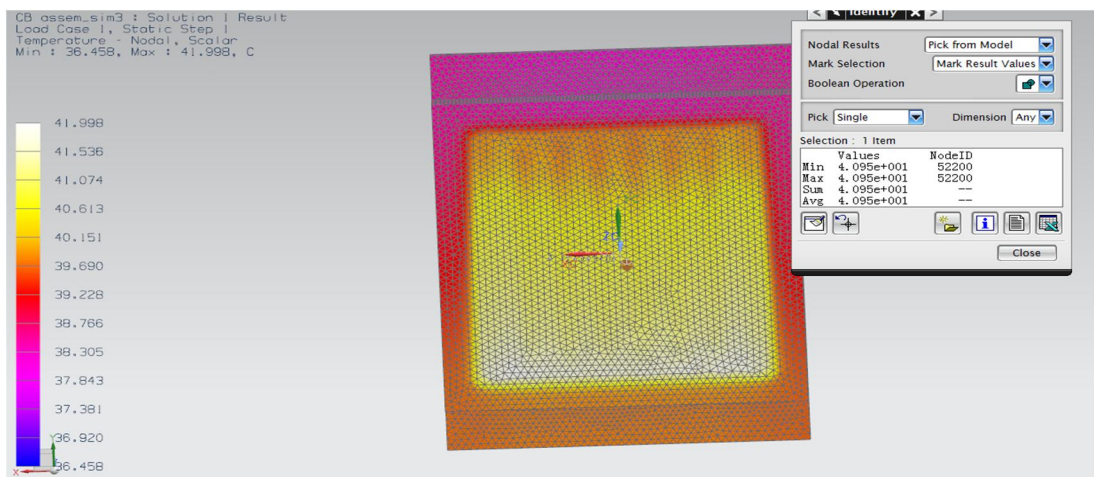
The following figures show the CFD simulation results for 0.43kg/s mass flow rate with water inlet temperature of 52°C at thermal load value from 600 W to 1000W :

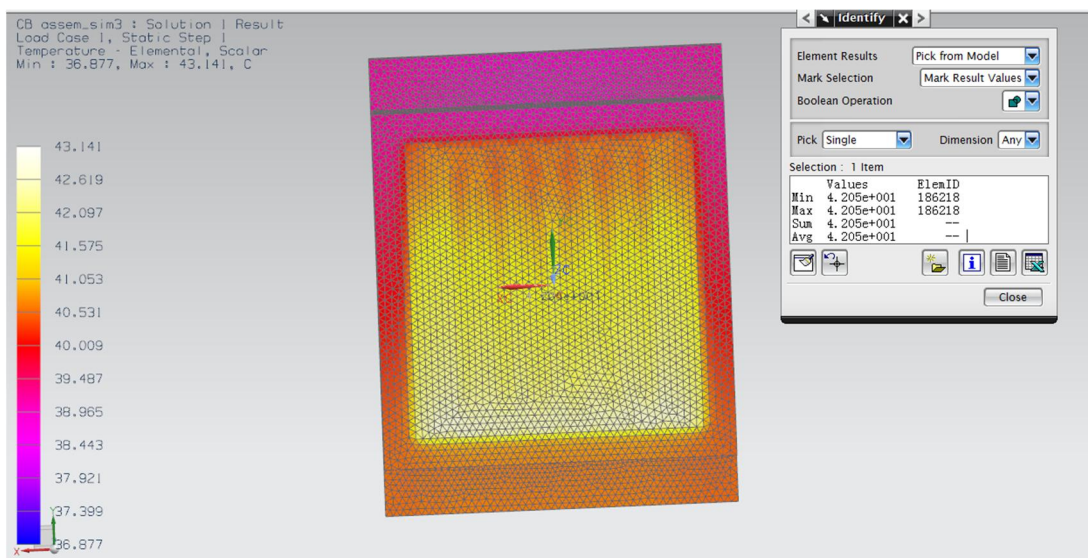
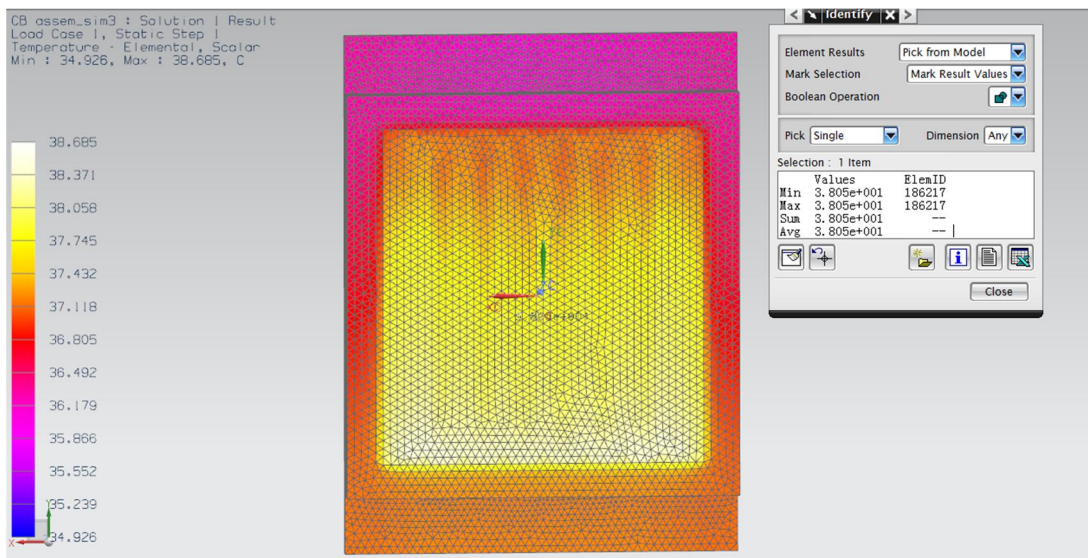
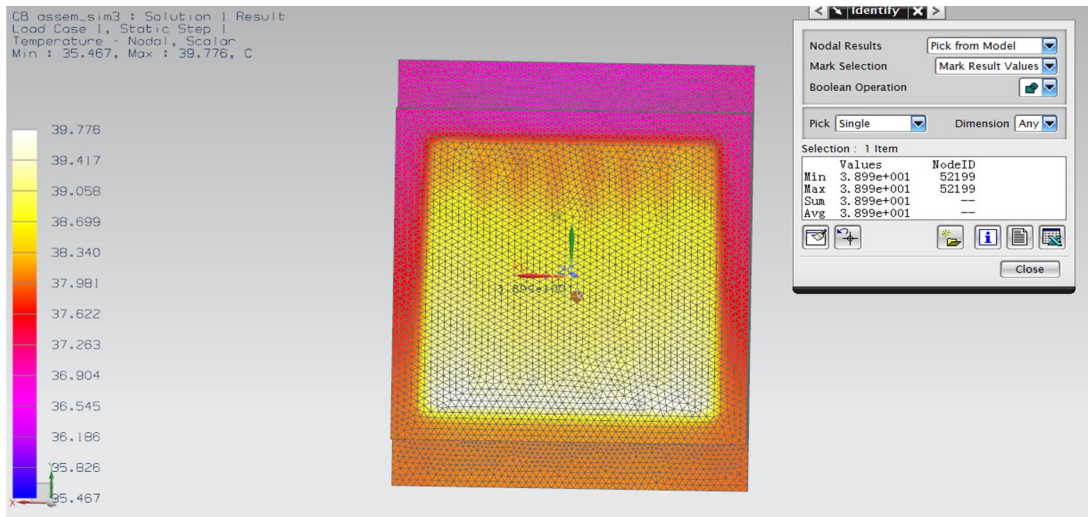




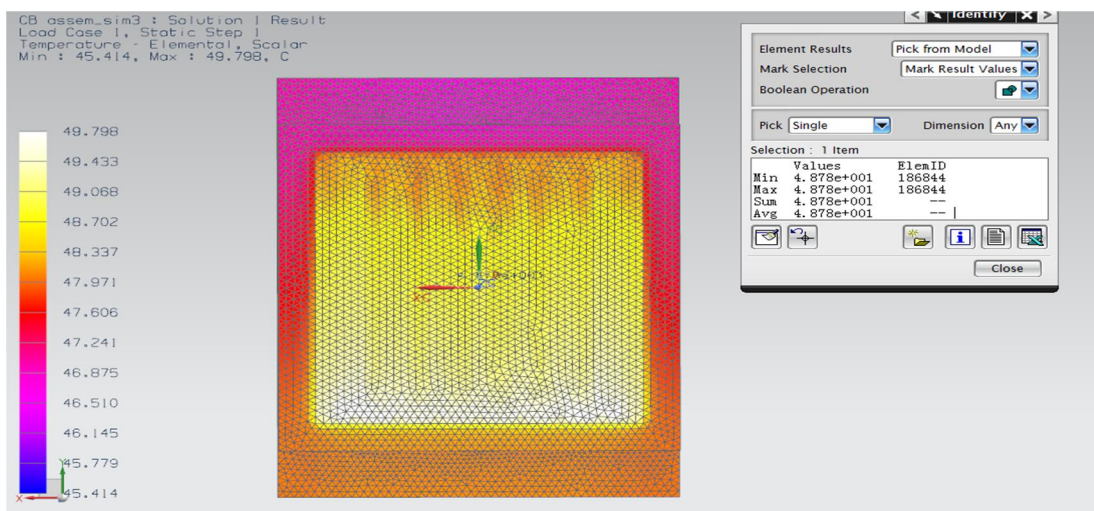
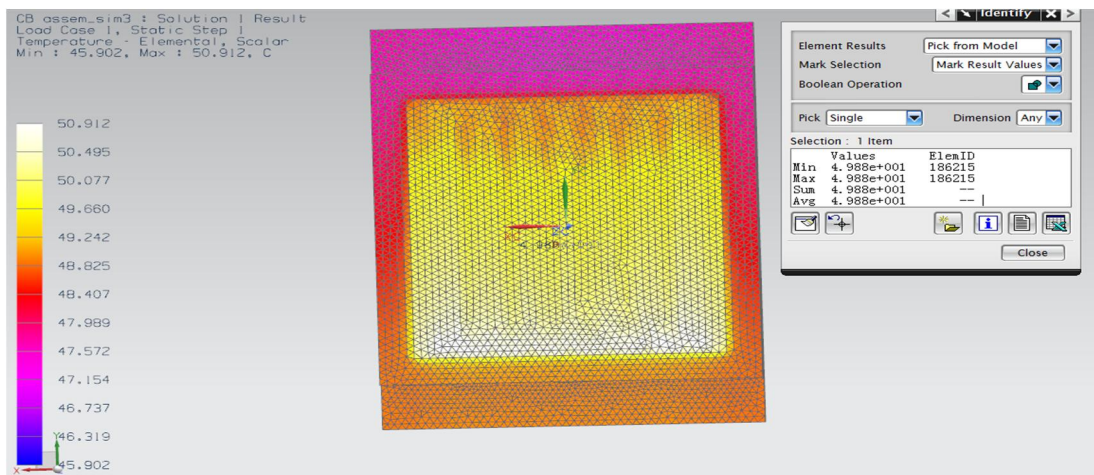
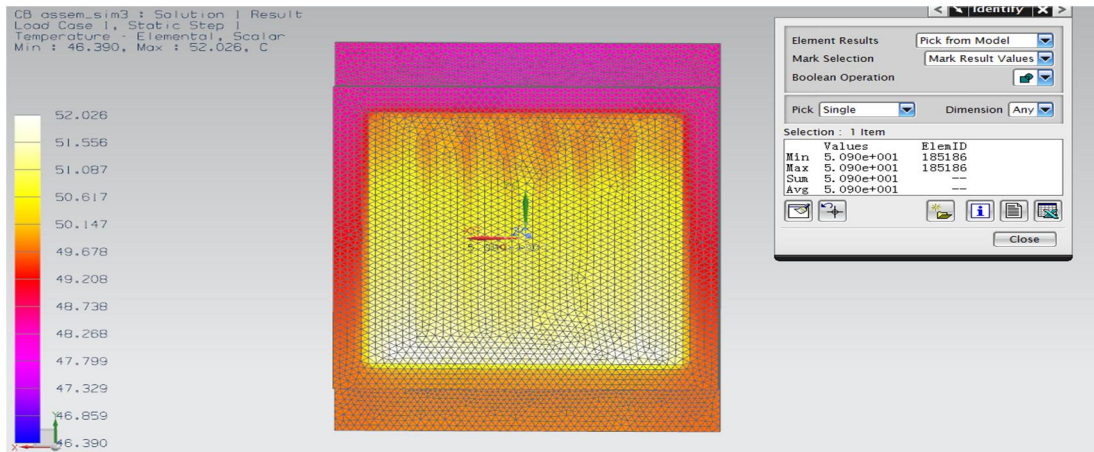


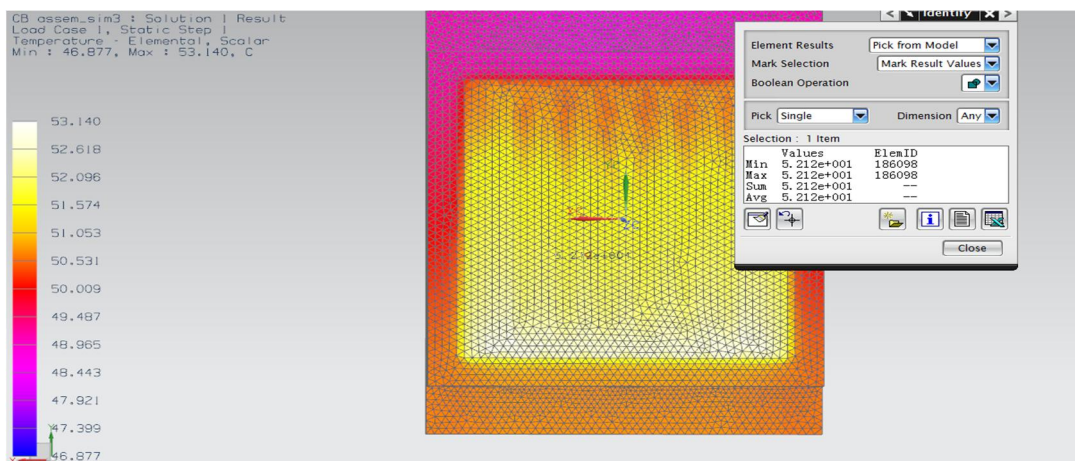
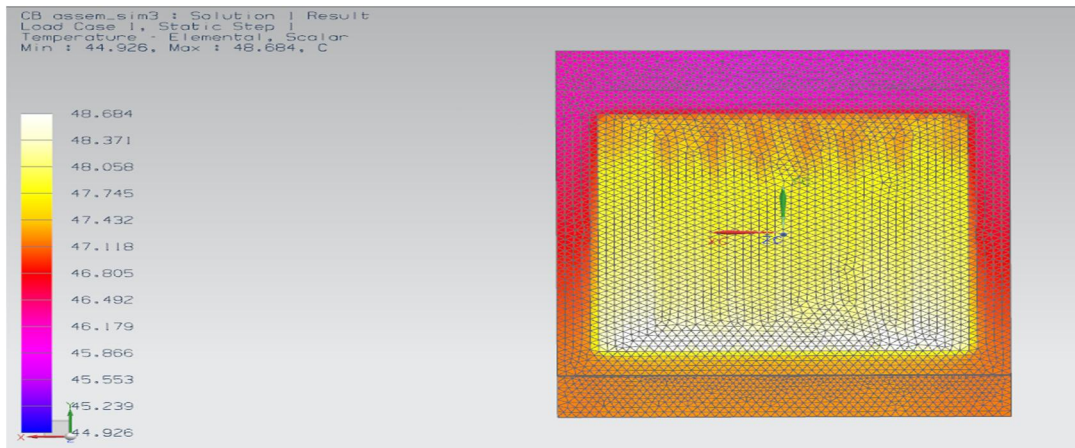
The following figures shows the CFD simulation results for 0.53kg/s mass flow rate with water inlet temperature of 32°C at thermal load value from 600 W to 1000W :



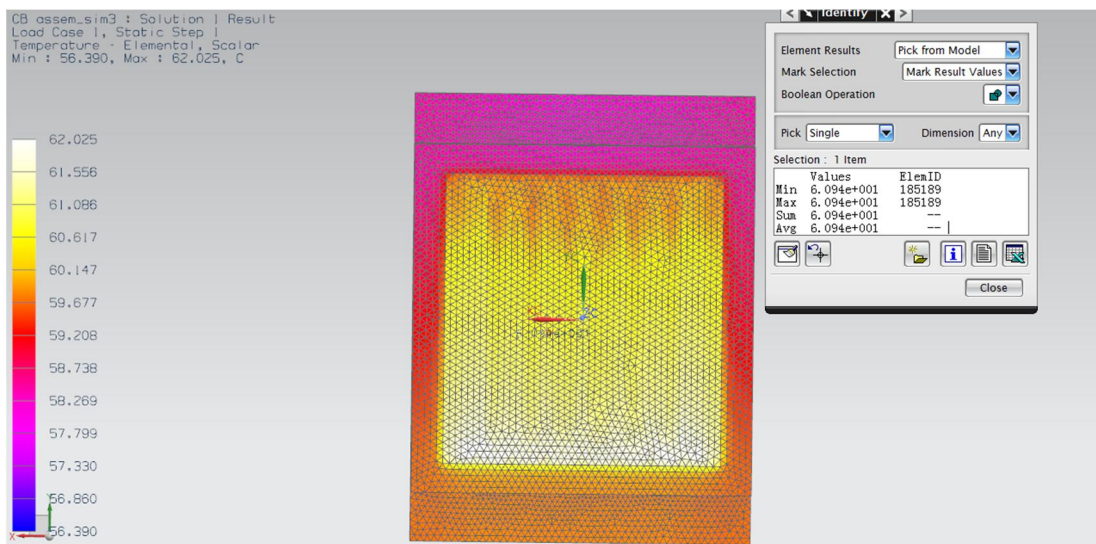


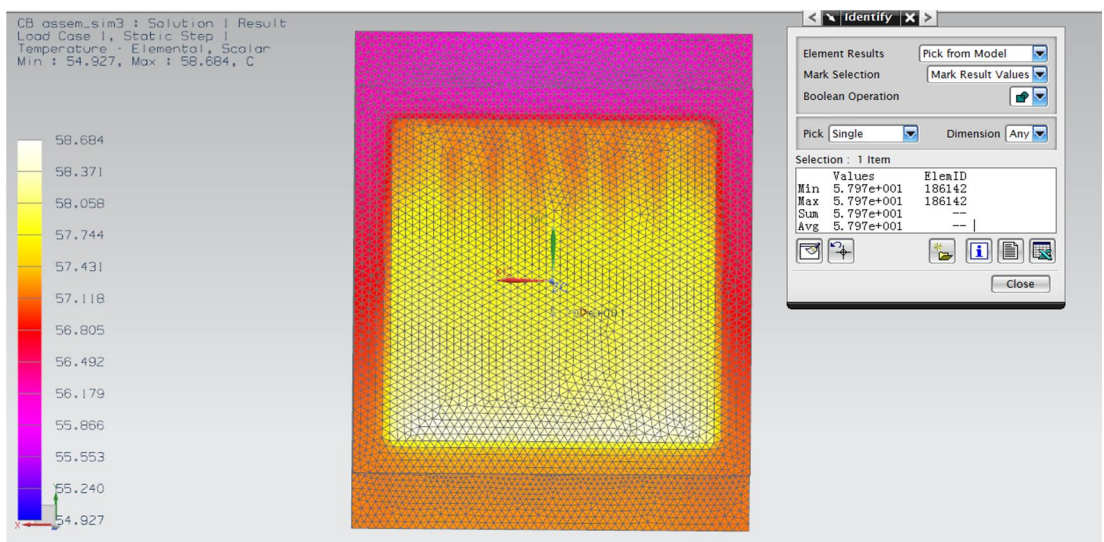
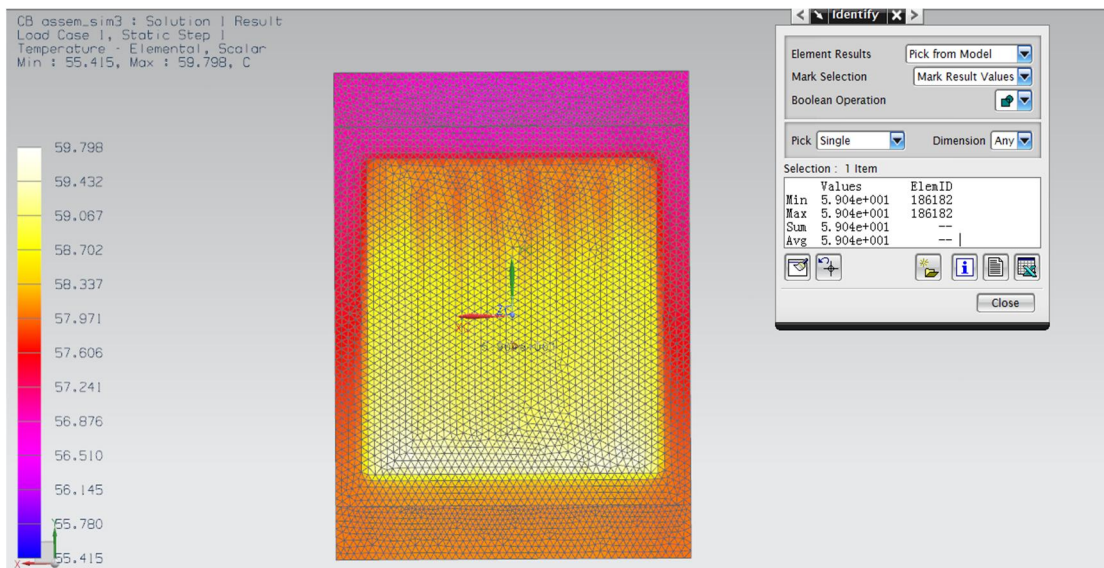
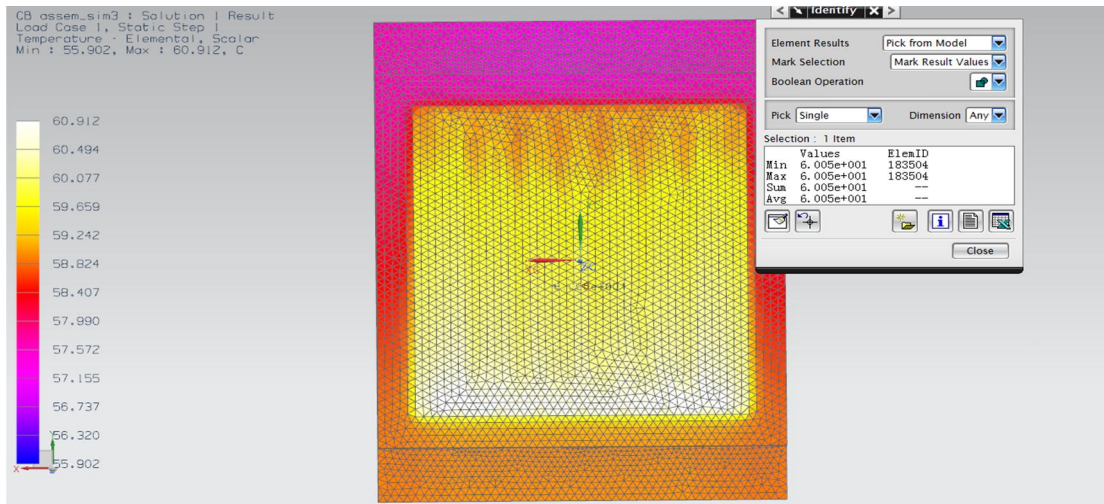
The following figures shows the CFD simulation results for 0.53kg/s mass flow rate with water inlet temperature of 42°C at thermal load value from 600 W to 1000W:

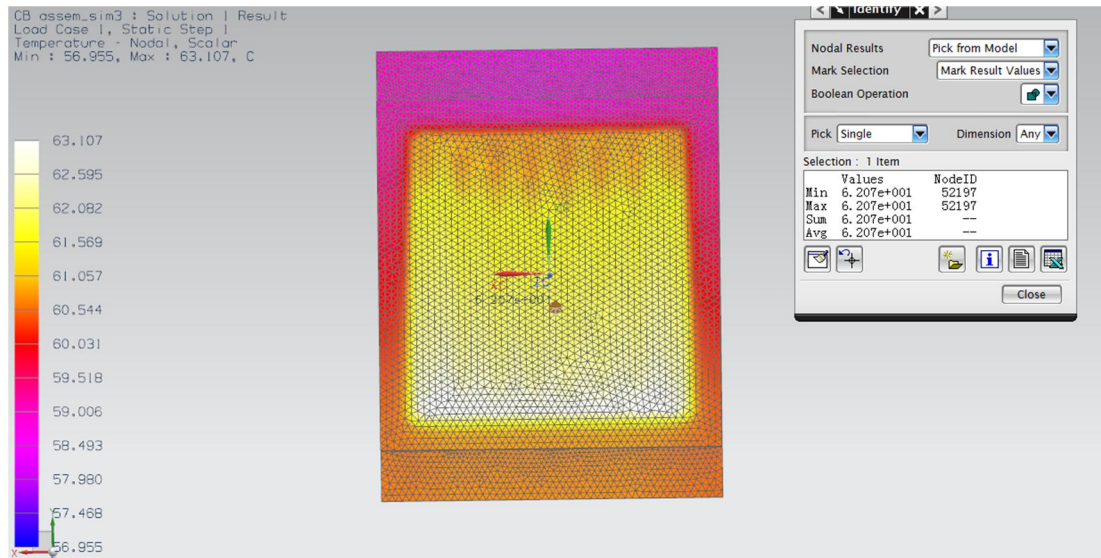




The following figures shows the CFD simulation results for 0.53kg/s mass flow rate with water inlet temperature of 52°C at thermal load value from 600 W to 1000W:







The detail resulting report generated by NX software for the final used parameter such as mass flow rate of 0.53kg/s, water inlet temperature of 32 degree and assumption of 3072W thermal load is at the following page.

APPENDIX D: Full Report of Software Generated Stress Analysis

Please refer to the following page for the full report of stress, strain and displacement simulation results generated by solidworks.

APPENDIX F: Detail Analysis on the Design of Spring

Please refer to the follow page for the detail analysis on the design of the spring for mirror tilting system.

APPENDIX G: Gantt Chart for the Project

Please refer to the follow page for the Gantt Chart of Project 1 and 2.